SYNTHESIS OF ZEOLITE MOLECULAR SIEVES FOR MEDICAL OXYGEN CONCENTRATOR

ABHIRAK SINCHANGREED

A Thesis Submitted in Partial Fulfillment of the Requirements for the
Degree of Doctor of Philosophy in Materials Engineering
Suranaree University of Technology
Academic Year 2025

การสังเคราะห์ซีโอไลท์โมเลกุลาร์ซีฟสำหรับเครื่องผลิตออกซิเจนทางการแพทย์

นายอภิรักษ์ สินจังหรีด

วิทยานิพนธ์นี้เป็นส่วนหนึ่งของการศึกษาตามหลักสูตรปริญญาปรัชญาดุษฎีบัณฑิต
สาขาวิชาวิศวกรรมวัสดุ
มหาวิทยาลัยเทคโนโลยีสุรนารี
ปีการศึกษา 2568

SYNTHESIS OF ZEOLITE MOLECULAR SIEVES FOR MEDICAL OXYGEN CONCENTRATOR

Suranaree University of Technology has approved this thesis submitted in partial fulfillment of the requirements for the Degree of Doctor of Philosophy

Thesis Examining Committee

.....

(Dr. Pattanaphong Janphuang)
Chairperson

.....

(Asst. Prof. Dr. Sukasem Watcharamaisakul)
Member (Thesis Advisor)

.....

(Assoc. Prof Dr. Jiratchaya Ayawanna)
Member

.....

(Asst. Prof. Dr. Siriwan Chokkha)
Member

.....

(Asst. Prof. Dr. Onlamee Kamon-in)
Member

.....

(Assoc. Prof. Dr. Yupaporn Ruksakulpiwat)
Acting Vice Rector for Academic Affairs
and Quality Assurance

.....

(Assoc. Prof. Dr. Pornsiri Jongkol)
Dean of Institute of Engineering

อภิรักษ์ สินจังหรีด: การสังเคราะห์ซีโอไลท์โมเลกุลาร์ซีฟสำหรับเครื่องผลิตออกซิเจนทางการแพทย์ (SYNTHESIS OF ZEOLITE MOLECULAR SIEVES FOR MEDICAL OXYGEN CONCENTRATOR)
อาจารย์ที่ปรึกษา : ผู้ช่วยศาสตราจารย์ ดร.สุขเกษม วัชรมัยสกุล, 111 หน้า.

คำสำคัญ: ซีโอไลท์, ดินบอลเคลย์, การแลกเปลี่ยนไอออน, การสังเคราะห์วิธีไฮโดรเทอร์มัล, เครื่องผลิตออกซิเจนทางการแพทย์

การวิจัยนี้มีวัตถุประสงค์เพื่อศึกษาการใช้ดินจากแหล่งภายในประเทศในการสังเคราะห์ซีโอไลต์ชนิดลิเทียมเอ (Li-A Zeolite) เพื่อนำไปประยุกต์ใช้ในเครื่องผลิตออกซิเจนแบบ Pressure Swing Adsorption (PSA) โดยใช้ดินจำนวน 3 ชนิด ได้แก่ ดินบอลเคลย์ (ดินดำ) ดินขาวระนอง และดินขาวลำปาง เพื่อหาวัสดุดินที่เหมาะสมที่สุดต่อการเกิดซีโอไลท์ ผลการทดลองพบว่า ดินบอลเคลย์ซึ่งมีอัตราส่วนซิลิกอนต่ออะลูมิเนียม (Si/Al) เท่ากับ 1.32 เป็นดินที่เหมาะสมที่สุดสำหรับการสังเคราะห์ ซีโอไลท์ชนิดเอ ดินบอลเคลย์ถูกนำมาเผาที่อุณหภูมิระหว่าง 400–800 องศาเซลเซียส เป็นเวลา 3 ชั่วโมง ผลการวิเคราะห์ด้วยเอกซ์เรย์ดิฟแฟรกชัน (XRD) พบว่า ที่อุณหภูมิ 600 องศาเซลเซียส ไม่ปรากฏพีคของแร่คาโอลิไนต์ (Kaolinite) ซึ่งแสดงถึงการเปลี่ยนโครงสร้างของดินบอลเคลย์ไปสู่เฟสกึ่งเสถียร (Metastable phase) หลังจากนั้นสามารถสังเคราะห์ซีโอไลท์ชนิดเอได้สำเร็จ โดยใช้สารละลายโซเดียมไฮดรอกไซด์ (NaOH) ความเข้มข้น 3 โมลาร์ ซึ่งทำให้ได้ผลึกซีโอไลท์ที่มีโครงสร้างสมบูรณ์ จากนั้นได้ทำการแลกเปลี่ยนไอออนโซเดียม (Na^+) ในซีโอไลท์กับไอออนลิเทียม (Li^+) โดยใช้สารละลายลิเทียมไฮดรอกไซด์ (LiOH) ความเข้มข้น 2 โมลาร์ เพื่อเพิ่มประสิทธิภาพการดูดซับ ซึ่งผลการวิเคราะห์ด้วยสเปกโทรสโกปีอินฟราเรดแบบฟูเรียร์ทรานส์ฟอร์ม (FTIR) ยืนยันการแลกเปลี่ยนไอออนดังกล่าวได้สำเร็จ ซีโอไลท์ที่ได้จากการสังเคราะห์ถูกนำมาขึ้นรูปด้วยวิธีสเปรย์ดราย (Spray Drying) เพื่อให้ได้อนุภาคทรงกลม โดยไม่ใช้สารยึดเกาะ (Binder) ซีโอไลท์ที่ได้ถูกทดสอบประสิทธิภาพในเครื่องผลิตออกซิเจน PSA โดยใช้ขนาดอนุภาคที่แตกต่างกัน ได้แก่ 450, 550 และ 650 ไมโครเมตร ผลการทดสอบพบว่า ซีโอไลท์ที่มีขนาดอนุภาค 450 ไมโครเมตร ให้ประสิทธิภาพในการผลิตออกซิเจนสูงที่สุดถึงร้อยละ 93 ซึ่งแสดงให้เห็นว่าซีโอไลท์ที่มีขนาดอนุภาคเล็กสามารถเพิ่มประสิทธิภาพการผลิตออกซิเจนได้ดีกว่าในระบบ PSA นอกจากนี้ การใช้ดินธรรมชาติภายในประเทศเป็นวัตถุดิบตั้งต้นช่วยลดต้นทุนการผลิตได้อย่างมีนัยสำคัญ เมื่อเทียบกับการใช้วัตถุดิบสังเคราะห์เชิงพาณิชย์ ดังนั้นงานวิจัยนี้แสดงให้เห็นถึงความเป็นไปได้ในการผลิตซีโอไลท์ชนิดลิเทียมเอที่มีต้นทุนต่ำ

และมีศักยภาพสำหรับการประยุกต์ใช้ในการผลิตออกซิเจนทางการแพทย์และอุตสาหกรรมการแยกก๊าซในประเทศไทย

สาขาวิชา วิศวกรรมเซรามิก ลายมือชื่อนักศึกษา .....

ปีการศึกษา 2568 ลายมือชื่ออาจารย์ที่ปรึกษา.....

ABHIRAK SINCHANGREED: SYNTHESIS OF ZEOLITE MOLECULAR SIEVES FOR MEDICAL OXYGEN CONCENTRATOR
THESIS ADVISOR : ASSIST.PROF. SUKASEM WATCHARAMAISAKUL, Ph.D. 111 PP.

Keywords: Zeolite, Ball clay, Ion-exchange, Hydrothermal synthesis, Oxygen concentrator

This study aimed to investigate the potential use of locally sourced clays for the synthesis of Li-A Zeolite to be applied in a pressure swing adsorption (PSA) oxygen concentrator. Three types of clays, namely ball clay, Ranong white clay, and Lampang white clay, were examined to determine the most suitable raw material for zeolite A formation. The results indicated that ball clay, with a Si/Al ratio of 1.32, was the most appropriate clay for synthesizing Zeolite A. The ball clay was calcined at temperatures ranging from 400 to 800 °C for 3 h. The X-ray diffraction (XRD) results revealed that at 600 °C, the kaolinite peak disappeared, indicating the transformation of ball clay into a metastable phase. Zeolite A was successfully synthesized from calcined ball clay using a 3 M NaOH solution, resulting in a well-crystallized structure. Furthermore, ion exchange of Na^+ with Li^+ was performed using a 2 M LiOH solution to enhance the adsorption performance of the zeolite. The ion exchange process was confirmed by Fourier-transform infrared spectroscopy (FTIR). The Li-A zeolite was then formed into spherical particles by spray drying without the use of a binder. The synthesized zeolites with different particle sizes (450, 550, and 650 μm) were tested in a PSA oxygen concentrator. The results showed that zeolite with a particle size of 450 μm provided the highest oxygen purity at 93 percent. This finding suggests that smaller zeolite particles can enhance oxygen production performance in PSA systems. Additionally, the use of locally available natural clay as a raw material significantly reduces production costs compared to using commercial synthetic sources. Therefore, this study demonstrates the feasibility of producing cost-effective Li-A zeolite for medical

oxygen production and industrial gas separation applications in oxygen concentrators using natural resources available in Thailand.

School of Ceramic Engineering

Academic Year 2025

Student's Signature .....

Advisor's Signature.....

ACKNOWLEDGEMENT

First and foremost, I would like to express my deepest gratitude to Asst. Prof. Dr. Sukasem Watcharamaisakul, who provided research guidance, encouragement, and support throughout the research course. Their expertise and valuable feedback have greatly contributed to the quality and completion of this thesis. I am also sincerely thankful to the members of my thesis committee, Assoc. Prof Dr. Jiratchaya Ayawanna, Asst. Prof. Dr. Siriwan Chokkha, and Asst. Prof. Dr. Onlamee Kamon-in, for their recommendations, comments, suggestions, and academic support. My appreciation also extends to my colleagues and friends in the Materials Engineering regarding their collaboration, assistance, and companionship made this academic journey productive and motivated. I am especially grateful to my family for their endless love, patience, and moral support. Their encouragement has been my greatest motivation throughout this academic journey.

Finally, I would like to acknowledge Suranaree University of Technology for providing scholarship support and the Synchrotron Light Research Institute for supporting the research fund and providing an oxygen concentrator for the experiment, particularly from Dr. Pattanaphong Janphuang. Without the support, the successful completion of this thesis would not have been possible.

ABHIRAK SINCHANGREED

TABLE OF CONTENTS

Page

TABLE OF CONTENTS (Continued)

Page

TABLE OF CONTENTS (Continued)

Page

LIST OF TABLES

Table **page**

LIST OF FIGURES

Figure **Page**

LIST OF FIGURES (continued)

Figure **Page**

LIST OF FIGURES (continued)

Figure **Page**

LIST OF FIGURES (continued)

Figure **Page**

CHAPTER I
INTRODUCTION

1.1 Introduction

Zeolite has been studied with the respect to its structure-property relationships, which are significantly dependent on synthesis conditions. To summary, Zeolites are hydrated aluminosilicates, which created from tetrahedral alumina $(AlO4)5-$ and silica $(SiO4)4-$ through the interlinkage of oxygen atoms. Zeolites contains high crystalline, porous aluminosilicate minerals with a three-dimensional network of tetrahedral SiO4 and AlO4 units, allowing cations to be located within the material's pores. In this framework, these cations neutralize the lattice's negative charge. Therefore, this cation mobility results from the unique ion-exchange and catalytic properties of zeolites. Zeolite has different applications. It can be used as a highly efficient catalyst (Y. Liu et al., 2019), adsorbent (Ramya et al., 2019), ion exchanger (Król, 2019), and detergent (Cardoso et al., 2015) for contaminated water treatment and other chemical processes. Moreover, zeolites is important for the process of biomass conversion, thermal energy storage, water purification, fuel cells, and air pollution remediation.

In the ordinary method, most synthesis methods require sodium aluminosilicate gel for both simple and complex methods. Especially the hydrothermal treatment, which involves a multiphase reaction-crystallization process (Cundy & Cox, 2003a) involving amorphous or crystalline phases, which is a liquid and a solid phase. The hydrothermal method has a significant impact on the synthesis of zeolites since its introduction by Barrer in 1948 (Kerr, 1983). Hydrothermal synthesis was described as an in situ reaction that occurs above room temperature and pressure in an aqueous solution. Synthesizing aluminosilicate zeolites under hydrothermal conditions is always

preferable. This method has several advantages, including low energy consumption, reduced air pollution, and a high tendency to form reactive products, as well as metastable and condensed phases. Synthetic zeolites are typically used than natural zeolites due to their higher purity and uniform particle size, which are particularly suitable for most engineering applications and scientific purposes. Most synthetic zeolites are synthesized from chemical sources integrated from silica and alumina in an aqueous alkaline medium at temperatures ranging from 8 to 200 ℃ for durations of 1 to 20 days. However, preparing synthetic zeolites from chemical sources of silica and alumina is relatively expensive (Johnson & Arshad, 2014). High-temperature, high-pressure, and long-period hydrothermal reactions are typically not considered "green" due to their low efficiency and potential for water pollution. The use of ecological materials, agro-waste, natural raw materials, and manufacturing waste has been studied and used as starting materials for synthesizing zeolite. For example, coal fly ash, rice husk ash, oil shale ash, bagasse fly ash, paper sludge, waste sandstone cake, waste porcelain, lithium slag, and kaolin. In general, there are two phases in the synthesis of zeolite from kaolin. The initial phase is calcination, which converts kaolin into a metastable phase through hydrothermal activation, as illustrated in Equation (1).

$$2Al_2Si_2O_5(OH)_4 \longrightarrow 2Al_2Si_2O_7 + 2H_2O \quad (1)$$

The second stage is hydrothermal treatment using an aqueous alkali solution to convert the product ($Al_2Si_2O_7$) obtained from the first stage into zeolite, as shown in Equation (2).

$$6Al_2Si_2O_7 + 12NaOH \longrightarrow Na_{12}(AlO_2)_{12}(SiO_2)_{12}27H_2O + 6H_2O \quad (2)$$

Therefore, this study aims to present an overview of current developments in the synthesis of zeolite from ball clay, with particular emphasis on identifying the

optimum calcination temperature and alkaline solution concentration for hydrothermal treatment. This study also examines the chemical and physical properties of the synthesized zeolite as a molecular sieve and evaluates its potential to enhance the performance of oxygen concentrator devices, leading to more efficient oxygen generation to achieve medical-grade concentration requirements.

1.2 Research objective

1.2.1 To synthesize the Li-A zeolite using ball clay as a starting material by hydrothermal treatment

1.2.2 To investigate the optimum calcining temperature of metastable phase ball clay and the concentration of the alkaline solution for hydrothermal treatment.

1.2.3 To study the chemical and physical properties of the synthesized zeolite as a molecular sieve.

1.2.4 To examine the efficiency of the synthesized zeolite as a molecular sieve in a Pressure swing adsorption (PSA) oxygen concentrator.

CHAPTER II
LITERATURE REVIEWS

2.1 Zeolite

The first scientific report of a zeolite was published by Cronstedt in 1765, when he described the mineral stilbite as "boiling stones." The name "zeolite" is created from the Greek terms called "zeo," which means "to boil," and "lithos," which means "stone." In 1862, St. Claire Deville produced zeolites in a laboratory (Zimmermann & Haranczyk, 2016). However, the most crucial early developments in the industrial synthesis of zeolites were achieved in the 1950s by Milton and Breck at Union Carbide.

Zeolites are crystalline and hydrated aluminosilicates that were characterized by the structural framework made from silica and alumina tetrahedra interconnected by shared oxygen atoms. This framework includes distinct channels and cavities filled with ions and water molecules, giving zeolites unique physical and chemical properties. Based on TO4 tetrahedra (where T can be either an aluminum or silicon atom), zeolites are valuable for various applications, such as ion exchange, molecular sieves, gas adsorption, and catalysis. Zeolite LTA (Linde Type A) has a cubic zeolitic framework that features sodalite cages (SOD-cages), formed by linked single four- and six-membered rings. In the LTA framework, zeolite A contains an α-cage made up of eight cuboctahedra connected by twelve cuboids. Each SOD cage in LTA is correlated with its six closest neighboring SOD cages through double T4-rings (D4R).

Regarding energy consumption, the carbon economy, and production costs, researchers have paid great attention to seeking cheap raw materials to replace high-cost pure synthetic materials in the synthesis of zeolite A. Clay minerals, coal ashes, natural zeolites, municipal solid wastes, and industrial sludge are known as alternative raw materials for the synthesis of zeolite A owing to their low cost and available

abundance in nature and industry. Among available raw materials, bentonite minerals with Si and Al sources have been recognized as highly promising precursors for the synthesis of zeolite A. Bentonite is a natural clay used in many industries, including bonding, plasticizing, and suspending. Bentonite is made from silica tetrahedral sheets and one central alumina octahedral sheet (J. Wang et al., 2017). The theoretical composition of Bentonite contains 71.62% of SiO_2, 15.22% of Al_2O_3, and 13.17% of water. Thus, Bentonite can be used as the starting material for the synthesis of zeolite since its SiO_2/Al_2O_3 ratio (around 4.7) is in a suitable range with that of synthesis zeolite A.

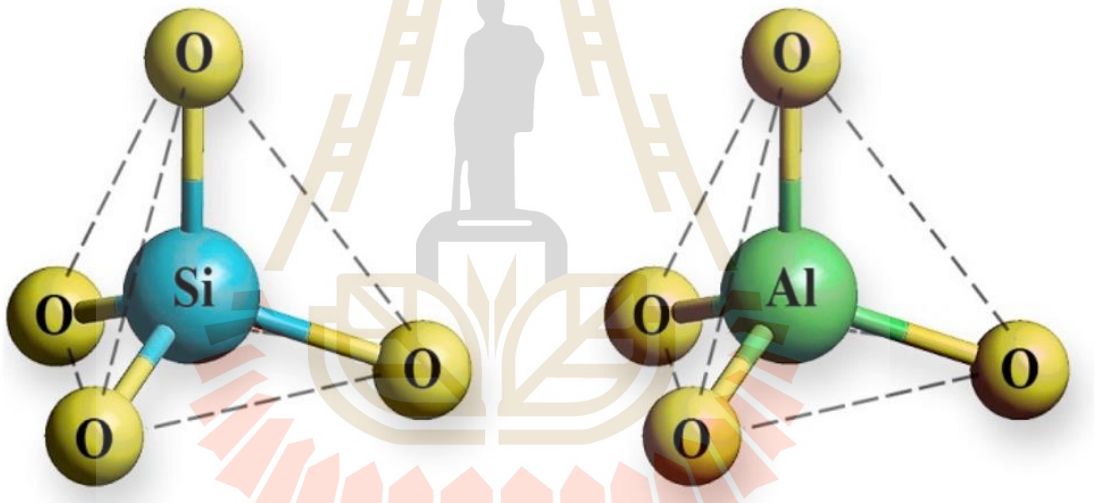

Figure 2.1 Representation of $[SiO_4]^{4-}$ or $[AlO_4]^{5-}$ tetrahedral
(Pavlović & Rajić, 2023)

Zeolites are crystalline aluminosilicates that possess microporous structures, with pore sizes between 3 and 7 Å. The latest Atlas of Zeolite Framework Types has cataloged approximately 176 different framework structures. The key attributes of these solid materials include their clearly defined structures, large surface areas,

effective adsorption of small molecules (acting as molecular sieves), and ion-exchange capability. Zeolites are composed of TO4 tetrahedra (T = Si, Al), which integrate oxygen atoms to form a 3D network. The extra framework cations can be ion-exchanged with other cations, for instance, alkali metals, alkaline earth metals, and transition metals. Besides, the Al content within the framework can vary from Si/Al≈1 to ∞ depending on the synthesis conditions. Moreover, Al or Si can be inserted into the framework during the post-synthesis modification process. Meanwhile, a higher Si/Al ratio of the framework can enhance both hydrophobicity and hydrothermal stability. Zeolite frameworks contain cages of different shapes, such as a spherical cage, which can be interconnected by channels with diameters determined by the number of T atoms as n-member rings. Large pore zeolites are constructed of 12-member rings (d > 7Å), medium pore zeolites contain 10-member rings (5Å < d < 6Å), while small-pore zeolites contain 6- or 8-member rings (diameter d: 2.8Å < d < 4Å. The Structure Commission of the International Zeolite Association (IZA-SC) assigns a three-letter code to each framework type. Table 2.1 illustrate essential zeolites with three-letter codes based on the Si/Al ratio or phosphate content

Table 2.1 Nomenclature and specifications of important zeolites

Low silica Si/Al ≤ 2		**Intermediate Silica** 2 < Si/Al ≤ 5		**High Silica** 5 < Si/Al		**Other elements**	
IUPAC name	Example	IUPAC name	Example	IUPAC name	Example	IUPAC name	Example
ANA	Analcime	BHP	Linde Q	BEA	Zeolite β	AEI	AlPO4-18
BIK	Bikitaite	FAU	NaY	FER	Ferrierite	AEL	AlPO4-11
CAN	Cancrinite	FER	Ferrierite	MEL	ZSM-11	AFN	AlPO4-14
EDI	Edintonite	LTL	Linde L	MFI	ZSM-5	AFR	SAPO-40
FAU	NaX	MAZ	Mazzite	MFS	ZSM-57	AFX	SAPO-56
FRA	Franzinite	MEI	ZSM-18	MSO	MCM-61	CAN	Tiptopite
LTA	Linde A	MER	Merlinoite	MTF	MCM-35	CHA	SAPO-47

Table 2.1 Nomenclature and specifications of important zeolites (Continued)

Low silica Si/Al ≤ 2		Intermediate Silica 2 < Si/Al ≤ 5		High Silica 5 < Si/Al		Other elements	
PHI	Phillipsite	MOR	Mordenite	MTT	ZSM-23	FAU	SAPO-56
SOD	Sodalite	OFF	Offretite	MWW	MCM-22	OSI	UiO-6
THO	Thomsonite	STI	Stilbite	ZSM	ZSM-48	SAV	Mg-STA-7

Low-silica zeolites, also known as aluminum-rich zeolites, have a nearly saturated aluminum content, with a molar ratio of Si/Al≈1. This structure allows for the maximum possible aluminum content in the tetrahedral framework (as seen in zeolites A and X). Low-silica zeolites contain the largest cation-exchange sites among zeolites, providing a strong hydrophilic surface selectivity. These zeolites have the largest pore volumes among known types, giving them a significant economic advantage in applications that require bulk separation and purification, where high capacity is essential.

Intermediate-silica zeolites were first developed at Union Carbide Laboratories in the early 1950s to provide enhanced thermal, hydrothermal, and acid stability. During production, these zeolites achieved significant commercial success as both adsorbents and hydrocarbon-conversion catalysts. The surfaces of these zeolites remain heterogeneous and demonstrate high selectivity for water and other polar molecules. Intermediate zeolites characterized by 2 < Si/Al < 5 in natural forms such as mordenite, erionite, clinoptilolite, and chabazite, also synthetic variants such as omega, mordenite, Y, and L. Within this Si/Al range, these materials retain hydrophilic properties.

High-silica zeolites are characterized by a silicon-to-aluminum (Si/Al) ratio greater than 5. This results in increased hydrophobicity and organophilicity, fewer intense Brønsted acidic sites, and enhanced thermal and hydrothermal stability. These materials can be synthesized directly by incorporating organic components into

aluminosilicate or silicate gels. Besides, they can be produced via post-synthesis modifications, such as hydrothermal steaming or treatment with aqueous (NH4)2SiF6, SiCl4, or F_2. Additionally, dealumination, which involves the removal of framework aluminum can improve catalytic properties and enhances thermal stability.

Many elements have been correlated with the zeolite framework, with the substitution of phosphorus by silicon within the zeolite structure. This led to the silica-aluminophosphates (SAPOs), which possess cation-exchange properties. Aluminophosphates (AlPOs) are composed of alternating AlO_2^- and PO_2^+ units to form a neutral, organophilic, and non-acidic framework. The incorporation of additional elements such as Si, Mg, Fe, Ti, Co, Zn, Mn, Ga, Ge, Be, Li, As, and B into the tetrahedral sites of AlPOs gives a vast number of element-substituted molecular sieves (MeAPO, MeAPSO, SAPO), which are essential heterogeneous catalysts.

Zeolites are widely used across multiple industries such as detergents, gas separation, desiccation, and catalysis. With lower cost, Natural zeolites are primarily utilized in bulk mineral applications. In 2008, the consumption of natural zeolites was estimated at 1.27×10^6 t. The second-largest application of zeolites is as catalysts, accounting for 17% by volume and over 55% of the market value, reflecting the higher cost of zeolites used in catalysis. Zeolite Y constitutes more than 95% of total zeolite catalyst consumption, primarily in the Fluid Catalytic Cracking (FCC) process. Smaller quantities are used in petrochemical synthesis and hydrocracking. In 2008, catalyst consumption was estimated at approximately 0.3×10^6 t. Zeolites also serve as adsorbents for drying and purifying petrochemical streams (such as ethylene and propylene), natural gas, and for bulk chemical separations (including normal paraffin and xylenes). Additionally, they are used in air separation industries to produce oxygen via pressure swing adsorption (PSA) or vacuum pressure swing adsorption (VPSA). In 2008, about 0.18×10^6 t (10%) of zeolite was used as an adsorbent. Other applications include the transformation of photochemical organics, sensor manufacturing, odor removal, paper fillers, solar energy conversion, plastic additives, soil conditioners and

fertilizers, pozzolanic cement and concrete, lightweight aggregates, and dietary supplements in animal nutrition. Global production of natural zeolites in 2008 was estimated at 3.0×10^6 t. China and Cuba are the largest consumers of additives used to enhance cement strength. Zeolite prices vary considerably depending on the application. In the United States, natural zeolite for bulk applications is priced between 0.04 and 0.25 USD per kilogram, whereas industrial adsorbent applications range from 1.5 to 3.5 USD per kilogram. For catalyst applications, prices range from 3 to 4 USD per kilogram for fluid catalytic cracking (FCC) and reach approximately 20 USD per kilogram for specialty catalysts. Adsorbent prices are generally 5 to 9 USD per kilogram, while detergent prices are around 2 USD per kilogram.

2.1.1 Zeolite A

Zeolite A or Linde Type A (LTA) is one of the most widely researched and applied synthetic zeolites. It possesses a highly crystalline aluminosilicate framework composed of interconnected TO_4 tetrahedra (where T = Si or Al) arranged in a cubic symmetry. The substitution of Si^{4+} by Al^{3+} in the framework generates negative charges that was balanced by exchangeable cations such as Na^+, Ca^{2+}, or K^+. This feature imparts zeolite A with remarkable cation-exchange capacity, therefore, it suitable for different applications. The framework of zeolite A is characterized by its three-dimensional pore system, featuring uniform pore openings of approximately 4.1 Å (for the NaA form), which enables selective adsorption and molecular sieving. Depending on the exchanged cation, the pore size can be adjusted; for example, the CaA form has an effective pore opening of ~5 Å, leading to the commercial terms 4A, 5A, and 3A zeolites. The unique structure of zeolite A has led to its extensive use in adsorption and ion-exchange processes. Its high affinity for polar molecules, particularly water, makes it an effective desiccant and drying agent in industrial processes. Additionally, the cation-exchange ability is exploited in water softening, where zeolite A efficiently removes calcium and magnesium ions, thereby reducing hardness. In environmental applications, zeolite A has been studied for the removal

of heavy metals, ammonium, and other toxic cations from contaminated water. Zeolite A has tunable ion-exchange selectivity to target specific contaminants for sustainable water treatment. Zeolite A also has a potential in adsorbing volatile organic compounds (VOCs) and greenhouse gases, thereby contributing to pollution control and energy-efficient separation technologies. Even though Zeolite A is less catalytically active than high-silica zeolites like ZSM-5, it still has niche applications in catalysis, especially when modified with metal cations. In the industrial sector, zeolite A is widely used as a detergent builder, which serve as an environmentally friendly alternative to avoid harmful phosphates. Its ion-exchange capability enhances washing efficiency by binding hardness ions, which increases the cleaning power of surfactants.

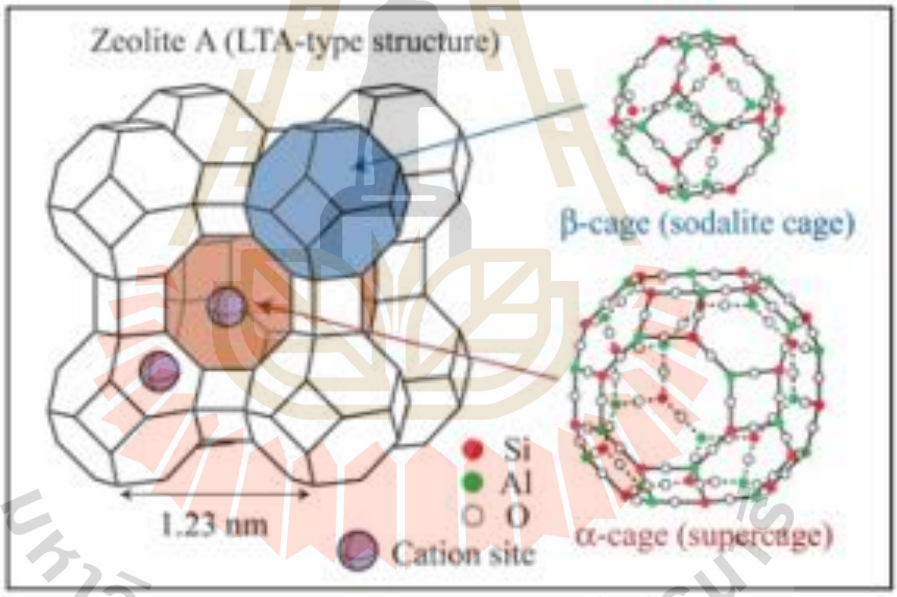

Figure 2.2 Features of the pores in zeolite A (IZA code LTA) (Petrov, 2012)

2.1.2 Zeolite properties

2.1.2.1 Zeolite as a catalyst

Table 2.2 illustrates the primary applications of zeolites as catalysts. Zeolites can be divided into three main categories: 1) Inorganic reactions,

2) Organic reactions, and 3) Hydrocarbon conversion. Zeolites exhibit several distinctive properties as catalysts, such as acidity, shape selectivity, high surface area, and structural stability. These characteristics will be discussed further in the following sections.

Table 2.2 Property of zeolites as a catalyst (Kianfar, 2020)

Inorganic reactions	Organic reactions	Hydrocarbon conversion
H_2S oxidation	Aromatisation (C4 hydrocarbons)	Allkylation
NO reduction of NH_3	Alkylation (naphthalene, benzene ethylbenzene, aniline, biphenyl, polyaromatics, etc.)	Cracking
CO oxidation, reduction	Aromatics (hydrogenation, oxidation, nitration, disproportionation, hydroalkylation, hydroxylation, oxyhalogenation, etc.)	Dehydration
Decomposition of H_2O	Chiral (enantioselective)	Fischer-Crafts alkylation
	Hydrogenation	Hydrocracking
	Cyclohexane (oxidation, isomerization, aromatization, ring opening)	Hydrogenation
		Dehydrogenation
		Hydrodealkylation
		Isomerization
		Methanol to gasoline
		Methanation
		Shape-selective reforming

2.1.2.2 Acidity and Basicity

Lewis acid is a species with electrons on its based that can be used for electron pairing. Brønsted states that acid-base contains protons, which appliable for transferring (H^+ ion) using acids as "proton donors" and bases as "proton acceptors." On solid surfaces, a Brønsted acid site can transfer a proton to an adsorbed molecule, while Lewis acid sites can accept electron pairs from those molecules. Besides, zeolites' acidity is primarily due to the presence of metal cations or hydroxyl protons in their extra-framework. In the case of aluminosilicate zeolites, the positive 4^+ charges on the silicon atoms in tetrahedral positions (T position) and the negative 2^- charges on the coordinating oxygen atoms result in neutral SiO_4 tetrahedra. Substitution of silicon atoms in the framework by aluminum atoms can change the corresponding tetrahedra charges from neutral to 1^-. These negative framework charges are balanced by extra-framework metal cations or hydroxyl protons, which form weak Lewis acid sites or strong Brønsted acid sites, respectively, and are responsible for the catalytic activity of the zeolite materials. Hydroxyl protons are found in zeolites, which are located on oxygen atoms that link silicon and aluminum atoms within the framework. Besides, the structural OH groups are referred to as Si-OH-Al groups (Figure 2.3a). Another hydroxyl group in zeolites is the silanol group (Si-OH), a terminal OH group found on the external surfaces of zeolite crystals (Figure 2.3b). The formation of these silanol groups results from dealumination of the zeolite framework via calcination, hydrothermal treatment, or strong-acid treatment. According to the specific treatment conditions, silicon migration, silanol group formation, and the generation of hydroxyl groups are correlated to an extra-framework aluminium (Figure 2.3c). In certain cases, dealumination results in the formation of Lewis acid sites at the extra-framework aluminium species and framework defects (Figure 2.3d). The proximity of these Lewis acid sites to bridging OH groups can generate superacidic Brønsted sites.

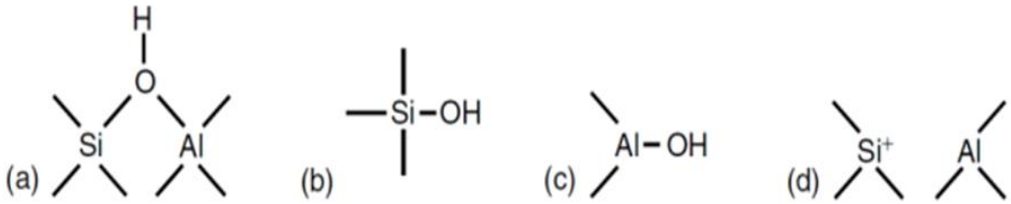

Figure 2.3 Different types of hydroxyl groups and acid sites in zeolites.
(Kianfar, 2020)

Despite the widespread use of acidic zeolites as solid catalysts in the chemical industry, relatively little attention has been given in the literature to their use as basic catalysts. These solid catalysts with basic properties have a considerable potential for several important industrial processes (e.g., Claus reaction). The nature of basic sites in zeolites is less well-defined than that of acid sites. The basic framework oxygen atoms or alkali metal cations in the zeolite framework contributes to their function as weak Lewis acid sites. The basicity of zeolites can be increased by modifying the framework's electronegativity or by incorporating basic components into their structure. Alkali-exchange of zeolites in aqueous solution or through solid-state ion exchange produces materials with basic framework oxygen atoms of relatively low base strength. Techniques such as IR spectroscopy, alkane cracking, UV-visible spectroscopy, temperature-programmed desorption of amines, microcalorimetry, and solid-state NMR spectroscopy have been used to quantify Brønsted and Lewis sites in solid-acid systems. However, these techniques do not readily distinguish between Lewis and Brønsted sites. Therefore, the combination of different characterization methods is often necessary to obtain comprehensive information.

2.1.2.3 Shape selectivity

Catalytic sites in zeolites can significantly affect reaction selectivity. Several classical concepts are valuable for catalyst designers in

understanding and predicting these influences. The size and shape of the pores, along with the properties of the reactants, determine whether molecules can be chemically activated at the active sites within the crystal structure. This phenomenon is referred to as reactant shape selectivity (RSS). When a mixture of product molecules desorbs from the intracrystalline active sites, the faster diffusing, "slimmer" molecules will be more prevalent, leading to a pseudothermodynamic equilibrium in the bulk phase. This effect is known as product diffusion shape selectivity (PDSS). Geometric constraints near the active site can hinder the formation of certain transition states, thereby affecting product selectivity. This phenomenon is known as transition-state shape selectivity (TSSS). Unlike other methods, crystallite-encapsulated sites are crucial for Reactive Selectivity and Product Distribution Selectivity (RSS and PDSS), while TSSS can also occur in half-open cages located at the ends of crystals. This phenomenon has primarily been observed in hydrocarbons and alkyl aromatics within medium-pore zeolites with 10-membered rings (10-MRs), and similar principles apply to functionalized organics and to different zeolite structures. The types of active sites extend beyond Bronsted acid sites; they also include metal and redox sites. This topic has been thoroughly reviewed in the literature. The application of these concepts implies that crystals can maintain compositional uniformity and that intracrystalline sites can display the same selectivity. It was initially suggested that factors such as pore size, tortuosity, and the pore structure defined by zeolite topology play significant roles in shaping the intrazeolitic fields and gradients. These factors, in turn, influence the rates of primary and secondary reactions and the overall selectivity. More recently, the impact of confinement on various kinetic and thermodynamic processes has been highlighted, shedding light on its effects on adsorption and diffusion. Configurational-bias Monte Carlo methods have enabled the simulation of slowly diffusing molecules confined within cages or adsorption sites in zeolite structures. This approach, which involves mapping the free-energy landscape in the intracrystalline space, overlooks the effects of local differences in site architecture or concentration on reaction selectivity. To account for several unexpected shape-selectivity phenomena observed

in long-alkane hydroconversion, the term inverse shape selectivity was coined. In zeolite pore widths of 0.65–0.74 nm, the opposite was encountered, that is, preferential formation of branched over linear hydrocarbons, viz., the formation of high yields of di-branched from n-alkanes over 10-MR zeolites like AFI (SAPO-5), the phenomenon being confirmed by adsorption experiments. The molecular basis of such effects has been attributed to purely entropic effects in monodimensional pores at high pressures, where smaller pores expel larger molecules. Several shape-selective phenomena were attributed to topology-dependent structural sites. Such nest effects resulted from tuning the curved catalyst surface to the configuration of adsorbed species, with entropic effects governing the fitting. A distinction has been established between two types of extra-framework catalysis, primarily in ZSM-22 (TON), namely pore-mouth and keylock selective catalysis. Alkanes can undergo hydroconversion to yield products that cannot be formed within or desorbed from the zeolite structure. The prevalent formation of specific molecules, such as 2-methylbranched alkanes from n-alkanes, has been attributed to transformation at a single pore mouth. In contrast, compounds like 2,4-dimethyloctane from n-decane are generated at adjacent pore mouths, with their selectivity influenced by both chain length and molecular topology.

Shape-selective catalysis varies based on the different dimensions of reactants, products, or intermediate molecules, and the pore size. Molecules with dimensions less than a critical size can enter the pores and react on the internal catalytic sites. However, molecules can leave the pores in the final product. Thus, shape-selective catalysis can be utilized to enhance the yield of desired products and prevent undesired products formation. Besides, shape selectivity is influenced by the pore-size constraints that govern the entry of reactant molecules, the diffusion or removal of product molecules from the pores, and the formation of specific transition states. These three factors may overlap, including:

1) Reactant selectivity

2) Product selectivity

3) Restricted transition state selectivity

Reactant selectivity is the ability to push material molecules pass through the zeolites' pores, while excluding larger molecules compared to pores size. In other words, only starting materials with specific sizes and shapes can penetrate the zeolite pores (see Figure 2.4a). This characteristic of zeolites is often described as a "molecular sieve." Table 2.3 compares kinetic molecular diameters of reagents with the pore openings of different zeolites. The analysis provides useful guidance for selecting an appropriate zeolite for a given starting material. However, the kinetic diameter offers only an approximate measure of molecular size, as molecules are not rigid structures. An example of reactant selectivity in zeolites is the dehydration of butanol over the CaA zeolite. The straight-chain alcohol is dehydrated much more quickly compared to iso-butanol, which has a larger molecular diameter. Product selectivity in zeolites occurs when the size of the molecule formed inside the pores is too large to diffuse out. Well-known examples of product selectivity in zeolites include the methylation of toluene and the disproportionation of toluene over the ZSM-5 zeolite. In both cases, all three isomers, including ortho, meta-, and para-xylene, are generated within the pores. Although the thermodynamic equilibrium corresponds to a p-xylene fraction (as the desired product) of only 24%, it can be obtained with a selectivity of more than 90%. This is because p-xylene has smaller dimensions and a diffusion rate that is 104 times faster than that of the other two isomers. In other words, although all isomers form relatively quickly within the zeolite cavity, p-xylene diffuses out of the cavity at a much faster rate.

Table 2.3 Pore sizes of zeolites and molecule diameters (Kianfar, 2020)

Zeolite	Pore size (Å)	Molecule	Kinetic diameter (Å)
KA	3.0	He	2.5
SAPO-34	3.8	NH_3	2.6
NaA	4.1	H_2O	2.8
CaA	5.0	N_2, SO_2	3.6
Erionite	3.8 x 5.2	Propane	4.3
ZSM-5	5.3 x 5.6	n-Hexane	4.9
Beta	5.6	Isobutane	5.0
CaX	6.9	Benzene	5.3
Mordenite	6.7-7.0	p-Xylene	5.7
NaX	7.4	CCL_4	5.9
AlPO-5	7.3	Cyclohexane	6.2
VPI-5	12.7	o-, m-Xylene	6.3

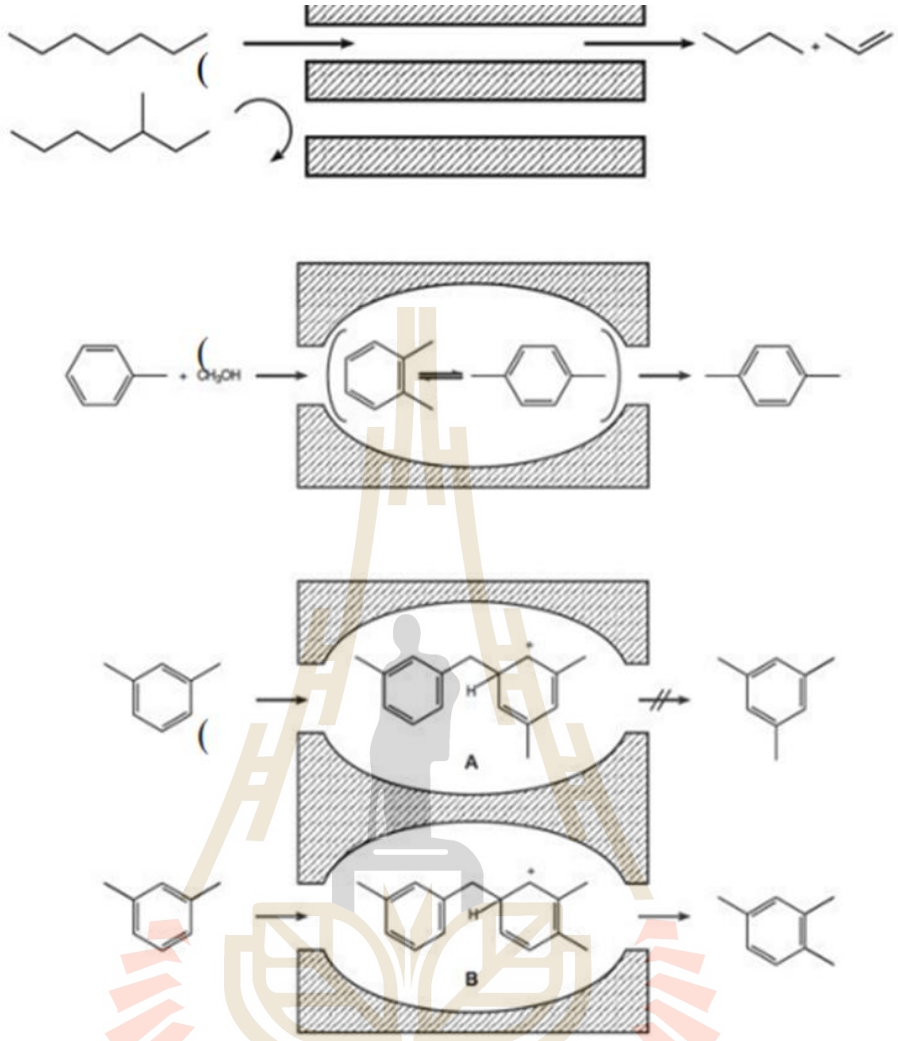

Figure 2.4 Shape selectivity of zeolites with examples of reactions: (Kianfar, 2020)

a) Reactant selectivity: cleavage of hydrocarbons,

b) Product selectivity: methylation of toluene

Since the Restricted transition-state selectivity depends on the available space within the zeolite's cavities or pores, the chemical reaction pathway is altered because specific reactions are prevented by the lack of space required for their corresponding transition states. Thus, intermediates with a geometrical fit to the zeolite

cavities can be formed during catalysis, and reactions that require smaller transition states can proceed with no hindrance. In practice, it is often difficult to distinguish between product selectivity and restricted transition state selectivity. Alkylation of benzene with ethylene over ZSM-5 to produce ethylbenzene exemplifies restricted transition-state selectivity. By limiting competing side reactions, the process can achieve high selectivity toward ethylbenzene.

2.1.2.4 Adsorption of zeolite

Zeolites are crystalline aluminosilicate minerals characterized by a highly ordered microporous framework consisting of interconnected channels and cavities. This unique structure endows them with exceptional adsorption properties, making them widely used in environmental remediation, gas separation, and catalysis. The adsorption behavior of zeolites arises primarily from their uniform pore size distribution, high surface area, cation-exchange capacity, and tunable hydrophilic/hydrophobic character. The adsorption capacity of zeolites is closely linked to their crystalline framework. The presence of tetrahedrally coordinated Si and Al atoms, connected via oxygen bridges, generates a negatively charged lattice that is balanced by the presence of extra-framework cations, such as Na^{+}, Ca^{2+}, or K^{+}. These cations not only stabilize the framework but also act as active sites for adsorption through ion-dipole interactions. The pore sizes of zeolites (typically ranging from 3 to 10 Å) provide molecular sieving ability, enabling selective adsorption of molecules based on size and shape. The structure of zeolites is made up of silicon-oxygen and aluminum-oxygen tetrahedra linked together by oxygen atoms. Zeolites can be classified based on their SiO_2/Al_2O_3 ratio into three categories: low siliceous zeolites (Si/Al mole ratio = 1–2), medium siliceous zeolites (Si/Al mole ratio = 3–10), and high siliceous zeolites (Si/Al mole ratio = 10^{+}). Low siliceous zeolites contain a high amount of AlO_4 units and Si–O–Al bonds, while high siliceous zeolites contain a lower amount. The Al–O bond consists of approximately 40% covalent and 60% ionic characteristics, whereas the Si–O bond is covalent. As a result, the Si–O–Al bond is much more polar

compared to the Si–O–Si bond. Highly polar water molecules (H_2O) interact more strongly with polar surfaces or groups than with relatively nonpolar ones. Therefore, the zeolites with a low SiO_2/Al_2O_3 ratio are generally more hydrophilic than those with a high SiO_2/Al_2O_3 ratio. Some typical zeolites with different types, Si/Al mole ratios, and water vapor adsorptions. The amount of water adsorbed on zeolites is strongly dependent upon the Si/Al ratio. In addition, there is little difference in water vapor adsorption between zeolite 3A and zeolite 13X with a similar Si/Al ratio, which indicates that water vapor adsorption (hydrophilicity) of zeolite is highly correlated with the Si/Al ratio rather than the zeolite type. For gas adsorption, zeolites have been widely studied for their gas adsorption capabilities such as CO_2, CH_4, and N_2. Studies have shown that zeolite A and zeolite X exhibit high selectivity for CO_2 due to their quadrupole moment and strong electrostatic interaction with the cations within the zeolite pores (Helfferich, 1985). The adsorption equilibrium and kinetics are influenced by the framework composition (Si/Al ratio) and the type of cation. For instance, NaA zeolite demonstrates superior CO_2 adsorption compared to CaA due to stronger interactions between CO_2 molecules and Na^+ sites. Beyond gas adsorption, zeolites are highly effective in adsorbing organic molecules such as dyes, phenols, and pesticides from aqueous media. The hydrophilic nature of low-silica zeolites favors the adsorption of polar molecules, while high-silica zeolites exhibit hydrophobicity, making them suitable for the removal of non-polar organic contaminants (S. Wang & Peng, 2010). For example, zeolite Y and ZSM-5 have been successfully applied in the removal of volatile organic compounds (VOCs). In contrast, zeolite A has demonstrated a strong affinity for methylene blue dye adsorption in wastewater treatment. Moreover, zeolites possess a significant ion-exchange capacity, which enhances their ability to adsorb heavy metal ions, such as Pb^{2+}, Cd^{2+}, and Cu^{2+}, from water. Natural zeolites, particularly clinoptilolite, have been widely studied for their application in water purification due to their low cost and high selectivity for divalent cations (Mumpton, 1999). The efficiency of adsorption depends different cation present types, the solution pH, and

the presence of competing ions. Surface modification of zeolites using surfactants or functional groups can further improve their affinity for specific pollutants.

Factors Affecting Adsorption Performance

1) Si/Al ratio: A Low Si/Al ratio can increase cation density, enhancing hydrophilicity and ion-exchange capacity, while a high Si/Al ratio improves hydrophobicity and thermal stability.

2) Cation type and exchange: Different cations alter the electrostatic field within the zeolite pores, thereby affecting adsorption affinity and selectivity.

3) Temperature and pressure: Adsorption of gases generally decreases with increasing temperature but increases with pressure.

4) Surface modification: Functionalization with organics or impregnation with metals enhances adsorption specificity toward target pollutants.

2.1.2.5 Modification of zeolites

The structure and composition of zeolites can be customized for specific applications through two main approaches: (1) Direct synthesis and (2) Post-synthetic treatment and modification. Direct synthesis is the primary method used to create zeolites. Several factors significantly influence the zeolite structure, including the composition of the synthesis mixture, synthesis temperature, reaction time, solution pH, aging and seeding conditions, as well as the directing agent or template used. However, in many cases, direct synthesis does not yield zeolites with the desired properties for their intended applications. To overcome this limitation, post-synthetic treatments such as ion exchange, the preparation of metal-supported zeolites, dealumination, the reinsertion of heteroatoms (such as boron, gallium, germanium, or aluminum) into the zeolite framework, and other modification methods offer practical alternatives to adjust zeolites for improved framework compositions and other properties. For instance, in the catalytic cracking process using HY zeolite, it is essential

to have strong acid activity along with high thermal and hydrothermal stability. It is well established that a higher SiO_2/Al_2O_3 ratio contributes to greater stability of the zeolite structure. However, few zeolites can be prepared using SiO_2/Al_2O_3 ratio through direct synthesis and this ratio is limited to a maximum value of around six. Dealumination in this case is a useful way to increase the SiO_2/Al_2O_3 ratio. Three dealumination methods have been used to produce the desired properties

1) Hydrothermal treatment (e.g., steaming).

2) Chemical treatment (e.g., reaction with EDTA, $(NH_4)2SiF_6$, $SiCl_4$, F_2 gas)

3) Combination of hydrothermal and chemical treatment (e.g., treatment with HCl, HNO_3, NaOH, KF).

The Si/Al ratio is important since the catalytic activity of a zeolite depends on the number of acidic hydroxyl (OH) groups associated with aluminum in its framework. This ratio directly influences the formation of carbonium or carbenium ions within the zeolite. Dealumination can improve the porous structure and enhance several important properties of zeolites, such as acidity, catalytic activity, thermal and hydrothermal stability, resistance to aging, and coking. However, excessive dealumination can reduce zeolite crystallinity. While dealumination is typically expected to lower zeolite catalytic activity, in some cases, if the increase in acid strength outweighs the decrease in acidic centers, dealumination can enhance catalytic activity. The increase in the acidity of hydroxyl (OH) groups is due to their interaction with aluminum species that have been displaced from the framework and are left within the cavities of the zeolite. The aluminosilicate structure of zeolites consists of ionic components, including Si^{4+}, $Al^{3+,}$ and O^{2-} ions. When Al^{3+} ions replace some Si^{4+} ions in the SiO_4 tetrahedra of the zeolite framework, this leads to the creation of an excess negative charge. To neutralize this negative charge, a compensating source of positive charge, in the form of cations, must be added. These non-framework cations

are crucial to determining the zeolite's catalytic properties. One method to incorporate cations into the zeolite is to use an aqueous salt solution, which allows the cations to enter the zeolite. Another method involves solid-state reactions between zeolites and cationic compounds intended to enter the porous structure. This approach offers several advantages over traditional liquid-phase ion-exchange processes as follow:

1) Prevention of handling large volumes of salt solutions

2) Less generation of waste salt solution

3) Introducing metal cations into narrow pore cavities where the ion exchange in aqueous solutions is not efficient.

2.1.3 Zeolite application

2.1.3.1 Microporous materials

Zeolites are crystalline aluminosilicates with three-dimensional framework of interconnected channels and cavities within the microporous range (< 2 nm). This structural feature provides them with high surface area, ion-exchange capacity, and molecular sieving ability, enabling selective adsorption and separation of molecules. Consequently, zeolites have become indispensable materials in industrial, environmental, and biomedical applications (Corma, 1997). One of the most prominent uses of zeolites is in gas separation and purification. Their uniform pore system allows them to differentiate molecules based on size and polarity. Zeolite A, in particular, possesses pore openings of approximately 0.41 nm, making it suitable for separating oxygen (kinetic diameter 0.346 nm) from nitrogen (0.364 nm). This property is utilized in pressure swing adsorption (PSA) oxygen concentrators, where nitrogen is preferentially adsorbed within the pores of the zeolite, resulting in an oxygen-enriched effluent. The efficiency and performance of such systems depend strongly on the crystallinity, purity, and adsorption capacity of the zeolite used. In addition to medical oxygen generation, zeolites are widely applied as heterogeneous catalysts in

petroleum refining and petrochemical industries, where they facilitate processes such as fluid catalytic cracking, isomerization, and hydrocracking. Their high thermal stability and shape-selective catalysis enable efficient conversion of hydrocarbons into fuels and valuable intermediates (Corma, 1995; Degnan, 2003). Zeolites also play a significant role in environmental protection and remediation. Due to their ion-exchange properties, they are utilized for water softening, removing heavy metals, and treating wastewater. Their strong adsorption capacity for gases such as CO, NH_3, and volatile organic compounds (VOCs) makes them effective in air purification and greenhouse gas mitigation (Mumpton, 1999; S. Wang & Peng, 2010). Additionally, zeolites are used as drying agents, odor absorbers, and carriers for fertilizers in agricultural applications. In the context of this thesis, the primary application of zeolite as a microporous material lies in the synthesis of Zeolite A for oxygen concentrators. Utilizing natural raw materials such as ball clay for zeolite synthesis provides a cost-effective and sustainable route for producing adsorbents that meet the growing demand for medical oxygen. This highlights the importance of zeolite's microporous framework in enabling selective adsorption processes, particularly in life-saving technologies such as PSA oxygen concentrators.

2.1.3.2 Applications of Zeolite A in Agriculture

Zeolite A has found increasing applications in agriculture because of its capability in high cation exchange, water retention ability, and environmental compatibility. While naturally occurring zeolites such as clinoptilolite are more commonly utilized, synthetic zeolite A has demonstrated comparable performance in improving soil quality, enhancing nutrient efficiency, and promoting sustainable agricultural practices (Reháková et al., 2004). One of the key agricultural applications of zeolite A is its use as a soil amendment. The porous framework of zeolite A enables high water absorption and slow release, which improves soil moisture retention in arid and semi-arid regions. This property has been particularly beneficial in countries with water scarcity, such as parts of the Middle East and Africa, where

zeolites have been applied to mitigate drought stress in crops (Karaca, 2004). Additionally, zeolite A acts as an ion exchanger, which can reduce the leaching of ammonium, potassium, and calcium, from the soil. By holding cations within its structure and releasing them gradually, zeolite A enhances fertilizer efficiency and reduces the need for repeated applications. Studies from Asia and Europe have reported that zeolite amendments improve nitrogen-use efficiency in rice and maize cultivation, thereby increasing yields while lowering fertilizer costs (Bansiwal et al., 2006; Leggo, 2000). Zeolite A has also been applied in animal husbandry and waste management. When incorporated into animal feed, it helps in binding excess ammonium ions, reducing odor emissions, and improving animal health. In regions with intensive livestock production, such as Europe and North America, zeolite A has been utilized to treat manure and control ammonia emissions, thereby contributing to environmental sustainability. Globally, the use of zeolite A in agriculture reflects its role as a multifunctional material for sustainable farming practices. Its contributions to soil improvement, fertilizer efficiency, water conservation, and waste treatment align with current global priorities in achieving food security and reducing environmental impacts. The potential for large-scale application of zeolite A, particularly when synthesized from inexpensive raw materials such as clays, further highlights its relevance for both developed and developing countries.

2.1.3.3 Applications of Zeolite A in Medicine

Zeolite A has attracted significant attention in the medical field due to its ion-exchange capability, adsorption capability, and biocompatibility. Its unique structure enables selective adsorption of ions and molecules, making it highly suitable for biomedical and pharmaceutical applications. One of the most prominent applications of zeolite A in medicine is as a drug delivery carrier. The porous structure allows for the encapsulation of therapeutic molecules, providing controlled release and enhanced bioavailability. For instance, zeolite-based systems have been used for the sustained release of antibiotics and anticancer drugs, where the zeolite framework

protects the drug from degradation and ensures targeted delivery. Zeolite A has also been reported to exhibit detoxifying effects within biological systems. Its ion-exchange properties have the capabilities to remove toxic from heavy metals and ammonium ions from the body, making it useful in therapies aimed at detoxification. Additionally, the high surface area and negative charge of zeolite A facilitate adsorption of harmful metabolites and pathogens, supporting its use as a dietary supplement in human and veterinary medicine. In wound healing and tissue regeneration, zeolite A has demonstrated potential as an antimicrobial and hemostatic agent. Studies have shown that zeolite-containing dressings can accelerate blood clotting by activating the coagulation cascade and simultaneously reducing infection risks through microbial adsorption. This dual functionality positions zeolite A as a valuable material in surgical and emergency medicine. Furthermore, zeolite A is being investigated for cancer therapy. Its adsorption properties may reduce oxidative stress and limit the proliferation of tumor cells. Some studies suggest that zeolite can enhance immune response and improve the efficacy of conventional cancer treatments (Pavelić et al., 2001). Although more clinical evidence is needed, these findings highlight its potential role in complementary oncology. Overall, the applications of zeolite A in medicine underscore its versatility as a biocompatible microporous material. Its roles in drug delivery, detoxification, antimicrobial activity, and tissue engineering continue to be the focus of research, contributing to the development of novel medical technologies.

2.1.3.4 Applications for industry

Since 2010, research has increasingly focused on using zeolite A as a supplementary cementitious material (SCM) to enhance the durability and sustainability of concrete. A key benefit is its pozzolanic activity, where it reacts with calcium hydroxide ($Ca(OH)_2$) to form calcium silicate hydrate (C-S-H) gel, which enhance the concrete matrix (Alexa-Stratulat et al., 2023). This densification leads to several improvements, for example, enhanced mechanical properties. Studies have shown that the addition of zeolite A can significantly improve the compressive strength and

flexural strength of mortars and concrete by refining the pore structure. Improved durability, achieved by using zeolite A, helps mitigate the harmful alkali-aggregate reaction (AAR), a major cause of concrete degradation, by consuming the free alkalis. Utilizing zeolite A as a partial substitute for Portland cement enhances environmental sustainability by reducing overall cement content, which consequently lowers the carbon footprint associated with concrete production. These recent findings solidify the role of zeolite A as a promising and eco-friendly additive for modern construction.

Zeolite A's unique molecular sieve properties and tunable acidity have made it a subject of extensive research in the catalyst industry since 2010. Its small pore size allows for shape-selective catalysis, controlling which molecules can enter and react within its framework.

Recent literature focuses on zeolite A's applications as both a catalyst and a catalyst support:

Catalyst Support: It serves as an excellent support for metal nanoparticles, preventing them from clumping and deactivating. This makes it a popular choice for reactions, including the selective catalytic reduction (SCR) of nitrogen oxides (NOx) from vehicle emissions (Cho et al., 2017).

Hydrogen Production and CO_2 Conversion: Zeolite-supported transition metal catalysts are being explored for hydrogen-related reactions and for the conversion of CO_2 to valuable products, addressing key challenges in clean energy (M. Liu et al., 2024).

Biomass Conversion: Researchers are utilizing zeolites to convert biomass into green fuels and high-value chemicals, a crucial step toward sustainable chemistry (Qazi et al., 2022)

2.1.3.5 Adsorption of Harmful Substances

Zeolites, crystalline aluminosilicates with a three-dimensional framework are widely studied due to their exceptional adsorption capabilities. Their unique pore architecture, high specific surface area, and ion-exchange properties make them highly effective in capturing and immobilizing harmful substances from air, water, and industrial effluents. Over the past decades, researchers have investigated natural and synthetic zeolites as adsorbents for heavy metals, dyes, organic pollutants, and toxic gases, demonstrating their versatility in environmental remediation. Zeolites possess uniform micropores (0.3–1 nm), which provide selective adsorption sites for molecules of compatible size. The negatively charged aluminosilicate framework, balanced by exchangeable cations (Na^+, K^+, Ca^{2+}), enhances their affinity toward polar and ionic species. The hydrophilic or hydrophobic nature of a zeolite depends on its Si/Al ratio, which in turn influences its adsorption capacity for water, organic compounds, and heavy metals. High thermal and chemical stability further enables their application in diverse adsorption processes. One of the most extensively studied applications of zeolites is the removal of toxic heavy metals from aqueous systems. Studies have demonstrated that clinoptilolite, a natural zeolite, effectively adsorbs Pb^{2+}, Cd^{2+}, Cu^{2+}, and Zn^{2+} ions through ion-exchange mechanisms. For instance, Wang and Peng (S. Wang & Peng, 2010) reported that zeolite-based adsorbents exhibit high selectivity toward lead ions due to their ionic radius compatibility with the zeolitic channels. Modified zeolites, such as those treated with surfactants or impregnated with iron oxides, have shown improved removal efficiency for arsenic and chromium species, highlighting the importance of surface modification in enhancing adsorption capacity. Zeolites also demonstrate potential in eliminating organic pollutants, including synthetic dyes, phenols, and pharmaceutical residues. Their adsorption mechanisms often involve hydrophobic interactions, electrostatic attraction, and molecular sieving effects. Studies indicate that high-silica zeolites, such as ZSM-5, exhibit a strong affinity for volatile organic compounds (VOCs) and aromatic

hydrocarbons due to their hydrophobic pore surfaces. In the textile industry, zeolite-based adsorbents have been explored for treating dye-contaminated wastewater, with surface-modified zeolites demonstrating enhanced uptake of both cationic and anionic dyes. Beyond water treatment, zeolites play a critical role in capturing harmful gases. Zeolites 13X and 5A are widely used for removing CO_2, SO_2, and NOx from flue gases. Their well-defined pore sizes and strong interactions with polar molecules enable selective adsorption even in mixed-gas environments. Furthermore, zeolites play a crucial role in pressure swing adsorption (PSA) systems for purifying air and natural gas. Recent studies have also highlighted their role in capturing ammonia and hydrogen sulfide, demonstrating their contribution to controlling industrial air pollutants.

2.1.3.6 Zeolite molecular sieve

The year 1979 marked the twenty-fifth anniversary of the commercial introduction of molecular sieve zeolites as a new class of industrial materials. These materials were first introduced in late 1954 as adsorbents for industrial separations and purifications. Since then, the interest in and appreciation for this unique class of materials have led to a substantial amount of scientific literature. To date, there are over 15,000 scientific articles and more than 10,000 issued patents dedicated to their synthesis, properties, structure, and applications. The molecular sieve industry is projected to have grown into an estimated quarter of a billion-dollar market, serving all major segments of the chemical process industries, including significant applications in the petroleum refining and petrochemical industries. It has generated a myriad of other adsorption, catalytic, and recent ion exchange applications. In 1967, Milton examined the origins and advancement of molecular sieve zeolites. Milton states that the initial findings and synthesis of new zeolites A, X, and Y, which subsequently led to their use in various commercial roles as selective adsorbents and catalysts. This study will discuss the progression of molecular sieve materials, including their synthesis, properties, and applications from 1954 to 1979, focusing on significant milestones and trends in these areas. It will not attempt to

replicate the comprehensive studies of zeolite molecular sieves by Breck or Barrer, nor the latest review articles on the use of molecular-sieve zeolites as adsorbents, catalysts, and ion exchangers, or on the applications of natural zeolites. The success of molecular sieve zeolites discovers new materials whose properties have been engineered to enhance existing processes and support the development of new ones. The application of molecular sieve zeolite adsorbents for various separations and purifications has become well established in the chemical process industries. Purification applications generally rely on surface selectivity for polar or polarizable molecules, such as water, CO_2, or sulfur compounds, as well as bulk separations based on molecular sieving principles. For instance, pressure swing adsorption in air separation was initially conceptualized by Milton as a molecular sieving operation based on the sizing difference between oxygen and nitrogen molecules. Also, the strong specific interaction between nitrogen's molecular quadrupole and the cation, with purification applications involving molecular sieving, where the selection of the zeolite adsorbent is determined by pore size, is designed to exclude potentially co-adsorbed molecules. For example, using type 3A molecular sieve for drying cracked gas effectively prevents the co-adsorption of ethylene and heavier unsaturated hydrocarbons. The unique structure of zeolite creates a system of uniform micropores and channels that can selectively adsorb molecules based on size, polarity, and shape. Due to their highly ordered pore system, zeolites are commonly referred to as molecular sieves, with pore sizes typically ranging from 3 to 10 Å, making them suitable for separating and adsorbing small gas molecules, such as nitrogen, oxygen, and carbon dioxide. The ion-exchange capacity of zeolites, resulting from the substitution of Si^{4+} by Al^{3+} in the framework, further enhances their adsorption and catalytic properties (Jha & Singh, 2016). This feature has led to their extensive use in industrial applications, including gas separation, purification, catalysis, and environmental remediation. In gas separation technologies, molecular sieves play a central role in processes such as pressure swing adsorption (PSA), where zeolites, particularly zeolite 5A and 13X, are employed to selectively adsorb nitrogen and enrich oxygen in medical and industrial

oxygen concentrators (Sircar, 2002). Moreover, the selectivity of zeolite molecular sieves can be tailored by adjusting the Si/Al ratio, framework topology, and cation-exchange properties, making them versatile materials for advanced applications. The stability, regenerability, and environmental compatibility of zeolite molecular sieves have positioned them as a key class of microporous materials in both traditional and emerging technologies.

2.2 Zeolite synthesis method

Zeolites can be synthesized from a variety of raw materials, both mineral and man-made. However, not all raw materials are economically viable for zeolite synthesis. Therefore, suitable raw materials should possess specific properties: they must be inexpensive, readily available, have low production costs, be selective in their reactions, yield high production levels, and contain minimal foreign substances. To date, several physicochemical and solvothermal methods have been adopted and developed to produce synthetic zeolites. This includes the hydrothermal method (Sugano et al., 2005), the alkali-fusion method, the sol-gel method, and the alkali-leaching method (Shoppert et al., 2017). The choice of synthesis method depends on the specific type of zeolite to be produced, as each technique has its own advantages and limitations.

2.2.1 Hydrothermal method

The hydrothermal technique is considered the primary method for synthesizing zeolites. This approach is essentially solvothermal, where water serves as a solvent and a base act as a mineralizer at varying temperatures and pressures. Conventionally, hydrothermal synthesis needs to use a sealed vessel usually made of polypropylene and Teflon-lined (PTFE) steel autoclave (Sangeetha & Baskar, 2016). Since the hydrothermal method requires lower temperature, this method is straightforward and more cost-effective. Zeolites are typically synthesized via a

hydrothermal approach (Cundy & Cox, 2003b) due to different advantages agreed by many researchers, which include low energy consumption, high reactivity of reactants, ease of maintenance over the solution, reduced air pollution, formation of metastable phases, and unique condensed phases. Numerous factors can influence the performance of hydrothermal methods, including temperature and pressure, batch composition, silica-to-aluminum ratio, reactant materials, overall alkalinity, aging time, template conditions, and seeding (Johnson & Arshad, 2014). To date, numerous attempts have been made to synthesize zeolites using the traditional hydrothermal technique. For instance, Wang et al. demonstrated the creation of synthetic zeolite (ZSM-5) from expanded perlite (or kaolin) through this method (P. Wang et al., 2007). Another research team successfully developed various hierarchical zeolite structures (BEA, LTA, FAU) using the conventional hydrothermal process (H. Chen et al., 2011). However, recent advancements have been made in this methodology. For example, Yao et al. produced Zeolite X powder from diatomite rich in silica and alumina using an eco-friendly and simplified hydrothermal approach (Yao et al., 2018). This Zeolite X shows significant promise for applications in industry, catalysis, and adsorption technology. Additionally, many researchers have reported the synthesis of zeolite A from aluminoborosilicate glass utilizing a hydrothermal method, with acid treatment applied beforehand to enhance the formation of a single-phase zeolite A with high crystallinity. There have also been efforts to produce zeolite A from municipal waste, an economical option with a higher alumina content (Terzano et al., 2015). Moreover, zeolite K–F was synthesized from recycled amber container glass using a one-pot hydrothermal technique (Taylor et al., 2020). The advantages of this process are that it does not require pre-treatment for the activation or the removal of hazardous components. However, the conventional hydrothermal method does not satisfy the severe terms of sustainability, as it uses structural directing agents that directly integrate and fill the pore volume of synthesized zeolites, which must be removed by high-temperature combustion. Therefore, there is a significant risk of hazardous and greenhouse gas emissions impacted by high-temperature combustion. Moreover, the

generation of high autogenous pressure in the (PTFE) lined steel autoclave, caused by heating the reaction mixture, can pose a severe threat to the equipment. Also, the conventional hydrothermal synthesis approach is often viewed as a high-energy-consuming method because it takes an extended time (1–20 days) to achieve final production. In the conventional hydrothermal method, controlling nucleation is difficult due to slow mixing hence, while uncontrollable nucleation leads to the formation of larger crystal sizes (Li et al., 2006). An agitator is often used to address issues, but it primarily promotes the movement of macroscopic layers. As a result, the mixing within these layers relies on the slow diffusion of reactant molecules. To enhance the the conventional hydrothermal strategy for zeolite synthesis, researchers have developed various sustainable methods. These include the microwave-assisted hydrothermal method, the alkali-fused hydrothermal method, the microwave-digested alkali-fusion-assisted hydrothermal method, and the ultrasound-assisted hydrothermal method. The microwave-assisted synthesis method is noted for its unique "microwave effects." Katsuki et al. (Katsuki et al., 2005) emphasized the synthesis of zeolites using microwave heating can significantly reduce the zeolite production time compared to traditional hydrothermal methods. They recognized that employing microwave heating throughout the synthesis can effectively shorten reaction time. For instance, NaY zeolite was synthesized by microwave heating in 10-15 minutes, yielding high crystallinity and purity. However, synthesizing zeolites from waste raw materials results in multiphase products and requires an extended process. Therefore, alkali fusion before hydrothermal treatment can reduce synthesis time and prevent the formation of inert multiphases (Bukhari et al., 2015). Several attempts have been made to synthesize zeolite using the alkali-assisted hydrothermal method. For example, the synthesis of zeolite X has also been carried out using a low-grade bauxite raw material through a two-step synthesis method. Meanwhile, Belviso et al. (Belviso et al., 2017) explored the use of clay minerals to synthesize various types of synthetic zeolites, including sodalite, faujasite, and A-type zeolite. They employed an alkaline hydrothermal method along with pre-alkali fusion, which could be done with or

without adding alumina. Additionally, they noted that industrial waste, specifically bauxite tailings, has been utilized for the synthesis of zeolite X. Other raw materials, such as waste perlite dust, fly ash, and steel slag, have also been used to synthesize faujasite, zeolite Y, and zeolite X through hydrothermal methods. It is important to note that the alkali fusion method requires high temperatures, exceeding 800°C. To reach a higher temperature within a short period, researchers have integrated a microwave heating system into the alkali fusion hydrothermal method. Mason and Peters described a method involving fusion pretreatment and microwave-assisted hydrothermal processes to create zeolite from fly ash generated by municipal solid waste incineration (MSWI). The fusion pretreatment transformed quartz into an amorphous state, allowing it to dissolve easily in a hydrothermal solution, thus speeding up the zeolite production process. Despite its drawbacks, the hydrothermal method holds significant promise for generating faujasite, X, Y, and ZSM-5-type zeolites tailored for specific uses. In conclusion, the hydrothermal synthesis of zeolites shows considerable potential, providing various advantages.

2.2.2 Sol-gel method

The sol–gel method is a physicochemical technique in which an inorganic colloidal suspension, or "sol," undergoes structural evolution to form a three-dimensional gel network within a continuous liquid phase, as illustrated in Figure 2.5 This process effectively facilitates the transition of a liquid solution into a solid gel. One of its key benefits is the enhanced control it provides, resulting in increased porosity and specific particle sizes. Several factors can affect the effectiveness of the sol-gel process, including (i) the rate of hydrolysis, (ii) temperature, and (iii) the rate of heating, and (iv) pH. There are many reports on this method. For example, Wu et al. (Wu et al., 2009) reported a two-step sol-gel route for the synthesis of MCM-22 zeolite regarding static hydrothermal conditions using the silica source from tetraethyl orthosilicate. Phiriyawirut et al. (Phiriyawirut et al., 2003) synthesized the MFI zeolite directly from the silatrane. The reaction temperature was varied using microwave

heating. They reported that a long aging time is more critical to achieve high crystallinity. Sathupunya et al. (Sathupunya et al., 2002) illustrated the synthesis of analcime (ANA) and gismondine-type (GIS) zeolites directly from the precursor of alumatrane and silatrane. This technique together with the microwave-assisted method and does not require specialized and expensive equipment. This method delivers high-quality, homogeneous product through molecular-level mixing. Besides various advantages, there are some limitations, such as the cost of precursors, which need to be overcome in the future.

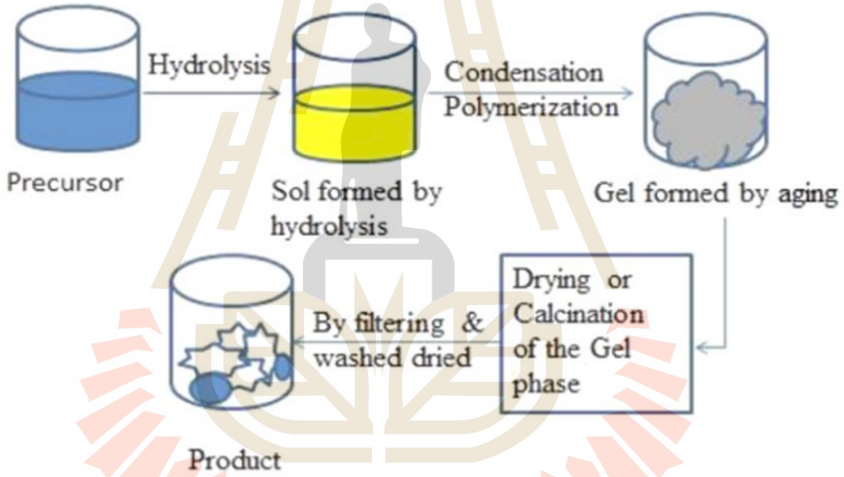

Figure 2.5 Sol-gel method for the synthesis of zeolite. (Khaleque et al., 2020)

2.2.3 Microwave method

Microwave heating is a fast, energy-efficient technique for synthesizing zeolites by applying microwave radiation. Microwaves act as high-frequency electric fields that ultimately generate heat to drive the reaction. Therefore, the energy can transfer from the microwave to the reactant material through resonance or relaxation. There are many advantages of using microwave methods. For example, it gives concise

time, which leads to small particle size and high-purity zeolite can be obtained (Fig 2.6). Factors that affect the microwave method are (i) SiO_2/Al_2O_3 molar ratio (Si/Al), (ii) alkalinity, (iii) wavelength produced from the magnetron, (iv) zeolization time and temperature, (v) crystallization time and temperature. In most cases, microwave-assisted synthesis of zeolites is combined with other methods, such as hydrothermal, solvothermal, and ionothermal methods. For example, Kim et al. used microwave irradiation to synthesize synthetic zeolite beta in fluoride media. In their experiment, they demonstrated that fluoride mineralization under microwave irradiation and seeding reduced particle size by increasing nucleation (Kim et al., 2004). Recently, a rapid microwave-heating method was developed for the liquid-phase synthesis of Y-type zeolite at high temperatures. The effects of microwave heating temperature, crystallization time, and silica-to-alumina ratio on the synthesis of Y-type zeolite are systematically investigated.

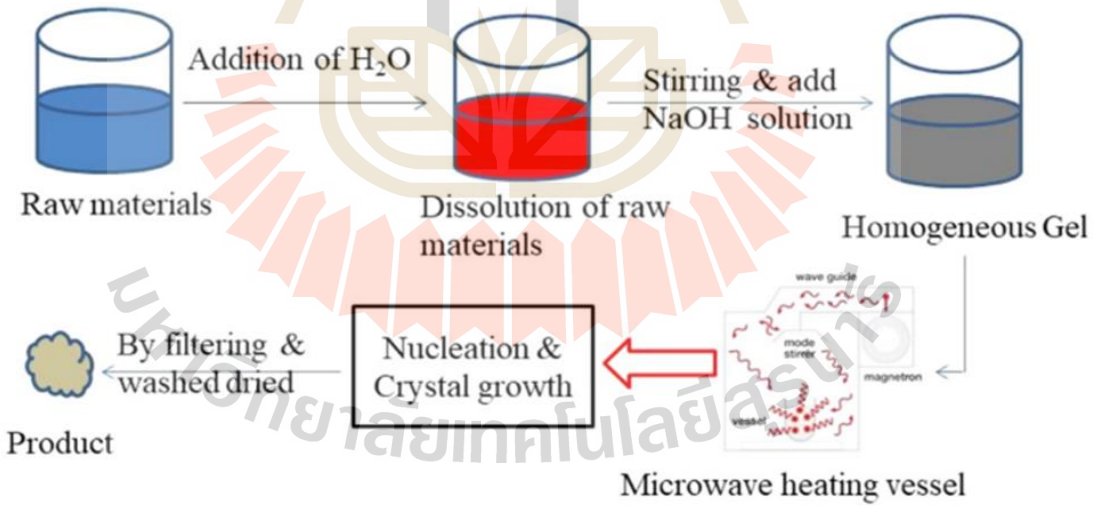

Figure 2.6 Microwave method for the synthesis of zeolite.

(Khaleque et al., 2020)

2.2.4 Ultra-sound energy method

Ultrasound with frequencies ranging from 20 kHz to 2 MHz is a branch of sonochemistry that is widely used in synthetic chemistry. Ultrasound has a significant influence on various types of synthesis cases, including the synthesis of amorphous or crystalline materials and polymerization reactions. Due to its significant influence on crystallization, ultrasound has received considerable attention in zeolite synthesis. The advantages of this method are straightforward: it has a rapid reaction, does not require complex facilities, provides a high crystal growth rate, offers a suitable particle size distribution and morphology, and allows control of the nucleation process. Ultrasound induces cavitation, the growth and explosive collapse of microscopic bubbles. Cavitation can also increase secondary nucleation rates and improve crystal purity during cooling crystallization. Owing to the various traditional and emerging applications of synthetic zeolites, the ultrasound energy method enables tunable zeolite synthesis. Temperature, time, and the molar ratio of reactants are considered the main parameters to determine the type and characteristics of the zeolite formed. Ultrasound energy methods have been used extensively to synthesize zeolites. For example, Pal et al. reported the synthesis of NaP zeolite nanocrystals at ambient temperature in a short crystallization time via ultrasound (Pal et al., 2013). Herein, sonication energy enables the formation of active radicals, which in turn lead to rapid crystallization of the zeolite phase. Synthesis of hierarchical ZSM-5 zeolites with long-term catalytic activity was also reported via ultrasound-assisted synthesis (Huang et al., 2016). Therefore, ultrasound energy-assisted methods are attractive to researchers due to their significant influence on zeolite synthesis.

2.2.5 Alkali-fusion and leaching method

In zeolite synthesis, the alkali fusion method is a general approach for decomposing materials rich in silica or alumina in the presence of alkali, which acts as an activator to form soluble aluminate and silicate salts. Solvothermal methods also use alkali (e.g., NaOH), but there are some differences between solvothermal and

alkali-fused methods. In the alkali fusion method, alkali is used to prevent multi-phase formation and is fused with the raw materials in a solid state before being introduced to any solvent. In contrast, in the solvothermal method, alkali is used in a solution state and acts as a mineralizer of the reaction medium. Generally, in the alkali-fusion method, the raw material is first fused with an alkali (e.g., NaOH) before a hydrothermal treatment (Fig2.7). During the hydrothermal treatment, the fused product is mixed with water and treated with the proper conditions, like heating at an appropriate temperature for the crystallization to form zeolite. Factors affecting the alkali-fusion methods are (i) the silicon-aluminum ratio of the raw material, (ii) concentrating the reacting alkali medium, (iii) temperature, and (iv) crystallization rate. Many studies have previously been conducted to synthesize zeolites using this method. For example, the synthesis of X-type zeolite by alkali fusion (e.g. sodium carbonate as an activator) followed by hydrothermal treatment using coal fly ash as a raw material. It was found that the alkali activator has a significant influence on the synthesis of synthetic zeolite. In addition, the alkali fusion method is usually used to synthesize zeolite A, zeolite X, and hydroxysodalite from the BFS. In a previous study, Chen et al. reported the synthesis of zeolite X from lithium slag through a hydrothermal reaction with alkali fusion. They mentioned the excellent properties of the zeolite (D. Chen et al., 2012). Moreover, in most processes, the alkali fusion technique is followed by a hydrothermal method for synthesizing zeolite. Both methods require high temperatures, time, and pressure. The primary sources for zeolite synthesis are commercial chemicals, which are very rich in alumina silicate, mineral resources in the earth's crust, and industrial by-products. By adjusting the experimental conditions, a range of zeolitic materials such as zeolite X, zeolite P, hydroxysodalite, tobermorite, and nepheline can be synthesized. This approach enables the use of low-grade raw materials without prior purification and produces high-purity anhydrous zeolites, offering a notable advantage. Alkali leaching is another approach in which the leachate maintains the silica-alumina ratio, such as with a NaOH solution. The factors that influence the alkali leaching method are (i) desalination rate, (ii) silica-alumina ratio of leachate-free solid product,

(iii) fusion temperature, (iv) concentration of leaching agent, and (v) crystallization rate. Several investigators have reported different zeolite syntheses via an alkali-alkali leaching approach. For instance, El-Naggar et al. synthesized pure zeolites using the alkaline leaching method from silica extracts obtained from fly ash. Their synthesized A-X zeolite blends showed the most significant potential for cesium ion sorption. The main benefit of this route is the production of a very efficient product at a low cost (El-Naggar et al., 2008).

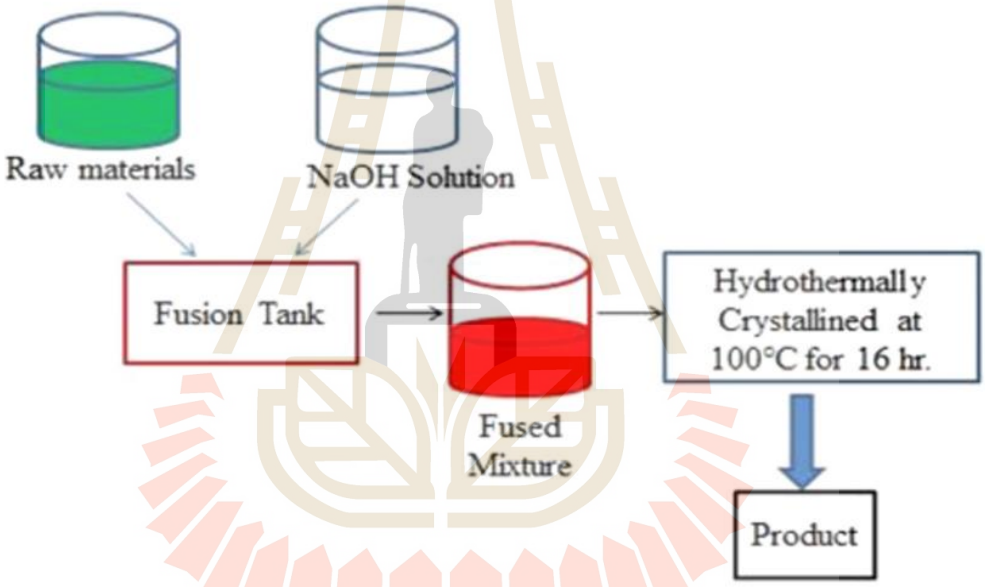

Figure 2.7 A schematic representation of zeolite synthesis via the alkali fusion method (Khaleque et al., 2020).

2.3 Ball clay

Ball clays are fine-grained and highly plastic sedimentary clays that fire to a light or nearly white color. They are used mainly in the manufacture of ceramic whiteware and are valued for their key properties of plasticity, which makes them easy

to mold, their unfired strength, and the fact that when fired, they have a light color. Normally, sedimentary clays fire to a reddish color. Some ball clays also have the ability to disperse in water to produce fluid slips (high solids aqueous suspensions). Ball clays exhibit highly variable compositions and consist not of a single mineral, as shown in Table 2.4. The clay is primarily composed of a mixture of three minerals: kaolinite, mica, and quartz. Each of these minerals contributes unique properties to the clay. Among them, kaolinite is the key component. The crystallinity, which refers to the degree of structural perfection, and the size of the kaolinite crystals present in various ball clays can significantly affect their performance in ceramics.

Table 2.4 Chemical composition of ball clay (Worrall, 2013)

Component	Wt%
SiO_2	40-60
Al_2O_3	25-40
Fe_2O_3	0.25-4.0
K_2O	0-0.75
TiO_2	0-0.4
CaO	0.0.5
MgO	0.0.3
Na_2O	0.5-4.0

Ball clays are primarily used as raw materials in ceramics. The main types of ceramic whiteware that include ball clay are sanitary ware, wall and floor tiles, and tableware. Additionally, ball clay is used in kiln furniture, enamels and glazes, building

bricks, fillers, and sealants. It is rare for ball clay to be used on its own; the amount employed varies depending on the specific product. Other key components of ceramic whiteware include kaolin, silica sand, and a flux, such as feldspar, which lowers the melting point of the other ingredients. Although it often accounts for only a small percentage of total raw materials, ball clay can be essential in certain ceramic products. Within a ceramic body, ball clay acts as a binding agent, enhancing plasticity, workability, and strength prior to firing. This allows the ceramic body to be formed and handled safely between the shaping and firing processes and also provides strength in the fired body. Some ball clays are particularly valued for their fluid and casting properties, which are important for slip-casting, especially in the manufacture of sanitary ware.

Figure 2.8 Ball Clay

2.4 Pressure Swing Adsorption Oxygen Concentrator

Air pollution is becoming a global issue that impacts both acute and chronic respiratory problems, concerning individuals and communities alike. Wearing disposable face masks has become a popular way to protect against exposure to

pollutants. However, a person with chronic obstructive pulmonary disease (COPD) could find it difficult to breathe through these masks. Consequently, there is an increasing demand for a lightweight and portable oxygen concentrator that provides a medical-grade oxygen supply with an O_2 concentration of approximately 88-92 vol%. Nowadays, oxygen concentration technologies are influenced by air separation processes, including cryogenic techniques, membrane separation, and pressure swing adsorption (PSA). These methods effectively produce enriched oxygen by utilizing ambient air as the source. Although cryogenic distillation is the leading process for air separation in industrial oxygen plants, the pressure swing adsorption (PSA) technique has the advantage of reducing energy consumption for small production scales. Compared with membrane separation methods, which require higher pressures and costly, selective, permeable materials, pressure swing adsorption (PSA), which uses nanosized zeolite adsorbents, offers a more practical approach for creating portable oxygen concentrators. The substantial microporous surface area of zeolite adsorbents enables the PSA-based portable oxygen concentrator to effectively capture nitrogen from air, producing a high-pressure stream of concentrated oxygen. The device can be regenerated by lowering the pressure, which releases the trapped nitrogen, thereby providing a continuous flow of oxygen to help individuals and increase the fraction of oxygen they inhale. Typically, this oxygen concentration system is combined with a filtration system that removes PM2.5 particles, improving the quality of the resulting gas stream. Finlayson and Sharp patented the pressure swing adsorption process in 1932 (GB Patent 365092), which describes an air separation technique involving pressurized adsorption and depressurized desorption phases (W. John Thomas, 1998). In 1958, two separate pressure swing adsorption units were patented: one that uses a fractional product purge flow during desorption, and another that employs pressure-vacuum swing adsorption (PVSA) (Sircar, 2002).

The selectivity of zeolite adsorbents for nitrogen over oxygen is attributed to the interaction between the electrostatic field of cationic zeolites and the quadrupole

moments of nitrogen and oxygen. Specifically, the quadrupole moment of nitrogen is three times greater than that of oxygen, which leads to selective adsorption on the zeolite surface (Drain, 1953). The most commonly used commercial zeolite in the oxygen concentration process is zeolite 13X, renowned for its excellent nitrogen-to-oxygen adsorption selectivity. Additionally, 13X zeolite modified through Li+ exchange demonstrates an enhanced nitrogen adsorption capacity at the active cation sites within the zeolite framework. The JLOX-101 LiX zeolite, provided by LUOYANG JIANLONG Chemical, is specifically designed for a Pressure Vacuum Swing Adsorption (PVSA) process, offering high oxygen selectivity. The Pressure Swing Adsorption (PSA) system was initially implemented in industrial plants as a cost-effective alternative to cryogenic separation plants, both in terms of capital investment and operating expenses. Over the past two decades, portable PSA oxygen concentrators have been developed, driven by advancements in the synthesis of more effective zeolites that offer higher gas adsorption capacity and selectivity. These PSA oxygen concentrators can deliver a continuous flow of oxygen by utilizing ambient air as their gas source. Two-bed or multi-bed PSA systems operate by alternately adsorbing and desorbing gases in the zeolite columns, allowing for continuous oxygen separation. For the production of medical-grade oxygen on-site, a cylinder gas source or several high-capacity air compressors are typically installed to enhance the rapid pressure swing adsorption process, thereby ensuring a consistent output of high-purity oxygen (Rao et al., 2014). Given the portable nature of small-scale concentrators, various simplified designs have been introduced to the PSA process to facilitate system miniaturization.

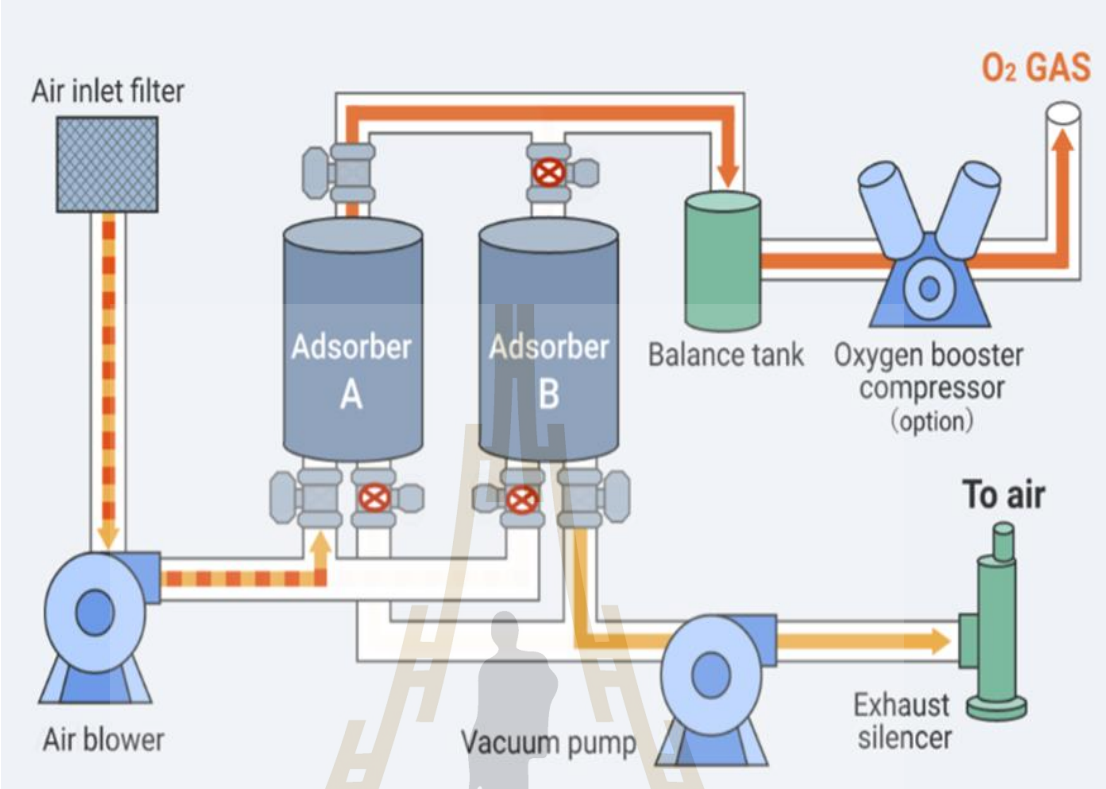

Figure 2.9 Schematics of the PSA oxygen concentrator

2.5 Research

2.5.1 Zeolite A synthesis

Mousa Gougazeh and J.-Ch. Buhl investigated the creation of zeolite materials by hydrothermally transforming natural kaolin from Jordan in sodium hydroxide (NaOH) solutions of different concentrations. This process was carried out at 100 °C over a duration of 20 hours. The mixture consisted of zeolite A, quartz, and hydroxy sodalite (HS), with zeolite A identified as the main product when NaOH concentrations were between 1.50 and 3.50 M, as evidenced by X-ray diffraction (XRD) and scanning electron microscopy (SEM). The study demonstrated that zeolite A can be derived from natural kaolin under these conditions, indicating that metakaolinization occurs at 650 °C. The successful hydrothermal synthesis of zeolite

A used kaolin as the primary raw material, and XRD analysis showed high relative crystallinity. SEM confirmed that the surface morphology of zeolite A was cubic in shape. Thus, kaolin was proposed as a viable and cost-effective raw material for the industrial production of zeolite A. (Gougazeh & Buhl, 2014).

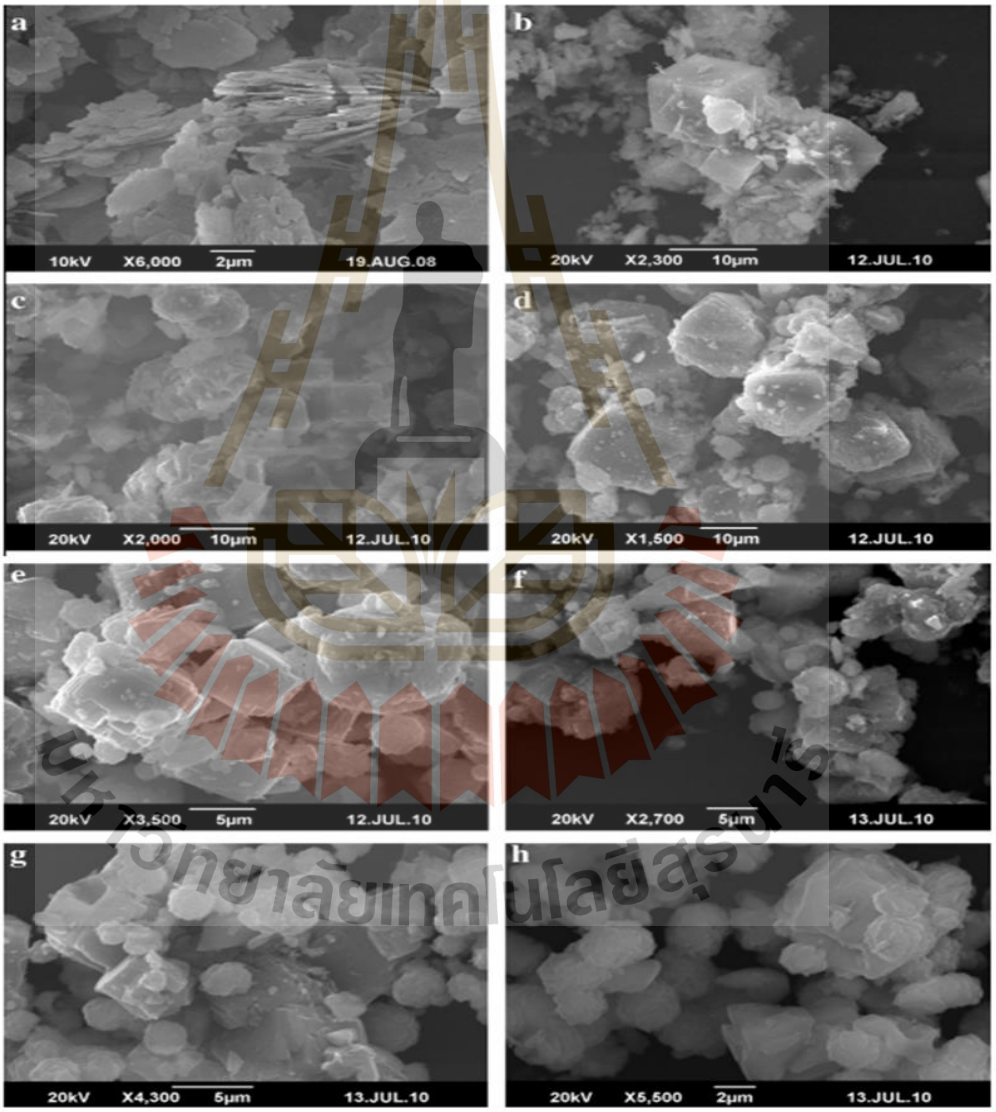

Figure 2.10 SEM micrographs illustrate the zeolite A's formation and related phases obtained through hydrothermal synthesis. In panel (a), hexagonal platy

crystals of untreated kaolin are shown. Panel (b) features well-developed cubes of zeolite A alongside remnants of metakaolin. In panel (c), zeolite A appears have formed prior to hydroxysodalite (HS), as indicated by the growth of HS crystals on the surface of zeolite A. Panels (d–f) display spheroidal aggregates of HS that developed on the surfaces of the cubic zeolite A crystals, demonstrating penetration twinning. Finally, panels (g–h) depict the lepispheric morphology of HS associated with the cubic crystals of zeolite A (Gougazeh & Buhl, 2014).

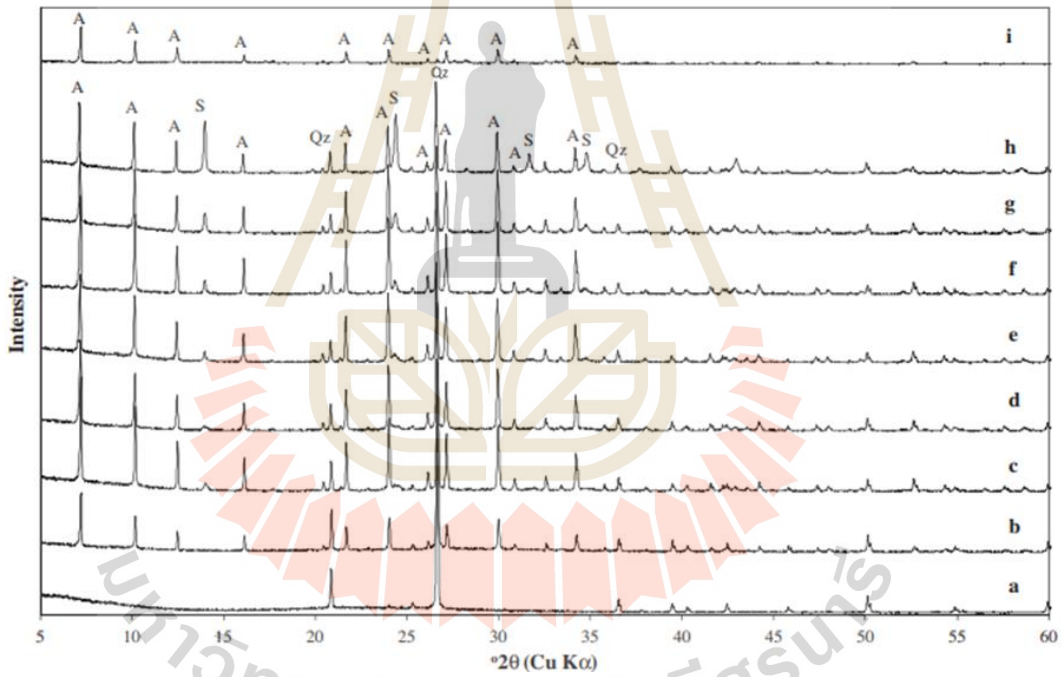

Figure 2.11 XRD patterns of zeolite A and associated phases obtained by Hydrothermal synthesis (a) unreacted metakaolin, (b) 1.0 M NaOH, (c) 1.5 M NaOH, (d) 2.0 M NaOH, (e) 2.5 M NaOH, (f) 3.0 M NaOH, (g) 3.5 M NaOH, and (h) 4.0 M NaOH, (i) commercial zeolite A. A: zeolite A, S: hydroxysodalite, Qz: quartz (Gougazeh & Buhl, 2014).

2.5.2 Ion exchange research

Lisa Price, Ka Ming Leung, and Asel Sartbaeva investigated local and average structural changes in zeolite A following ion exchange. Solid-state FTIR revealed changes to the local structure of the LTA framework upon ion exchange with NH^{4+} and Ca^{2+}. Exchange with Li^{+}, K^{+}, and Rb^{+} ions does not significantly affect the long-range crystal order. The FT-IR spectra for Li-A, Na-A, K-A, and Rb-A all display the fundamental zeolite framework vibration at Vmax/cm−1 of 959, 968, 972, and 969, respectively, corresponding to the asymmetric V(O–T–O) stretch, as shown in Figure 2.12. In addition, the framework symmetric $V_{(O-T-O)}$ stretch occurs at $V_{/cm-1}$ 684, 664, 663, and 666 for Li-A, Na-A, K-A, and Rb-A, respectively. The broad peaks at 3350–3450 cm^{-1} and the weaker peaks at 1650 cm^{-1} observed in all spectra correspond to the $V_{(O-H)}$ stretching and $\delta_{(H-O-H)}$ bending vibrations of water molecules in the hydrated samples. The only noticeable differences in the spectra are that the framework $V_{(O-T-O)}$ asymmetric stretch shifts slightly to a higher wavenumber and the $V_{(O-T-O)}$ symmetric stretch shifts slightly to a lower wavenumber, with increasing cation size, $Li^{+} < Na^{+} < K^{+}$

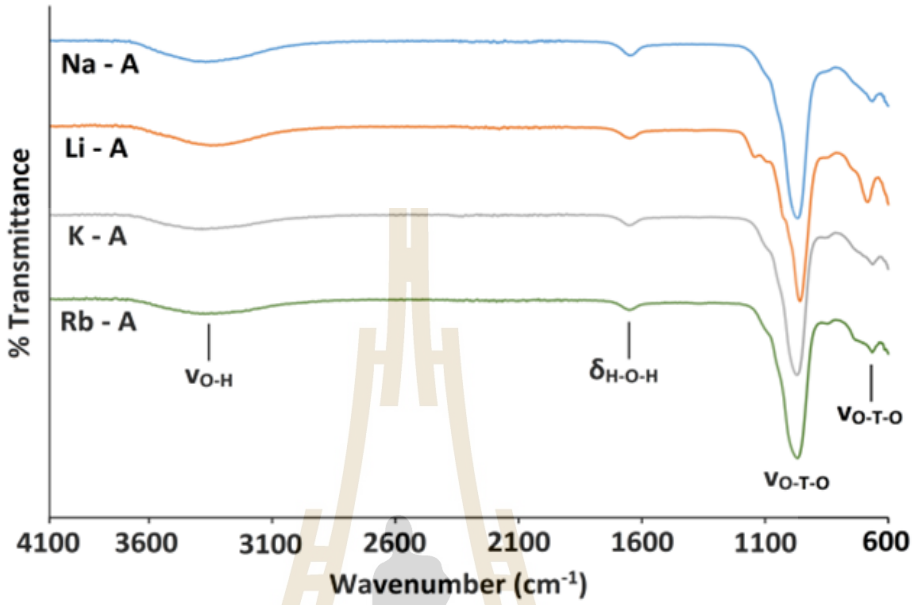

Figure 2.12 FT-IR spectra for Na-A (blue line) and cation-exchanged Li-A (orange line); K-A (grey line) and Rb-A (green line) (Price et al., 2017).

2.5.3 Spray drying research

Tuiana Shoinkhorova and her colleagues conducted a study on shaping ZSM-5-based catalysts using spray drying techniques. In their research, they explored a method for formulating catalysts through this process. They incorporated ZSM-5 zeolite, which has a silica-to-alumina molar ratio of 23, along with various commercially available clays, including kaolin, talc, montmorillonite, attapulgite, and sepiolite, into the composites. The researchers optimized the spray-drying parameters to produce particles with sizes ranging from 30 to 100 μm. They demonstrated that varying the gas flow rate, nozzle aperture, pretreating the slurry with ball milling, and adjusting the ratio of the slurry components allowed for the production of composite particles with different sizes and morphological characteristics. Among all the variables studied, the

most critical factor in the slurry formulation was the total solid content of the sprayable slurry. This content is significantly influenced by the components of the catalyst, particularly the binder and clay. Slurry dilutions below 30 wt% resulted in loosely packed, surface-defective composite materials with poor attrition resistance. In contrast, higher loadings under optimal spraying conditions produced much better-shaped particles (Shoinkhorova et al., 2019).

2.5.4 Zeolite molecular sieve

Ehsan Javadi Shokroo and colleagues conducted a comparative study examining the use of zeolite 5A and zeolite 13X for air separation through pressure swing adsorption (PSA) (Shokroo et al., 2016). The simulation results indicated that zeolite 13X exhibited a slightly higher nitrogen adsorption capacity compared to zeolite 5A. However, under the same operating conditions, zeolite 5A had a larger mass transfer zone than its counterpart. When comparing the equal volume of nitrogen adsorbed by both materials, zeolite 5A demonstrated a greater ability to desorb a larger volume of nitrogen within a specific timeframe. Additionally, to achieve oxygen purity of 96%, using zeolite 5A proved to be more cost-effective than using zeolite 13X.

2.5.5 Studies on adsorption-based air separation for medical-grade oxygen production

Various studies in the literature have examined alternative adsorption cycles and materials for air separation (Jareteg et al., 2020). Farooq et al. investigated a 2-bed, 4-step PSA method for air separation utilizing 5A zeolite through simulation and testing (Farooq et al., 1989). Kopaygorodsky et al. investigated the use of 5A zeolite in ultra-rapid PSA cycles to enhance air separation efficiency (Kopaygorodsky et al., 2004). Santos et al. tested three possible adsorbents and examined the 4-step PSA and PVSA cycles for Oxygen generation (Santos et al., 2006). A two-step pulsed PSA approach was developed by Rao et al. to investigate the potential level of shrinking in medical applications (Rao et al., 2010). A four-step rapid PSA process was developed

by Rao et al. A rapid PSA process based on LiX zeolite was developed in Refs. (Zhu et al., 2017). The process characteristics and performance measures for various literature studies are summarized in Table 2.5

Table 2.5 Literature Studies on adsorption-based air separation for medical-grade oxygen production

Adsorbent	Cycle type	Duration (s)	Operating Pressure		Purity (%)	Reference
			P_a	P_d		
5A zeolite	2-bed 4-StepSA	100	1.5	1.01	93.4	49
5A zeolite	2-step PSA	<3	1.52	1.01	85	50
LiX zeolite	4-step PSA	3-5	3.04-4.05	1.01	90	4
LiLSX zeolite	4-step PSA	3-9	4.0	1.0	90	53
LiLSX zeolite	5-step PVSA	7	2.4	0.6	90	54
LiLSX zeolite	4-bed 6-step VPSA	5	2.53	1.01	92	47
LiLSX zeolite	2-bed 6-step VPSA	3.8-6.8	1.95	0.43	92-93	43

CHAPTER III

RESEARCH METHODOLOGY

3.1 Preparation

3.1.1 Chemicals, equipment, and characterization

Table 3.1 Chemicals, Chemical formula

Chemicals	Chemical formula	Figure
Ball clay	$Al_2Si_2O_5(OH)_4$	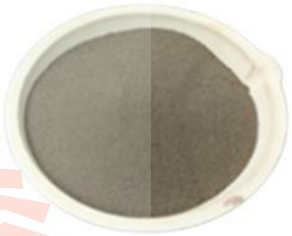 Figure 3.1
Ranong white clay	$Al_2Si_2O_5(OH)_4$	 Figure 3.2

Table 3.1 Chemicals, Chemical formula (Continued)

Chemicals	Chemical formula	Figure
Lampang white clay	$Al_2Si_2O_5(OH)_4$	 Figure 3.3
Sodium hydroxide	NaOH	 QReC Figure 3.4
Lithium hydroxide Monohydrate 99.5%	LiOH	 Loba Chemie Figure 3.5

3.1.2 Equipment

Table 3.2 Research Equipment

Equipment	Figure
Oxygen concentrator	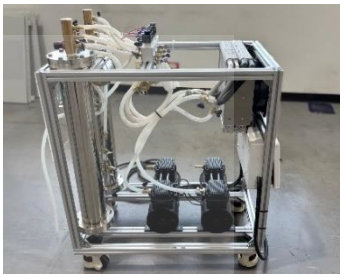 Figure 3.6
Oxygen gas detector	 Figure 3.7
Magnetic stirrer and Magnetic bar	 Figure 3.8

Table 3.2 Research Equipment (Continued)

Equipment	Figure
Furnace	 Figure 3.9
Oven	 Figure 3.10
Alumina crucible	 Figure 3.11

Table 3.2 Research Equipment (Continued)

Equipment	Figure
Mortar	 Figure 3.12
Spray dryer	 Figure 3.13
Deionization water	 Figure 3.14

Table 3.2 Research Equipment (Continued)

Equipment	Figure
Beaker	 Figure 3.15
Buchner Funnel	 Figure 3.16
Erlenmeyer Flask	 Figure 3.17

Table 3.2 Research Equipment (Continued)

Equipment	Figure
Filter paper	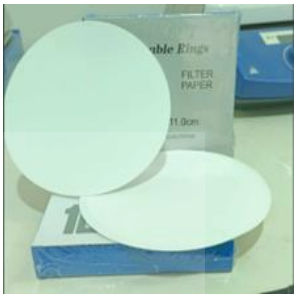 Figure 3.18
litmus paper	 Figure 3.19

3.1.3 Characterization techniques

Table 3.3 Characterization techniques

Characterization techniques	Figure
X-ray Diffractometer: XRD (D2 PHASER)	 Figure 3.20
Scanning Electron Microscope/Energy Dispersive X-ray Spectroscopy: SEM-EDS (JEOL JSM-6010LV)	 Figure 3.21

Table 3.3 Characterization techniques (Continued)

Characterization techniques	Figure
Thermogravimetric Analyzer: TGA (Mettler Toledo TGA/DSC1)	 Figure 3.22
BET Surface Area Pore Size and Pore Volume Distribution Analyzer micrometric (ASAP2020P)	 Figure 3.23
Energy Dispersive Spectrometer X-ray Fluorescence (ED-XRF) (Horiba/XGT-5200)	 Figure 3.24

Table 3.3 Characterization techniques (Continued)

Characterization techniques	Figure
Fourier Transform Infrared Raman Spectrophotometry (FT-IR-Raman/Vertex 70)	 Figure 3.25
X-ray Tomographic Microscopy (XTM)	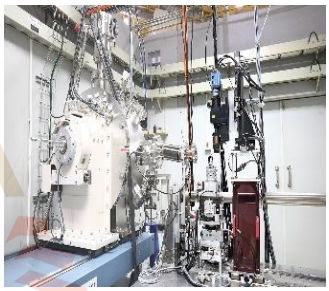 Figure 3.26

3.2 Experimental flow chart

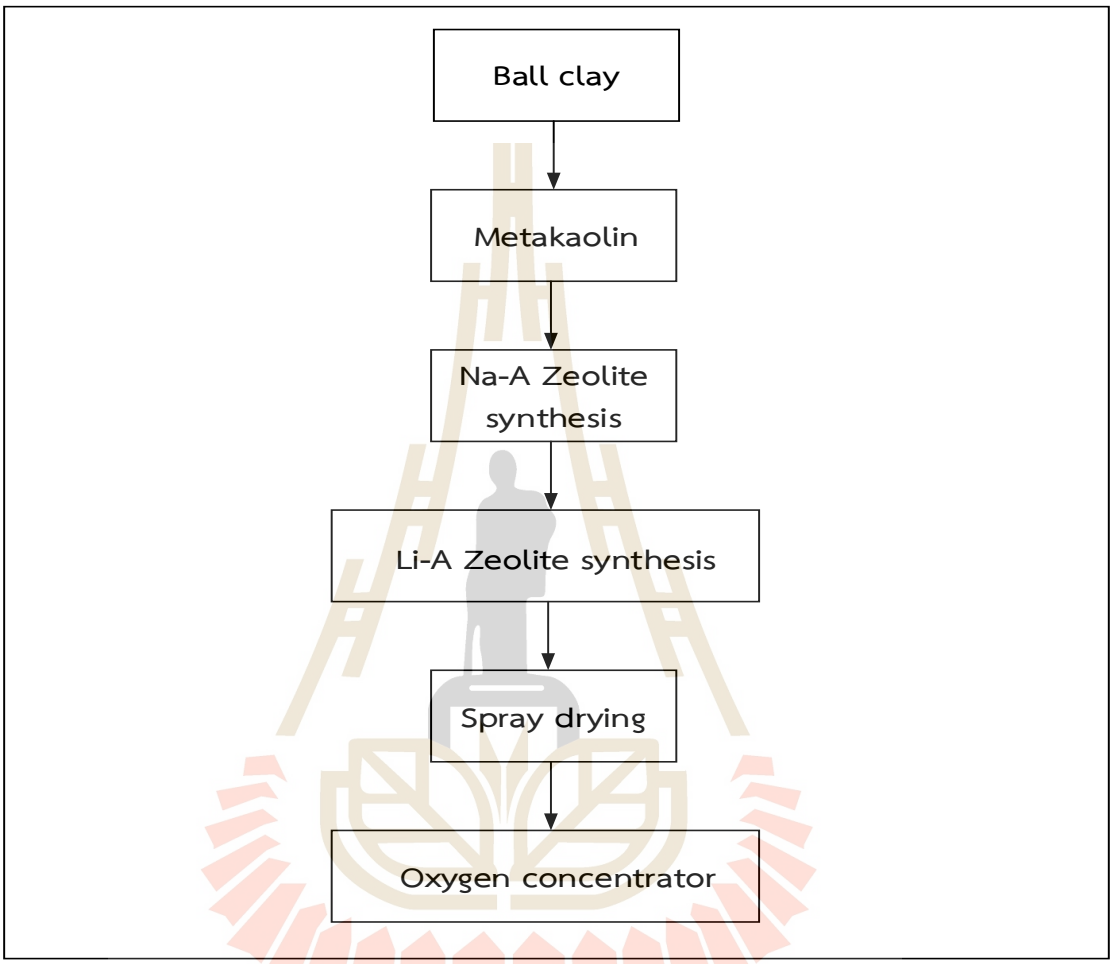

Figure 3.27 Experimental flow chart

The synthesis of Li-A zeolite from ball clay for medical oxygen production involves a sequential process beginning with the thermal pretreatment of the raw material. Initially, Ball clay is calcined to produce Metakaolin, which acts as the reactive aluminosilicate precursor. This Metakaolin is then subjected to a hydrothermal treatment with a sodium hydroxide solution to synthesize Na-A zeolite through a crystallization process. Following this, an essential ion-exchange step is performed,

where the the synthesized Na-A zeolite is treated with a lithium hydroxide solution to replace the sodium ions with lithium ions, yielding the final adsorbent, Li-A zeolite. Finally, the Li-A zeolite slurry is prepared for industrial application via spray drying, a technique that converts the slurry into free-flowing, spherical particles with controlled size and morphology. These optimized particles are then loaded into a pressure swing adsorption (PSA) system, forming the core component of the oxygen concentrator for efficient air separation by selectively adsorbing nitrogen.

3.3 Na-A zeolite synthesis

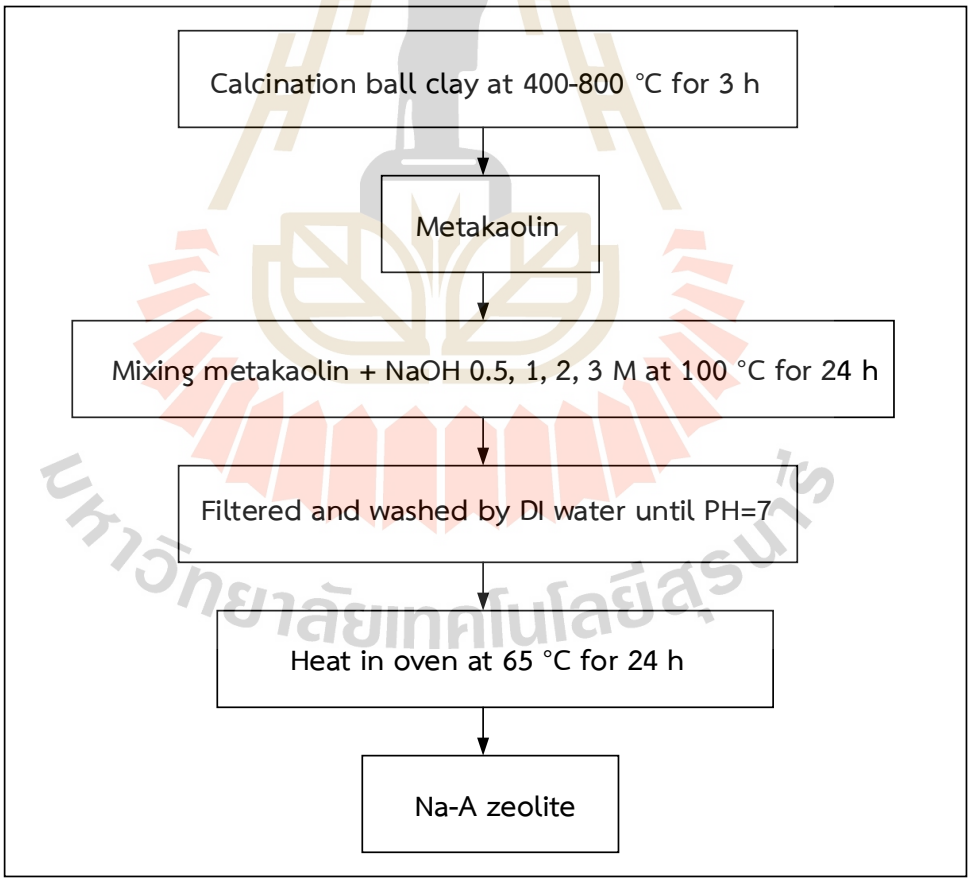

Figure 3.28 Flow chart for Na-A zeolite synthesis

The process for synthesizing Na-A zeolite from ball clay consisted of two fundamental steps: calcination and hydrothermal treatment. During calcination, the ball clay was heated at temperatures of 400, 500, 600, 700, and 800 °C for 3 h. This thermal treatment initiated a structural transformation within the ball clay, resulting in the formation of a metastable phase. Following calcination, the metastable phase samples underwent hydrothermal treatment with an aqueous NaOH solution to form Na-A zeolite. 20 g of ball clay was mixed with 100 mL of NaOH solutions at various concentrations (0.5, 1, 2, and 3 M) at 100 °C for 24 h. Subsequently, the samples were filtered and washed with deionized water until a neutral pH was achieved, thereby removing excess NaOH. Finally, they were dried in an oven at 65 °C for 24 h.

3.4 Li-A zeolite synthesis

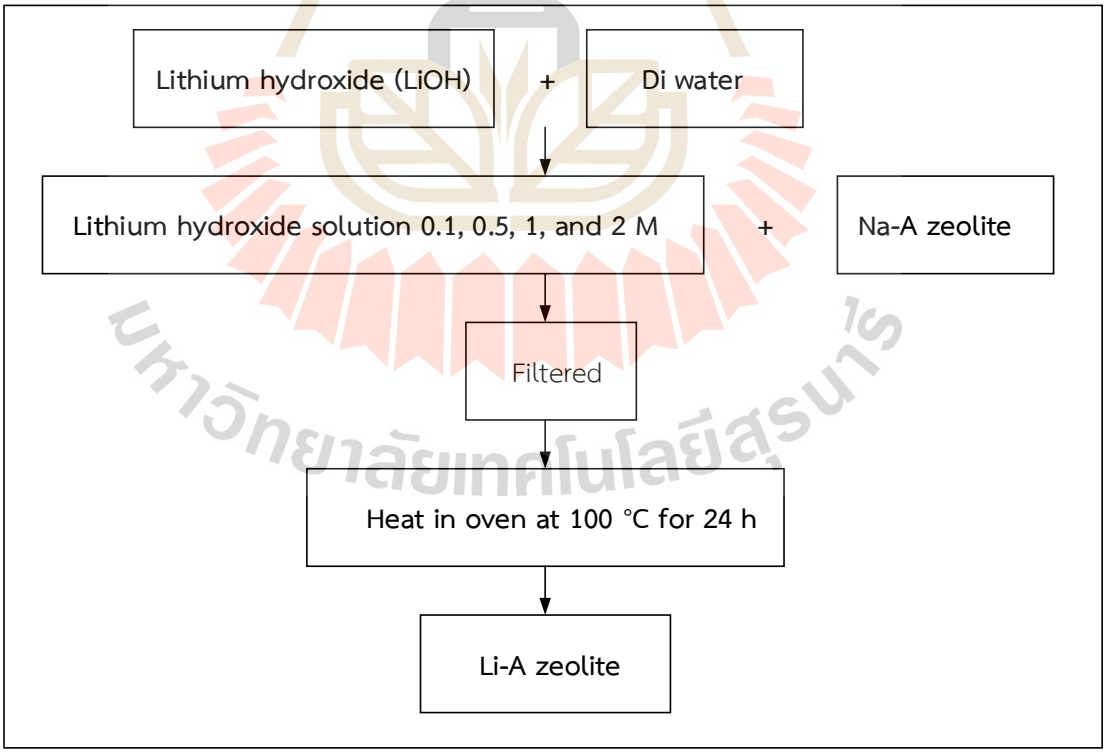

Figure 3.29 Flow chart for Li-A zeolite synthesis

In this experiment, varying amounts of LiOH powder were added to distilled water to prepare solutions with different concentrations of 0.1, 0.5, 1, and 2 M. Then, 50 g of Na-A zeolite was added to 1000 mL of LiOH solution at room temperature, with continuous stirring using a magnetic stirrer for 24 h. The samples were then filtered and dried overnight.

3.5 Spray Drying

The Li-A zeolite slurry was prepared by mixing 50 g of Li-A zeolite with 100 mL of deionized water as a solvent. The Li-A zeolite was thoroughly mixed with a magnetic stirrer and then ball-milled for 24 h. The spray drying process was performed using a spray dryer operated with a maximum inlet temperature of 220 °C, an air flow rate of 35 m^3/h, slurry feed rate of 15 ml/min, and spraying air flow rate of 357 L/h. The Li-A zeolite slurry was continuously mixed during the spray drying using a magnetic stirrer. Moreover, fluid nozzles with diameters of 450 μm were used in this study.

3.6 The efficiency of Li-A zeolite synthesized as a molecular sieve in a Pressure swing adsorption (PSA) oxygen concentrator

Medical oxygen concentrators are devices that generate high-purity oxygen by selectively eliminating nitrogen from the air. Natural zeolites are effective adsorbents in these devices thanks to their unique physical and chemical properties. The effectiveness of nitrogen absorption in natural zeolites is closely associated with their specific attributes. A significant factor that impacts nitrogen-selective absorption is the distribution of pore sizes within the zeolites. By customizing the uniformity of these pore sizes, zeolites can be aligned with the dimensions of nitrogen molecules, enabling efficient adsorption while excluding other gases. Thus, refining the pore-size distribution is essential for selective nitrogen capture. Moreover, the ion-exchange

capacity of natural zeolites is crucial to their function in medical oxygen concentrators. Zeolites can exchange ions with their environment, thereby enhancing their nitrogen adsorption capacity. By replacing specific ions in the zeolite with others that have a greater affinity for nitrogen, the material can become more efficient at capturing nitrogen gas. In addition to these factors, the surface area and porosity of natural zeolites are significant for their nitrogen-selective absorption performance. A greater surface area and increased porosity provide additional sites for nitrogen molecules to adhere to the zeolite, improving both the capacity and selectivity of the adsorbent. In conclusion, natural zeolites are highly valuable adsorbents for medical oxygen concentrators due to their pore size distribution, ion-exchange capacity, surface area, and porosity. Optimizing these characteristics can improve nitrogen-selective absorption efficiency. By understanding these properties, researchers and engineers can develop more effective medical oxygen concentrators using natural zeolites. Valuable insights can be gained from research aimed at developing more efficient oxygen-selective adsorbents and optimizing related methods for medical oxygen concentrators. Initial studies recognized that the oxygen-selective trait of various zeolites was due to the lower quadrupole moment of O_2 compared to N_2. In parallel with process research conducted by engineers, chemists, and materials scientists focused on adsorbents, a comparison of the numerous properties of well-characterized synthetic and natural zeolites can offer substantial learning opportunities. Collaborating, materials scientists and process engineers can likely achieve greater success than working independently in developing cost-effective, high-quality oxygen concentrators. However, selecting the appropriate natural zeolite for oxygen separation can pose challenges, and cost and quality considerations must always be kept in mind. Li-A zeolite synthesized from ball clay is employed in this study to capture N_2 in molecular sieve beds with a diameter of 98.20 mm and 649 mm. The Li-A zeolite prepared samples with several grain sizes (450 μm, 550 μm, and 650 μm) were prepared in the laboratory.

The compressed air moves to the sieve bed filters, which play a crucial role in removing nitrogen from the air. Inside the sieve bed, a material called zeolite, shaped like a six-sided microscopic cube with holes on each side, is responsible for this nitrogen removal.

There are two sieve beds located in the concentrator. After the air is first compressed, it is directed into the first sieve bed, where oxygen is separated and sent to the product tank. As a result, the first sieve bed becomes filled with nitrogen. In addition, the gas flow is switched, and the compressed air is directed to the second sieve bed. The compressor associated with the first sieve bed is vented to the outside, while the air from the product tank is returned to the first sieve bed.

As pressure drops in the first sieve bed and oxygen concentration decreases, the zeolite releases the trapped nitrogen. The released nitrogen recombines with the oxygen and is vented back into the room as regular air. The air is then compressed again and sent to the second sieve bed, where oxygen is once more separated and directed to the product tank. This entire cycle repeats itself every few seconds, starting again with the first sieve bed.

CHAPTER IV

RESULTS AND DISCUSSION

4.1 XRF Analysis

X-ray fluorescence (XRF) spectroscopy was used to characterize the composition of the white clay feedstock and the synthesized zeolite A. The analysis aimed to evaluate the extent of clay transformation during synthesis and to confirm the formation of a zeolitic structure by monitoring compositional changes, particularly variations in the Si/Al ratio and sodium content. Table 4.1 presents the comparative XRF results for the different white clay samples and the resulting zeolite products. The raw clay was predominantly composed of silica (SiO_2) and alumina (Al_2O_3), with minor amounts of iron oxide (Fe_2O_3) potassium oxide (K_2O), calcium oxide (CaO), and magnesium oxide (MgO).

The raw ball clay was analyzed for its elemental composition using X-ray fluorescence spectroscopy (XRF). The results of the analysis are shown in Table 4.1. It was found that the raw ball clay contained 55.946% w/w SiO_2 and 36.085% w/w Al_2O_3, with a molar ratio of 1.32. The Si/Al molar ratio of 1.32 was used to synthesize the Na-A zeolite without any adjustment. In addition, the raw ball clay also contained small amounts of elements such as iron oxide (Fe_2O_3), potassium oxide (K_2O), calcium oxide (CaO), titanium dioxide (TiO_2), and manganese dioxide (MnO_2). Moreover, the SiO_2/Al_2O_3 molar ratio closely matches the theoretical ratio for zeolite A synthesis, as confirmed by the calculation below Table 4.1, indicating a successful structural transformation. These results demonstrate the effectiveness of using white clay as a raw material for synthesizing zeolite A and achieving the elemental composition through the applied synthesis process.

Following the synthesis, a notable increase in the Na_2O content was detected in the zeolite A sample, which indicates that sodium was effectively integrated into the crystal structure during the hydrothermal treatment. This substantial rise in Na_2O correlates strongly with both the mechanism of formation and the stabilization of the zeolite framework. Sodium ions (Na^+), sourced from Na_2O, are crucial as structure-directing and charge-compensating agents, especially in low-silica zeolites like zeolite A (LTA-type). Their presence aids in the formation of a well-organized aluminosilicate framework by balancing the negative charges caused by the isomorphic substitution of Si^{4+} by Al^{3+} in the tetrahedral structure. An increase in Na_2O concentration also boosts the alkalinity of the reaction medium, which is vital for enhancing the dissolution of silica and alumina sources. This improved solubility speeds up the nucleation and crystallization processes of zeolite structures through a dissolution–reprecipitation mechanism. Furthermore, the Na_2O levels have a direct effect on phase selectivity during hydrothermal synthesis. Lower sodium levels typically result in amorphous or poorly crystalline phases, while higher Na_2O concentrations promote the formation of sodium-rich crystalline zeolite phases like zeolite A. This phenomenon is linked to the role of Na^+ in stabilizing intermediate aluminosilicate species and facilitating the assembly of the desired microporous framework.

Table 4.1 The chemical XRF composition of raw materials and zeolite A

Element	Ball clay (wt%)	Lampang white clay (wt%)	Ranong white clay (wt%)	Na-A Zeolite (wt%)
SiO_2	55.946	64.478	73.519	42.856
Al_2O_3	36.085	24.763	13.223	36.619
Fe_2O_3	1.141	1.268	2.209	1.207

Table 4.1 The chemical XRF composition of raw materials and zeolite A (Continued)

Element	Ball clay (wt%)	Lampang white clay (wt%)	Ranong white clay (wt%)	Na-A Zeolite (wt%)
K_2O	0.377	3.973	3.285	2.123
TiO_2	0.346	0.046	0.089	0.030
CaO	0.096	0.212	0.104	0.124
MnO_2	0.009	0.246	0.071	0.020
Na_2O	3.178	4.196	5.232	16.456
MgO	2.822	0.818	2.268	0.565

1. Si/Al calculation of Ball Clay

$$SiO_2 = \frac{55.946 \times 258.18}{100 \times 60.08} = 2.40 \text{ mol}$$

$$Al_2O_3 = \frac{36.085 \times 258.18}{100 \times 101.96} = 0.91 \text{ mol}$$

$$Si/Al = \frac{2.40}{0.91 \times 2} = 1.32$$

2. Si/Al calculation of Lampang white clay

$$SiO_2 = \frac{64.478 \times 258.18}{100 \times 60.08} = 2.77 \text{ mol}$$

$$Al_2O_3 = \frac{24.763 \times 258.18}{100 \times 101.96} = 0.63 \text{ mol}$$

$$Si/Al = \frac{2.77}{0.63 \times 2} = 2.20$$

3. Si/Al calculation of Ranong white clay

$$SiO_2 = \frac{73.519 \times 258.18}{100 \times 60.08} = 3.16 \text{ mol}$$

$$Al_2O_3 = \frac{13.223 \times 258.18}{100 \times 101.96} = 0.33 \text{ mol}$$

$$Si/Al = \frac{3.16}{0.33 \times 2} = 4.79$$

4. Si/Al calculation of Na-A Zeolite

$$SiO_2 = \frac{42.856 \times 1807.26}{100 \times 60.08} = 12.89 \text{ mol}$$

$$Al_2O_3 = \frac{36.619 \times 1807.26}{100 \times 101.96} = 6.49 \text{ mol}$$

$$Si/Al = \frac{12.89}{6.49 \times 2} = 0.99$$

Notation:

SiO_2 = 60.08 g/mol

Al_2O_3 = 101.96 g/mol

Ball clay, Ranong white clay, Lampang white clay = 258.18 g/mol

Zeolite A = 1807.26 g/mol

SiO_2 (wt%) of ball clay = 55.946 g/mol

Al_2O_3 (wt%) of ball clay = 36.085 g/mol

SiO_2 (wt%) of Lampang white clay = 64.478 g/mol

Al_2O_3 (wt%) of Lampang white clay = 24.763 g/mol

SiO_2 (wt%) of Ranong white clay = 73.519 g/mol

Al_2O_3 (wt%) of Ranong white clay = 13.223 g/mol

SiO_2 (wt%) of Na-A zeolite = 42.856 g/mol

Al_2O_3 (wt%) of Na-A zeolite = 36.619 g/mol

In calculating the molar ratio of silicon to aluminum (Si/Al) within the zeolite framework (or the precursor mix used for synthesis), meticulous consideration must be given to the atomic stoichiometry of the corresponding oxide sources. Specifically, silicon dioxide (SiO_2) contributes one atom of silicon (Si) per formula unit, while aluminum oxide (Al_2O_3) contributes two atoms of aluminum (Al) per formula unit. Therefore, if the starting molar ratio is defined based on the quantities of SiO_2 and Al_2O_3, the true atomic ratio of Si/Al requires a correction factor. This correction involves multiplying the number of moles of Al_2O_3 by a factor of 2 to accurately reflect the actual number of aluminum atoms present in the mixture.

4.2 Thermal Analysis

The thermal behavior of the ball clay sample was investigated by thermogravimetric analysis (TGA) and differential thermal analysis (DTA), as shown in Figure 4.1 The TGA curve (blue line) and DTA curve (red line) reveal the mass changes and corresponding thermal behavior occurring during heating from 30 °C to 1000 °C in an oxygen atmosphere at 10 °C/min.

In the first stage, approximately 1–2% weight loss occurred at the heat below 100°C, accompanied by a small endothermic effect in the DTA curve. This change

corresponds to the evaporation of physically adsorbed and interlayer water molecules, indicating the removal of surface moisture and loosely bound water from the ball clay structure.

The second stage, occurring in the temperature range of 280–560 °C, exhibits a major endothermic peak with a maximum at 510 °C corresponding to the dihydroxylation of kaolinite, the principal mineral phase in ball clay. During this process, the structural hydroxyl groups within the kaolinite structure are removed.

This transformation leads to the formation of metakaolin, an amorphous and highly reactive aluminosilicate phase. The endothermic peak observed at 510 °C confirms the energy absorption associated with the breakdown of the kaolinite crystal structure. Beyond 680 °C, the TGA curve gradually levels off, indicating that the dehydroxylation process is nearly complete. No significant mass loss is detected above this temperature. The material thus transitions into a thermally stable metastable phase, suitable as a precursor for zeolite synthesis. The formation of metakaolin within the 510–680 °C temperature window is of particular importance for zeolite synthesis because it increases the reactivity of silicon and aluminum species during hydrothermal treatment. This ensures more efficient dissolution and reassembly of the aluminosilicate network into the crystalline framework of zeolite A. Therefore, based on the thermal analysis results, the optimal calcination temperature range for preparing reactive ball clay lies between 510 °C and 680°C, ensuring complete dehydroxylation and maximizing the potential for zeolite A formation.

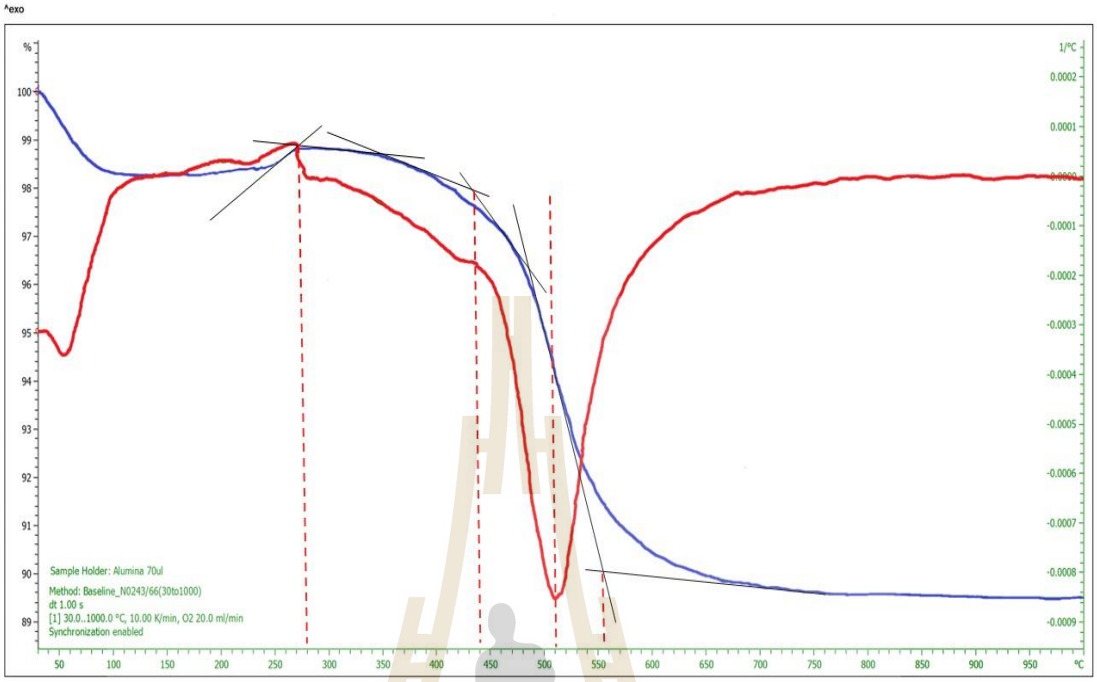

Figure 4.1 TGA and DTA curves of ball clay.

4.3 X-Ray Diffraction (XRD) Analysis

Figure 4.2 illustrates the X-ray diffraction (XRD) patterns of the raw clay materials. The major crystalline phases identified in Lampang white clay, Ranong white clay, and ball clay are kaolinite, illite, and quartz, which are considered impurity phases. In addition, ball clay was selected as the raw material for subsequent hydrothermal synthesis based on its chemical composition determined by X-ray fluorescence (XRF) analysis. The Si/Al ratio of ball clay was found to be 1.32, which is close to the theoretical Si/Al ratio of zeolite A. This appropriate compositional ratio makes ball clay a suitable precursor for the successful synthesis of Na-A zeolite under hydrothermal conditions. After calcination at 600 °C, the XRD pattern of ball clay metakaolin shows the disappearance of the characteristic kaolinite peaks when compared with that of the raw ball clay. This indicates that the kaolinite phase was

destroyed during thermal treatment as a result of dihydroxylation of the structural hydroxyl groups within the clay minerals. Consequently, the crystal structure of ball clay was transformed into an amorphous phase. This transformation is consistent with the Differential Thermal Analysis (DTA) results presented in Figure 4.1, which reveal a significant endothermic reaction associated with the loss of structural water due to dehydroxylation at the calcination temperature. Furthermore, calcination plays a crucial role in the synthesis of Na-A zeolite from ball clay, as it disrupts the original lattice structure and converts the clay into a highly reactive amorphous (metastable) phase. XRD analysis confirms that ball clay undergoes complete amorphization at approximately 600 °C, as evidenced by the absence of kaolinite reflections, with only the diffraction peaks corresponding to quartz remaining, as shown in Figure 4.3.

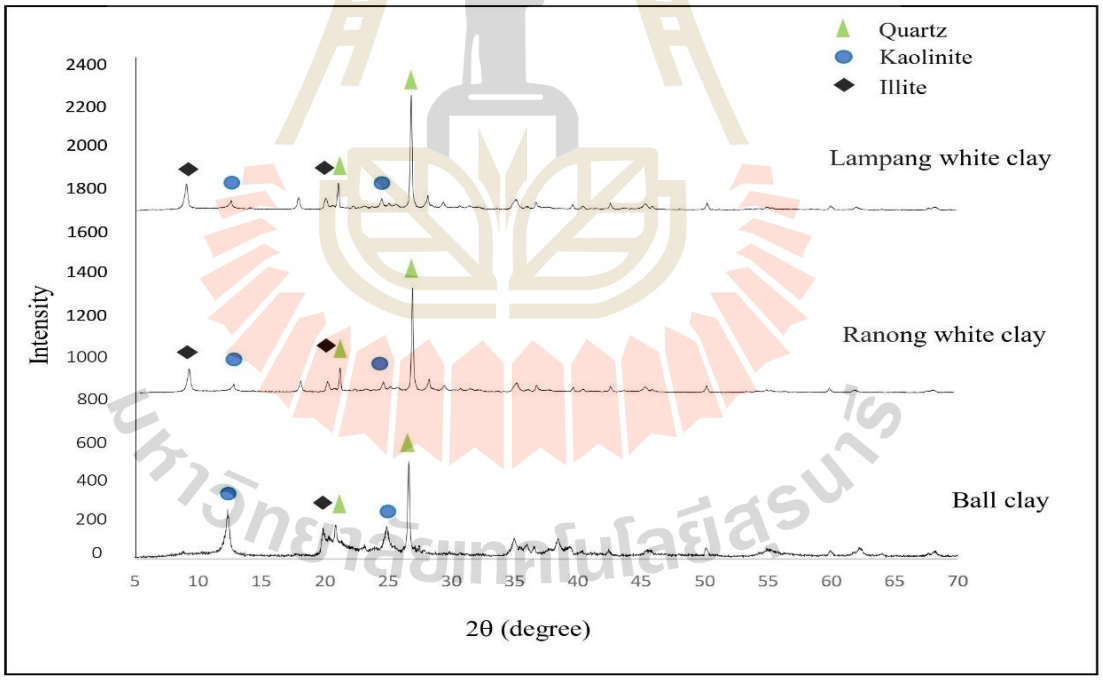

Figure 4.2 XRD pattern of clay in Thailand

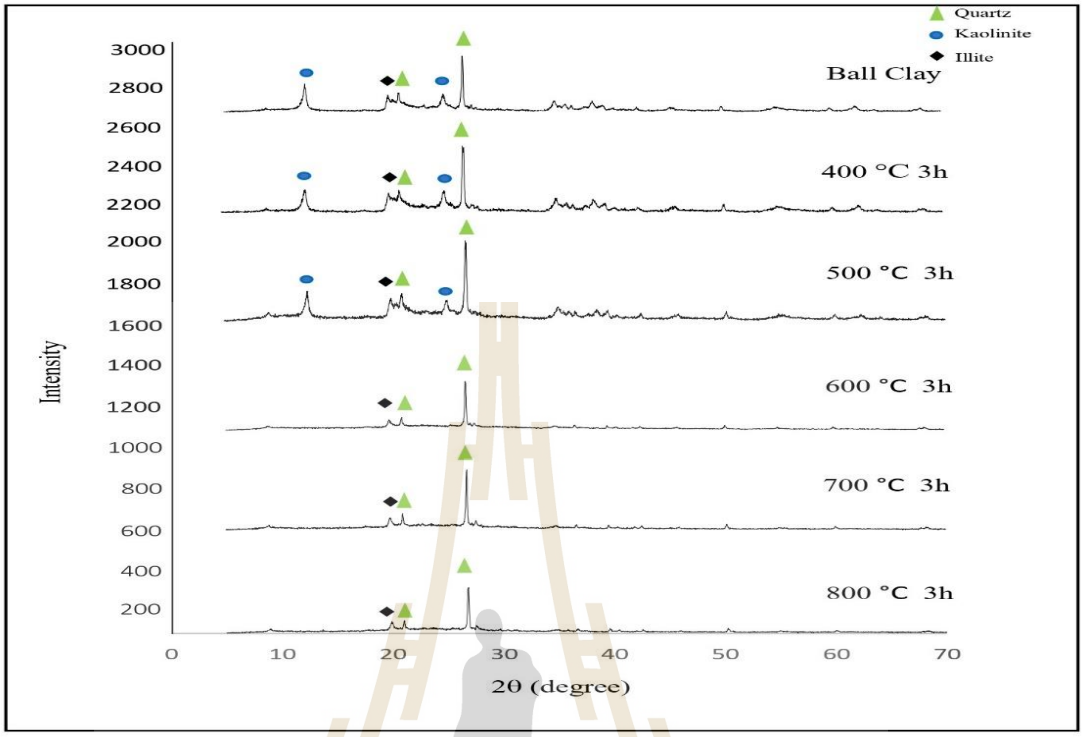

Figure 4.3 XRD pattern of ball clay and metastable phase samples calcined at a temperature range of 400 – 800 ℃ for 3 h.

Metakaolin obtained from the calcination of ball clay at 600 ℃ was used as the aluminosilicate precursor for the synthesis of Na-A zeolite via the hydrothermal method. Various factors influence the synthesis of Na-A zeolite. This study observed that the factors affecting the synthesis of Na-A zeolite were the concentrations of sodium hydroxide solution. Figure 4.4 demonstrates the XRD patterns of Na-A zeolite synthesized using different concentrations of NaOH solution. At 0.5 and 1 M NaOH, no zeolite crystal phase was observed, demonstrating that these conditions did not yield Na-A zeolite. The optimum conditions for synthesizing Na-A zeolite were achieved using NaOH concentrations of 2 and 3 M, a hydrothermal treatment temperature of 100 ℃, and a reaction time of 24 hours, which agrees with the corresponding patterns available in the literature (Silva et al., 2021). Among these conditions, the Na-A zeolite

synthesized using 3 M NaOH exhibited the highest crystallinity, as evidenced by the sharp and intense characteristic diffraction peaks of the LTA-type structure. Therefore, this sample was selected as the precursor material for the subsequent synthesis of Li-A zeolite via the cation exchange process. The ion exchange was carried out using LiOH solutions with different concentrations to investigate the effect of lithium content on the structural characteristics of the resulting Li-A zeolite. Moreover, Figure 4.5 demonstrates the XRD patterns of Li-A zeolite after cation exchange. Moreover, Figure 4.5 demonstrates the XRD patterns of Li-A zeolite after cation exchange. The reduced cation radius of Li in comparison to Na results in a structural contraction, along with minor alterations in peak intensity ratios and shifts when Na cations are substituted by other alkali metals (Price et al., 2017). X-ray diffraction (XRD) patterns of Na-A zeolite 3M and after ion exchange with lithium ions, Li-A zeolite. The diffraction peaks of both samples correspond well to the characteristic reflections of the LTA-type zeolite structure, indicating that the framework structure was preserved after the ion exchange process. A slight shift of the diffraction peaks toward higher 2 theta values was observed for the Li-A zeolite compared to the Na-A zeolite sample. For example, the characteristic reflection shifted from approximately 7.18° in Na-A zeolite to 7.25° in Li-A zeolite, while similar trends were observed for other major reflections, such as (220), approximately 10.20° in Na-A zeolite to 10.14° in Li-A zeolite, and (222), approximately 12.50° in Na-A zeolite to 12.70° in Li-A zeolite. This peak shift can be attributed to a decrease in the interplanar spacing (d-spacing), which is associated with lattice contraction caused by the replacement of Na^+ ions with smaller Li^+ ions. The ionic radius of Li^+ (0.76 Å) is smaller than that of Na^+ (1.02 Å), resulting in stronger electrostatic interactions between Li^+ ions and the negatively charged AlO_4^- units in the zeolite framework. Consequently, the unit cell parameter of the Li-A zeolite slightly decreased. Despite the observed peak shift, no additional diffraction peaks corresponding to impurity phases were detected, confirming that the ion exchange process did not alter the crystalline phase of the zeolite A structure.

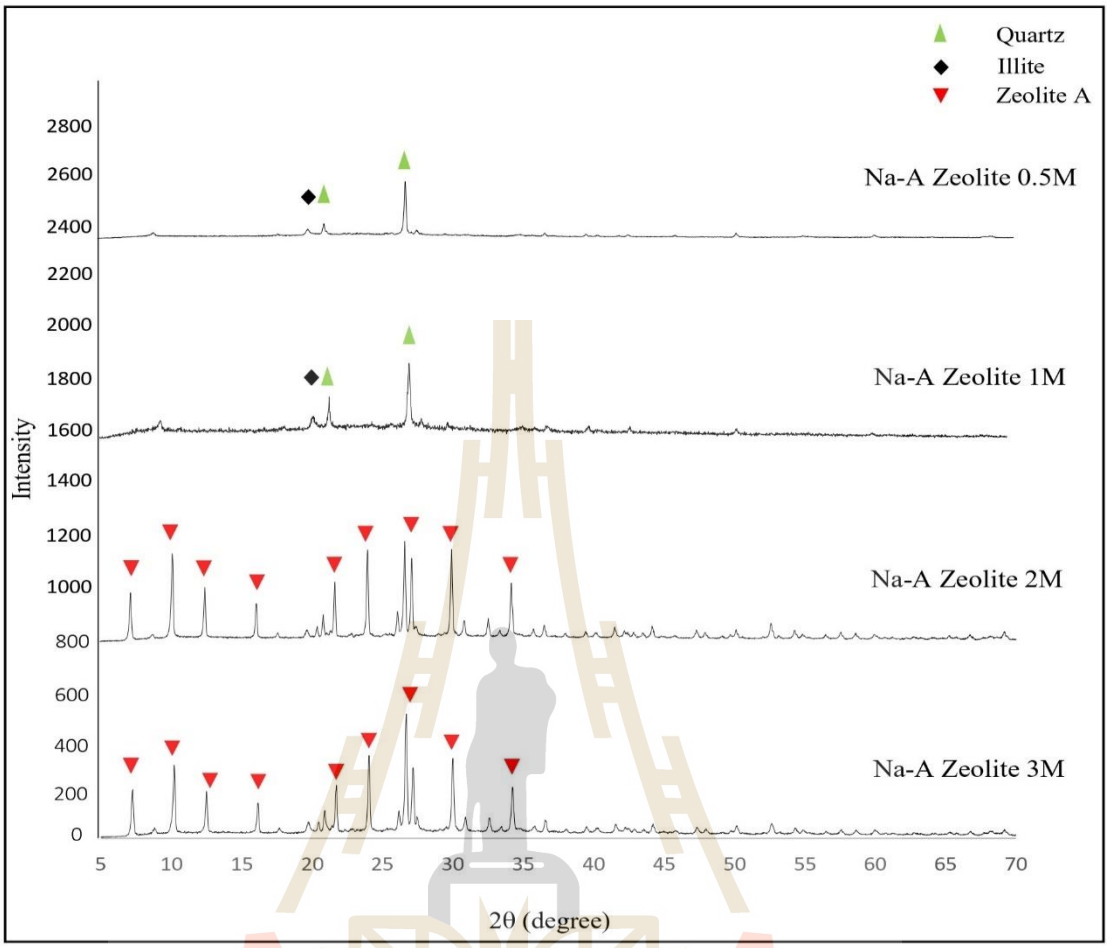

Figure 4.4 The XRD patterns of Na-A zeolite prepared by hydrothermal treatment at 100 °C in the NaOH solution at different concentrations (0.5, 1, 2, and 3 M).

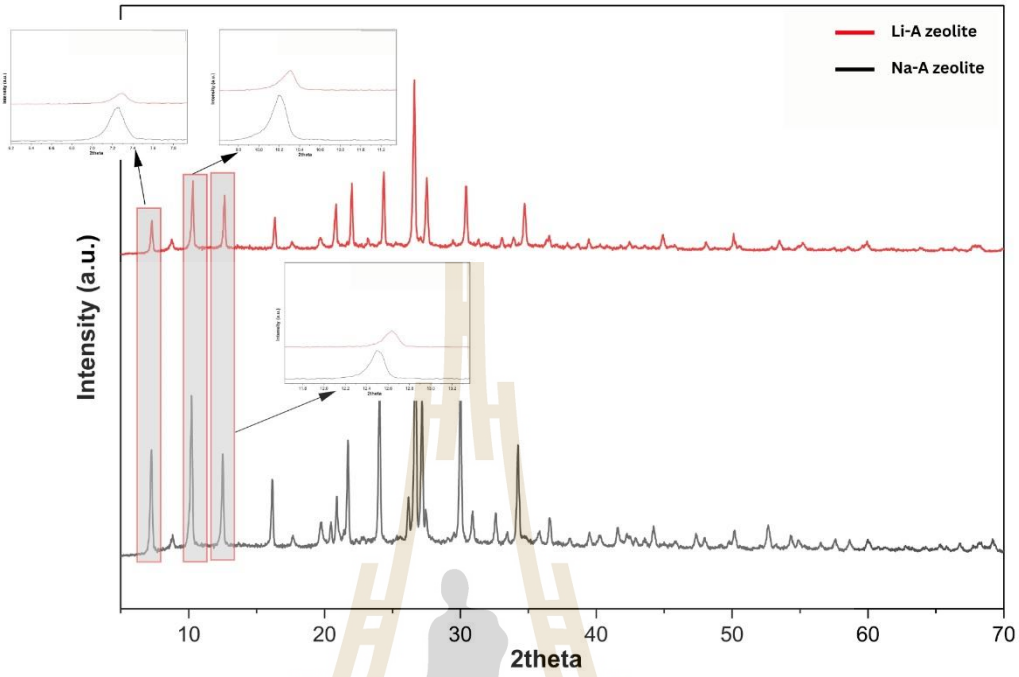

Figure 4.5 The XRD patterns of Na-A zeolite prepared by hydrothermal treatment at 100 °C in the NaOH solution 3M, and Li-A zeolite prepared by an ion-exchanger at room temperature in the LiOH solution 2M.

4.4 Fourier Transform Infrared (FTIR) Spectrum Analysis

The FTIR spectra for Na-A and Li-A zeolite display the fundamental V_{max} framework vibrations at 977 and 964 cm^{-1}, consistent to the asymmetric $V_{(O\text{-}T\text{-}O)}$ stretch. Moreover, the symmetric $V_{(O\text{-}T\text{-}O)}$ stretch occurs at 655 and 683 cm^{-1} for Na-A and Li-A zeolite, respectively. The band located at 1635 cm^{-1} is corresponded to the interstitial bonded water, and the band located between 2900 – 3750 cm^{-1} results from intra-and intermolecular hydrogen bonding (Cui et al., 2018). The FTIR results correspond with the XRD data, the framework $V_{(O\text{-}T\text{-}O)}$ asymmetric stretch shifts to a slightly lower wavenumber with increasing cation size, $Li^+ < Na^+$, as shown in Figure 4.6

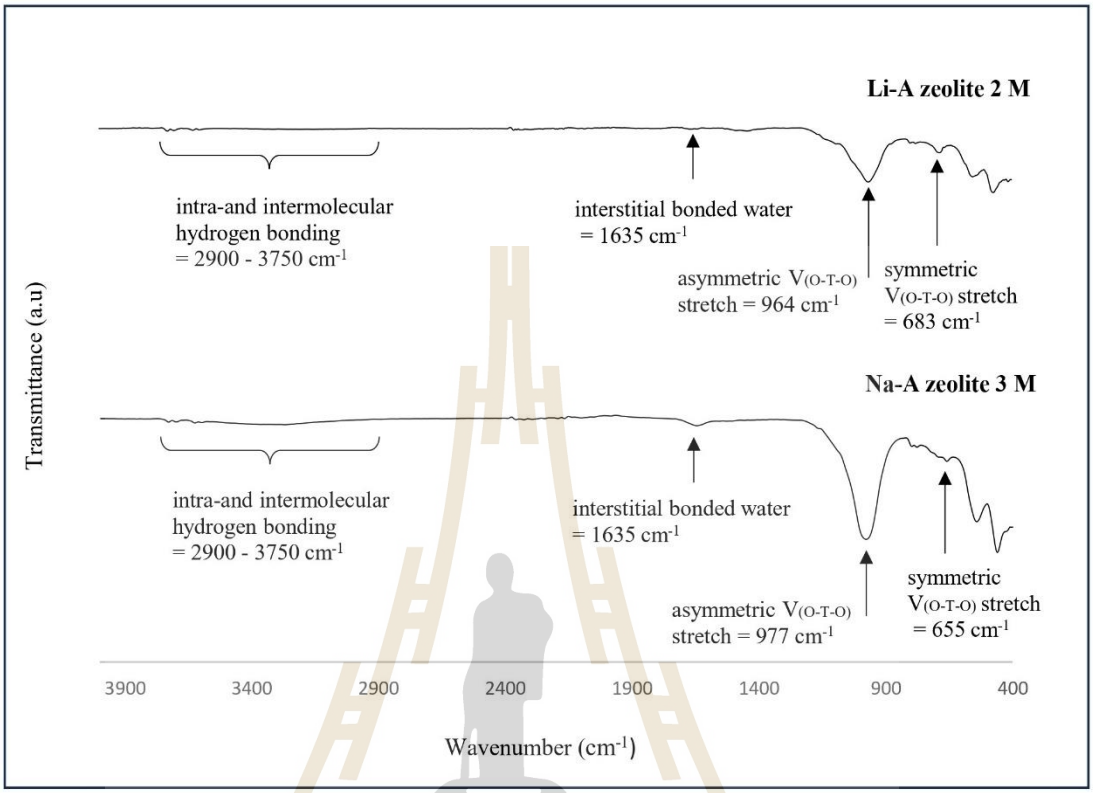

Figure 4.6 Fourier transform infrared (FTIR) spectrum of Na-A zeolite 3M and Li-A zeolite 2M.

4.5 Scanning Electron Microscope (SEM), Energy Dispersive X-Ray Spectroscopy (EDS) Analyses, and X-Ray Tomographic Microscopy (XTM)

The micrographs in Figure 4.7a, 4.7b, and 4.7c show that the crystallites of ball clay, Lampang white clay, and Ranong white clay are in a random orientation before treatment. In contrast, the morphology of the Na-A zeolite samples after hydrothermal treatment in NaOH solutions of varying concentrations was analyzed using scanning electron microscopy (SEM). Figure 4.8 (a-d) presents the effect of NaOH concentration on the formation of Na-A zeolite obtained after activation of metakaolin at 100 °C for 24 h. The results demonstrated that the morphologies of Na-A zeolites were similar to those reported in studies on the XRD patterns of Na-A zeolite prepared by hydrothermal treatment at 100 °C in NaOH solution concentrations of 0.5, 1, 2, and 3 M. A well-defined cubic-shaped morphology of Na-A zeolite was observed at high concentrations of NaOH (2 and 3 M), as shown in Figures 4.8c and 4.8d. At NaOH concentrations of 0.5 and 1 M, the formation of Na-A zeolite was not observed, as evidenced by the absence of cubic morphology, as depicted in Figures 4.8a and 4.8b. Of all NaOH concentrations investigated, 3 M NaOH was the most suitable concentration for obtaining Na-A zeolite with a cubic morphology.

Figure 4.9a illustrates the morphology of Li-A zeolite after cationic exchange. The results demonstrated the presence of a cubic-shaped morphology in Li-A zeolite. Moreover, Figure 4.9b presents the spherical shape with a smooth surface of Li-A zeolite granules prepared by a spray dryer.

The X-ray Tomographic Microscopy experiment was conducted at beamline 1.2 at the Synchrotron Light Research Institute, Nakhon Ratchasima, Thailand. There is a distribution of particle sizes, shapes, and morphologies of ball clay (Figure 4.10a, 4.10c), and some of the ball clay particles contain inter-voids to appear hollow. The equivalent spherical diameter distribution (Figures 4.10b and 4.10d) shows particles with an average equivalent spherical diameter of 450 μm. At this magnification, the differences in greyscale are directly proportional to the atomic number of the

component that absorbs the X-ray. Moreover, the individual components of the Li-A zeolite inside each particle were resolved.

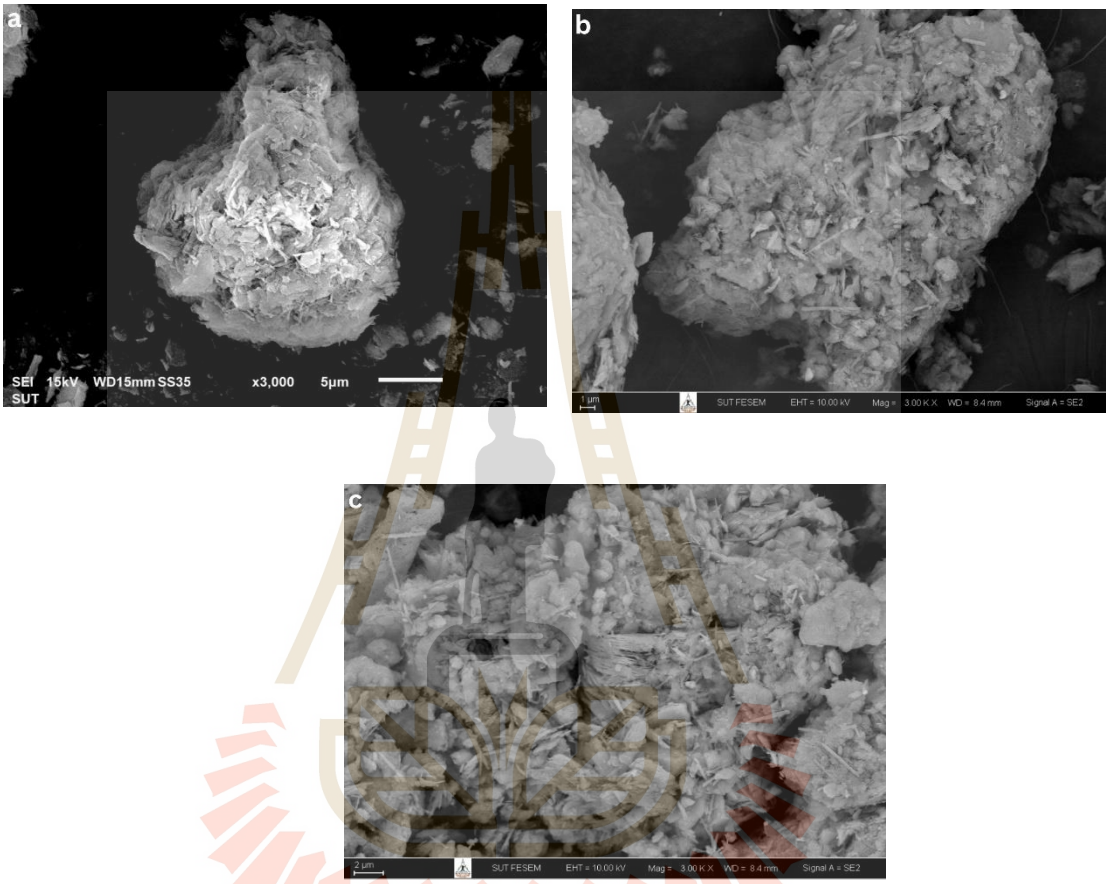

Figure 4.7 Scanning electron microscope (SEM) images of clay in Thailand (a) Ball clay, (b) Lampang white clay, and (c) Ranong white clay

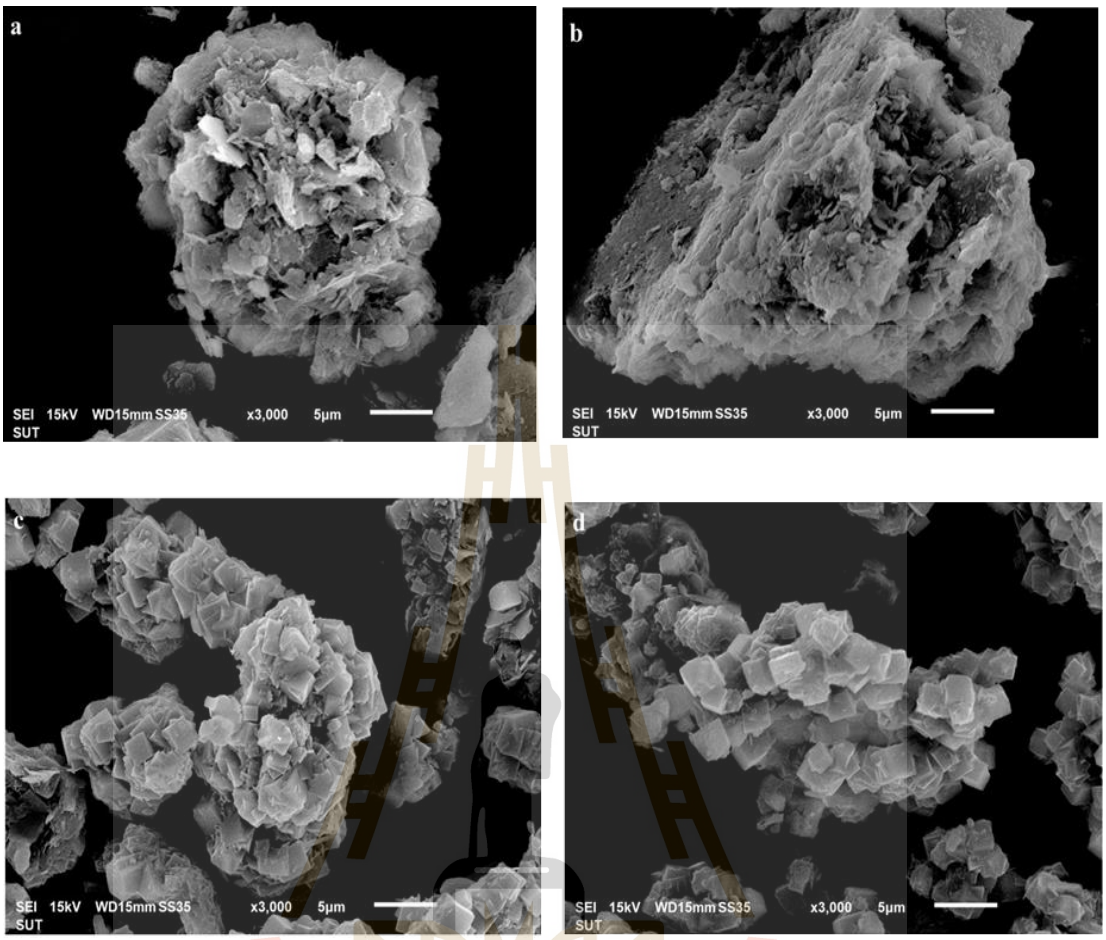

Figure 4.8 Scanning electron microscope (SEM) images of Na-A zeolite after hydrothermal treatment in NaOH solution at various concentrations: (a) 0.5 M, (b) 1 M, (c) 2 M, and (d) 3 M

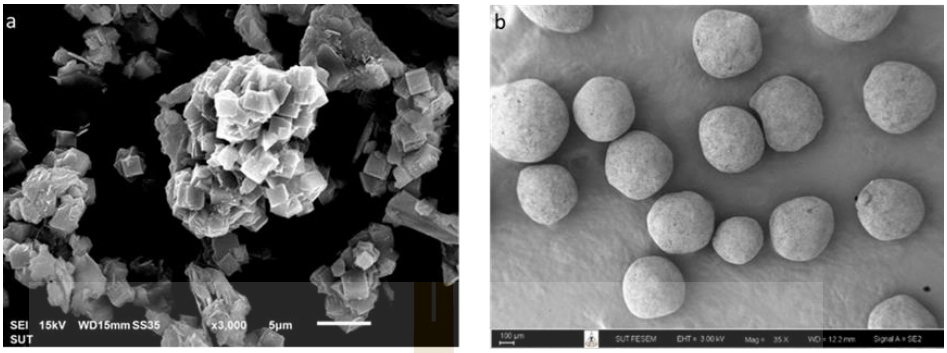

Figure 4.9 Scanning electron microscope (SEM) images of (a)Li-A zeolite after a cationic exchange in LiOH solution at 2M and (b)Li-A zeolite granules prepared by a spray dryer

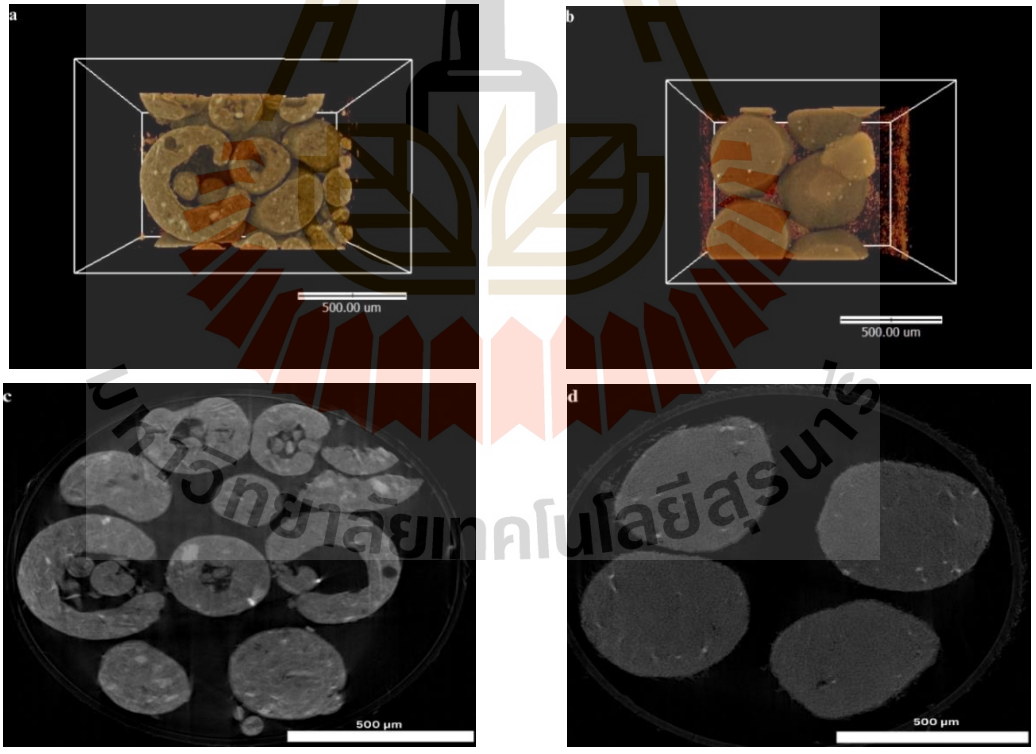

Figure 4.10 Cross-section of the 3D image of (a)ball clay, (b) Li-A zeolite granules and a single slice of the tomogram of (c) ball clay and (d) Li-A zeolite granules

4.6 Specific Surface Area of Li-A Zeolite

The textural properties of the synthesized Li-A zeolite were analyzed by Brunauer–Emmett–Teller (BET) surface area analysis using nitrogen adsorption–desorption measurements at 77 K. The synthesized Li-A zeolite exhibited a specific surface area of 450 m^2/g, depending on synthesis temperature, NaOH, and LiOH concentration. These values are slightly lower than those of commercial zeolite A (Typically 500-800 m^2/g). This relatively high surface area indicates the successful development of a well-defined microporous framework characteristic of zeolite A. The total pore volume of the synthesized Li-A zeolite is 0.25 cm^3/g, which is comparable to previously reported values in the range of 0.20–0.35 cm^3/g for conventional zeolite A materials. The pore volume is mainly attributed to the intrinsic microporous structure of zeolite A, consisting of sodalite cages interconnected by uniform pore openings. The average pore size of the synthesized Li-A zeolite is 0.4 nm, confirming that the material predominantly exhibits microporosity. This value is consistent with reported average pore sizes for zeolite A, which are generally below 2 nm, corresponding to the characteristic pore opening of approximately 0.4 nm. Such pore dimensions are favorable for molecular sieving and selective adsorption applications. Overall, the specific surface area, total pore volume, and average pore size of the synthesized zeolite A are in good agreement with values reported in previous studies, indicating that the synthesized material possesses typical textural properties of zeolite A and is suitable for adsorption and molecular sieving applications.

4.7 Zeolite molecular sieve for oxygen concentrator

This chapter presents the experimental results of the zeolite samples with particle sizes of 450 μm, 550 μm, and 650 μm, tested in the oxygen concentrator system. The main objective was to evaluate the relationship between particle size and oxygen purity (%).

4.7.1 Oxygen Purity of Different Zeolite Particle Sizes

The results demonstrated a clear relationship between zeolite particle size and oxygen purity produced by the oxygen concentrator. The performance evaluation was conducted over three independent test cycles, with each cycle operated continuously for 2 h to ensure reproducibility and operational stability. The obtained results showed consistent trends across all test runs. As the zeolite particle size decreased, the oxygen purity increased. Specifically, the zeolite with a particle size of 450 μm exhibited the highest performance, achieving a maximum oxygen purity of 93%. In comparison, the 550 μm zeolite sample reached a maximum oxygen purity of 92%, while the 650 μm sample showed the lowest performance, with a maximum oxygen purity of 90%. These results indicate a gradual decrease in oxygen separation efficiency with increasing particle size. The improved performance observed for smaller particle sizes can be attributed to the increased surface area, which promotes more effective nitrogen adsorption during the pressure swing adsorption (PSA) process. Importantly, oxygen purity levels exceeding 90% are generally considered acceptable and suitable for typical medical oxygen concentrator applications. Therefore, all tested zeolite particle sizes met the minimum requirement for medical use; however, the 450 μm zeolite demonstrated superior performance and is the most suitable particle size among the samples investigated.

Table 4.2 Oxygen purity at different zeolite particle sizes

Time (min)	O_2 Purity (%)								
	450 µm			550 µm			650 µm		
	1st	2nd	3rd	1st	2nd	3rd	1st	2nd	3rd
5	92	92	92	91	92	91	90	90	88
10	92	92	92	92	92	92	88	90	90
15	93	93	93	92	92	92	88	89	88
20	91	92	91	91	91	91	89	89	89
25	92	91	92	90	90	92	89	90	90
30	92	92	92	90	90	90	90	90	90
35	93	93	93	91	90	91	89	89	89
40	91	92	91	91	91	91	90	88	90
45	91	91	91	91	91	91	90	89	89
50	91	91	91	91	91	91	90	90	90
55	91	91	91	91	91	91	88	88	88
60	90	92	93	90	90	90	90	90	90
65	90	90	93	92	92	92	89	89	89
70	90	91	92	90	90	90	90	90	90
75	91	91	91	91	91	91	88	88	88
80	91	91	93	91	91	91	88	89	89
85	90	92	92	90	90	90	90	90	90

Table 4.2 Oxygen purity at different zeolite particle sizes (Continued)

Time (min)	O_2 Purity (%)								
	450 µm			550 µm			650 µm		
	1st	2nd	3rd	1st	2nd	3rd	1st	2nd	3rd
90	91	93	91	91	92	91	88	88	90
95	91	91	91	91	92	91	89	88	89
100	91	91	91	91	91	91	89	89	89
105	91	91	91	91	91	91	89	90	90
110	93	93	93	92	92	92	90	90	90
115	93	93	93	91	91	91	90	88	90
120	92	92	92	90	92	90	90	90	89

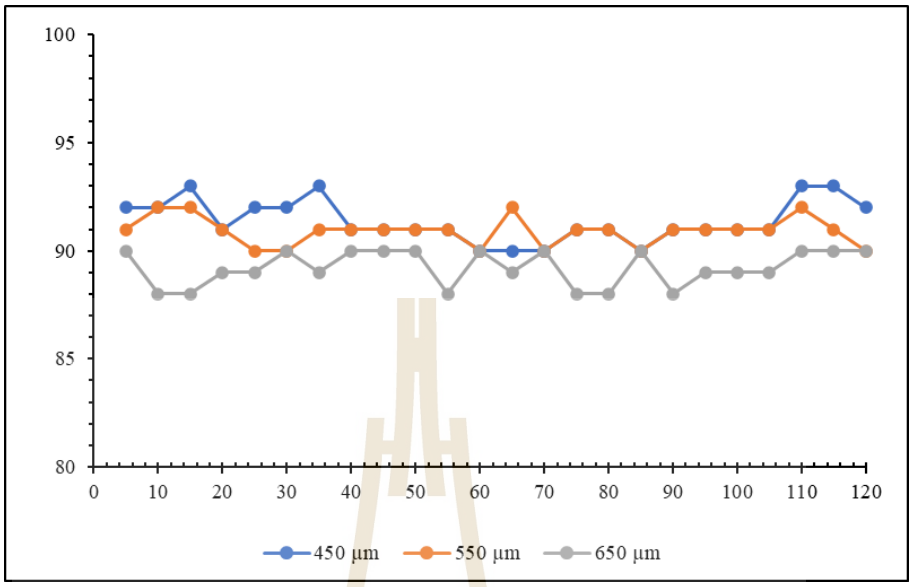

Figure 4.11 The first cycle of the oxygen concentrator at different zeolite particle sizes

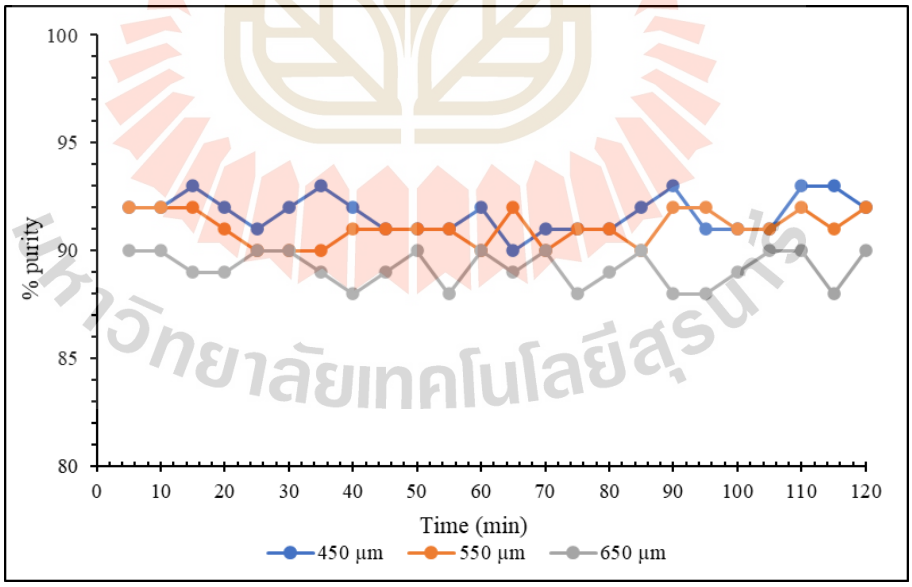

Figure 4.12 The second cycle of the oxygen concentrator at different zeolite particle sizes

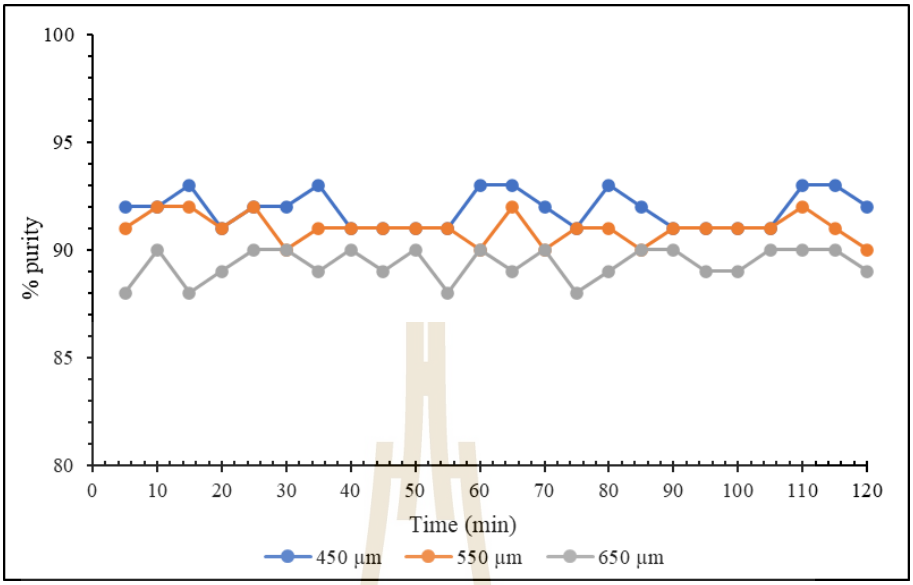

Figure 4.13 The third cycle of the oxygen concentrator at different zeolite particle sizes

CHAPTER V

CONCLUSION AND RECOMMENDATION

5.1 Conclusion

In this research, zeolite A was successfully synthesized using various types of local clays, including ball clay, Ranong white clay, and Lampang white clay, to determine the most suitable raw material for zeolite formation. The results revealed that ball clay, with a Si/Al ratio of 1.32, exhibited the most appropriate composition for zeolite A synthesis. In general, starting materials for synthesizing zeolite A should ideally possess a Si/Al ratio in the range of approximately 1.00 - 1.30 to ensure proper framework formation and phase purity. The composition of ball clay closely matched this optimal range, making it a promising raw material for zeolite A production. Ball clay was calcined at different temperatures ranging from 400℃ to 800℃ for 3 hours. It was found that at 600℃, the XRD pattern exhibited a kaolinite peak, indicating the transformation into a metastable phase of ball clay, which is favorable for zeolite formation. Zeolite A was successfully synthesized from ball clay at a NaOH concentration of 3 M. Furthermore, ion exchange between Na^+ and Li^+ ions was achieved using a 2 M LiOH solution, confirmed by FTIR analysis, indicating the successful formation of Li-zeolite. The synthesized zeolite was formed into particles using a spray drying method without the need for a binder, which simplified the shaping process and maintained the material's purity. Performance testing of zeolite with different particle sizes (450, 550, and 650 μm) in an oxygen concentrator demonstrated that the 450 μm zeolite particles provided the highest oxygen purity, reaching 93 percent after 15 min of operation. This result indicates that smaller particle sizes enhance the adsorption efficiency and improve the overall performance of the oxygen

concentrator. Overall, this study confirms that locally sourced ball clay is a suitable and sustainable raw material for synthesizing Li-A zeolite, which can be applied effectively in oxygen concentrator systems.

5.2 Recommendation

5.2.1 Ion Exchange Exploration:

Additional studies using different cations, such as Ca^{2+}, Mg^{2+}, and K^{+}, may be conducted to evaluate their impact on adsorption performance and selectivity in oxygen concentrator applications.

5.2.2 Long-term Performance Testing:

Extended operational testing of Li-A zeolite in real oxygen concentrators should be conducted to assess its stability, regeneration behavior, and performance over multiple adsorption cycles.

5.2.3 Scale-up and Economic Feasibility:

A techno-economic assessment should be performed to evaluate the cost-effectiveness of large-scale Li-A zeolite synthesis from ball clay and its potential for industry application.

REFERENCES

REFERENCES

Alexa-Stratulat, S.-M., Olteanu, I., Toma, A.-M., Pastia, C., Banu, O.-M., Corbu, O.-C., & Toma, I.-O. (2023). The Use of Natural Zeolites in Cement-Based Construction Materials—A State of the Art Review. *Coatings*, *14*(1), 18. https://doi.org/10.3390/coatings14010018

Bansiwal, A. K., Rayalu, S. S., Labhasetwar, N. K., Juwarkar, A. A., & Devotta, S. (2006). Surfactant-Modified Zeolite as a Slow Release Fertilizer for Phosphorus. *Journal of Agricultural and Food Chemistry*, *54*(13), 4773–4779. https://doi.org/10.1021/jf060034b

Belviso, C., Cavalcante, F., Niceforo, G., & Lettino, A. (2017). Sodalite, faujasite and A-type zeolite from 2:1dioctahedral and 2:1:1 trioctahedral clay minerals. A singular review of synthesis methods through laboratory trials at a low incubation temperature. *Powder Technology*, *320*, 483–497. https://doi.org/10.1016/j.powtec.2017.07.039

Bukhari, S. S., Behin, J., Kazemian, H., & Rohani, S. (2015). Conversion of coal fly ash to zeolite utilizing microwave and ultrasound energies: A review. *Fuel*, *140*, 250–266. https://doi.org/10.1016/j.fuel.2014.09.077

Cardoso, A. M., Horn, M. B., Ferret, L. S., Azevedo, C. M. N., & Pires, M. (2015). Integrated synthesis of zeolites 4A and Na–P1 using coal fly ash for application in the formulation of detergents and swine wastewater treatment. *Journal of Hazardous Materials*, *287*, 69–77. https://doi.org/10.1016/j.jhazmat.2015.01.042

Chen, D., Hu, X., Shi, L., Cui, Q., Wang, H., & Yao, H. (2012). Synthesis and characterization of zeolite X from lithium slag. *Applied Clay Science*, *59–60*, 148–151. https://doi.org/10.1016/j.clay.2012.02.017

Chen, H., Wydra, J., Zhang, X., Lee, P.-S., Wang, Z., Fan, W., & Tsapatsis, M. (2011). Hydrothermal Synthesis of Zeolites with Three-Dimensionally Ordered Mesoporous-Imprinted Structure. *Journal of the American Chemical Society*, *133*(32), 12390–12393. https://doi.org/10.1021/ja2046815

Cho, C. P., Pyo, Y. D., Jang, J. Y., Kim, G. C., & Shin, Y. J. (2017). NOx reduction and N2O emissions in a diesel engine exhaust using Fe-zeolite and vanadium based SCR catalysts. *Applied Thermal Engineering*, *110*, 18–24. https://doi.org/10.1016/j.applthermaleng.2016.08.118

Corma, A. (1995). Inorganic Solid Acids and Their Use in Acid-Catalyzed Hydrocarbon Reactions. *Chemical Reviews*, *95*(3), 559–614. https://doi.org/10.1021/cr00035a006

Corma, A. (1997). From Microporous to Mesoporous Molecular Sieve Materials and Their Use in Catalysis. *Chemical Reviews*, *97*(6), 2373–2420. https://doi.org/10.1021/cr960406n

Cui, Y., Zheng, Y., & Wang, W. (2018). Synthesis of 4A Zeolite from Kaolinite-Type Pyrite Flotation Tailings (KPFT). *Minerals*, *8*(8), 338. https://doi.org/10.3390/min8080338

Cundy, C. S., & Cox, P. A. (2003a). The Hydrothermal Synthesis of Zeolites: History and Development from the Earliest Days to the Present Time. *Chemical Reviews*, *103*(3), 663–702. https://doi.org/10.1021/cr020060i

Cundy, C. S., & Cox, P. A. (2003b). The Hydrothermal Synthesis of Zeolites: History and Development from the Earliest Days to the Present Time. *Chemical Reviews*, *103*(3), 663–702. https://doi.org/10.1021/cr020060i

Degnan, T. F. (2003). The implications of the fundamentals of shape selectivity for the development of catalysts for the petroleum and petrochemical industries.

Journal of Catalysis, *216*(1–2), 32–46. https://doi.org/10.1016/S0021-9517(02)00105-7

Drain, L. E. (1953). Permanent electric quadrupole moments of molecules and heats of adsorption. *Transactions of the Faraday Society*, *49*, 650. https://doi.org/10.1039/tf9534900650

El-Naggar, M. R., El-Kamash, A. M., El-Dessouky, M. I., & Ghonaim, A. K. (2008). Two-step method for preparation of NaA-X zeolite blend from fly ash for removal of cesium ions. *Journal of Hazardous Materials*, *154*(1–3), 963–972. https://doi.org/10.1016/j.jhazmat.2007.10.115

Farooq, S., Ruthven, D. M., & Boniface, H. A. (1989). Numerical simulation of a pressure swing adsorption oxygen unit. *Chemical Engineering Science*, *44*(12), 2809–2816. https://doi.org/10.1016/0009-2509(89)85090-0

Gougazeh, M., & Buhl, J.-Ch. (2014). Synthesis and characterization of zeolite A by hydrothermal transformation of natural Jordanian kaolin. *Journal of the Association of Arab Universities for Basic and Applied Sciences*, *15*(1), 35–42. https://doi.org/10.1016/j.jaubas.2013.03.007

Helfferich, F. G. (1985). Principles of adsorption & adsorption processes, by D. M. Ruthven, John Wiley & Sons, 1984, xxiv + 433 pp. *AIChE Journal*, *31*(3), 523–524. https://doi.org/10.1002/aic.690310335

Huang, L., Qin, F., Huang, Z., Zhuang, Y., Ma, J., Xu, H., & Shen, W. (2016). Hierarchical ZSM-5 Zeolite Synthesized by an Ultrasound-Assisted Method as a Long-Life Catalyst for Dehydration of Glycerol to Acrolein. *Industrial & Engineering Chemistry Research*, *55*(27), 7318–7327. https://doi.org/10.1021/acs.iecr.6b01140

Jareteg, A., Maggiolo, D., Larsson, A., Thunman, H., Sasic, S., & Ström, H. (2020). Effects of bed aging on temperature signals from fixed-bed adsorbers during industrial

operation. *Results in Engineering*, *8*, 100156. https://doi.org/10.1016/j.rineng.2020.100156

Jha, B., & Singh, D. N. (2016). *Fly Ash Zeolites* (Vol. 78). Springer Singapore. https://doi.org/10.1007/978-981-10-1404-8

Johnson, E. B. G., & Arshad, S. E. (2014). Hydrothermally synthesized zeolites based on kaolinite: A review. *Applied Clay Science*, *97–98*, 215–221. https://doi.org/10.1016/j.clay.2014.06.005

Karaca, M. (2004). *Use of Natural Zeolite (Clinoptilolite) in Agriculture*. https://www.researchgate.net/publication/269709768

Katsuki, H., Furuta, S., Watari, T., & Komarneni, S. (2005). ZSM-5 zeolite/porous carbon composite: Conventional- and microwave-hydrothermal synthesis from carbonized rice husk. *Microporous and Mesoporous Materials*, *86*(1–3), 145–151. https://doi.org/10.1016/j.micromeso.2005.07.010

Kerr, G. T. (1983). **Hydrothermal Chemistry of Zeolites** , by R. M. Barrer. Academic Press, London and New York, 1982. 360 + ix pages, $57.50. *Clays and Clay Minerals*, *31*(4), 319–320. https://doi.org/10.1346/CCMN.1983.0310414

Khaleque, A., Alam, M. M., Hoque, M., Mondal, S., Haider, J. Bin, Xu, B., Johir, M. A. H., Karmakar, A. K., Zhou, J. L., Ahmed, M. B., & Moni, M. A. (2020). Zeolite synthesis from low-cost materials and environmental applications: A review. *Environmental Advances*, *2*, 100019. https://doi.org/10.1016/j.envadv.2020.100019

Kianfar, E. , & M. A. (2020). Zeolites: properties, applications, modification and selectivity. *Zeolites: Advances in Research and Applications, 1.*

Kim, D. S., Chang, J.-S., Hwang, J.-S., Park, S.-E., & Kim, J. M. (2004). Synthesis of zeolite beta in fluoride media under microwave irradiation. *Microporous and*

Mesoporous Materials, *68*(1–3), 77–82. https://doi.org/10.1016/j.micromeso.2003.11.017

Kopaygorodsky, E. M., Guliants, V. V., & Krantz, W. B. (2004). Predictive dynamic model of single-stage ultra-rapid pressure swing adsorption. *AIChE Journal*, *50*(5), 953–962. https://doi.org/10.1002/aic.10093

Król, M. (2019). Hydrothermal synthesis of zeolite aggregate with potential use as a sorbent of heavy metal cations. *Journal of Molecular Structure*, *1183*, 353–359. https://doi.org/10.1016/j.molstruc.2019.02.011

Leggo, P. J. (2000). An investigation of plant growth in an organo-zeolitic substrate and its ecological significance. *Plant and Soil*, *219*(1–2), 135–146. https://doi.org/10.1023/A:1004744612234

Li, H., Li, H., Guo, Z., & Liu, Y. (2006). The application of power ultrasound to reaction crystallization. *Ultrasonics Sonochemistry*, *13*(4), 359–363. https://doi.org/10.1016/j.ultsonch.2006.01.002

Liu, M., Miao, C., & Wu, Z. (2024). Recent advances in the synthesis, characterization, and catalytic consequence of metal species confined within zeolite for hydrogen-related reactions. *Industrial Chemistry & Materials*, *2*(1), 57–84. https://doi.org/10.1039/D3IM00074E

Liu, Y., Han, S., Guan, D., Chen, S., Wu, Y., Yang, Y., & Jiang, N. (2019). Rapid green synthesis of ZSM-5 zeolite from leached illite clay. *Microporous and Mesoporous Materials*, *280*, 324–330. https://doi.org/10.1016/j.micromeso.2019.02.027

Mumpton, F. A. (1999). *La roca magica* : Uses of natural zeolites in agriculture and industry. *Proceedings of the National Academy of Sciences*, *96*(7), 3463–3470. https://doi.org/10.1073/pnas.96.7.3463

Pal, P., Das, J. K., Das, N., & Bandyopadhyay, S. (2013). Synthesis of NaP zeolite at room temperature and short crystallization time by sonochemical method. *Ultrasonics Sonochemistry*, *20*(1), 314–321. https://doi.org/10.1016/j.ultsonch.2012.07.012

Pavelić, K., Hadžija, M., Bedrica, L., Pavelić, J., Đikić, I., Katić, M., Kralj, M., Bosnar, M. H., Kapitanović, S., Poljak-Blaži, M., Križanac, Š., Stojković, R., Jurin, M., Subotić, B., & Čolić, M. (2001). Natural zeolite clinoptilolite: new adjuvant in anticancer therapy. *Journal of Molecular Medicine*, *78*(12), 708–720. https://doi.org/10.1007/s001090000176

Pavlović, J., & Rajić, N. (2023). Clinoptilolite—An Efficient Carrier for Catalytically Active Nano Oxide Particles. *Minerals*, *13*(7), 877. https://doi.org/10.3390/min13070877

Petrov, I. and T. Michalev. (2012). Synthesis of zeolite A: a review. *Scientific Papers of the University of Ruse, 51*, 30–35.

Phiriyawirut, P., Magaraphan, R., Jamieson, A. M., & Wongkasemjit, S. (2003). MFI zeolite synthesis directly from silatrane via sol–gel process and microwave technique. *Materials Science and Engineering: A*, *361*(1–2), 147–154. https://doi.org/10.1016/S0921-5093(03)00509-4

Price, L., Leung, K., & Sartbaeva, A. (2017). Local and Average Structural Changes in Zeolite A upon Ion Exchange. *Magnetochemistry*, *3*(4), 42. https://doi.org/10.3390/magnetochemistry3040042

Qazi, U. Y., Javaid, R., Ikhlaq, A., Khoja, A. H., & Saleem, F. (2022). A Comprehensive Review on Zeolite Chemistry for Catalytic Conversion of Biomass/Waste into Green Fuels. *Molecules*, *27*(23), 8578. https://doi.org/10.3390/molecules27238578

Ramya, G., Crittenden, B., Smith, M., Camus, O., Chew, Y. M. J., & Perera, S. (2019). Synthesis of novel regenerable 13X zeolite-polyimide adsorbent foams. *Chemical Engineering Journal*, *361*, 736–750. https://doi.org/10.1016/j.cej.2018.12.096

Rao, V. R., Farooq, S., & Krantz, W. B. (2010). Design of a two-step pulsed pressure-swing adsorption-based oxygen concentrator. *AIChE Journal*, *56*(2), 354–370. https://doi.org/10.1002/aic.11953

Rao, V. R., Kothare, M. V., & Sircar, S. (2014). Novel design and performance of a medical oxygen concentrator using a rapid pressure swing adsorption concept. *AIChE Journal*, *60*(9), 3330–3335. https://doi.org/10.1002/aic.14518

Reháková, M., Čuvanová, S., Dzivák, M., Rimár, J., & Gaval'ová, Z. (2004). Agricultural and agrochemical uses of natural zeolite of the clinoptilolite type. *Current Opinion in Solid State and Materials Science*, *8*(6), 397–404. https://doi.org/10.1016/j.cossms.2005.04.004

Sangeetha, C., & Baskar, P. (2016). Zeolite and its potential uses in agriculture : A critical review. *Agricultural Reviews*, *of*. https://doi.org/10.18805/ar.v0iof.9627

Santos, J. C., Portugal, A. F., Magalhães, F. D., & Mendes, A. (2006). Optimization of Medical PSA Units for Oxygen Production. *Industrial & Engineering Chemistry Research*, *45*(3), 1085–1096. https://doi.org/10.1021/ie0504809

Sathupunya, M., Gulari, E., & Wongkasemjit, S. (2002). ANA and GIS zeolite synthesis directly from alumatrane and silatrane by sol-gel process and microwave technique. *Journal of the European Ceramic Society*, *22*(13), 2305–2314. https://doi.org/10.1016/S0955-2219(02)00042-0

Shoinkhorova, T., Dikhtiarenko, A., Ramirez, A., Dutta Chowdhury, A., Caglayan, M., Vittenet, J., Bendjeriou-Sedjerari, A., Ali, O. S., Morales-Osorio, I., Xu, W., & Gascon, J. (2019). Shaping of ZSM-5-Based Catalysts via Spray Drying: Effect on

Methanol-to-Olefins Performance. *ACS Applied Materials & Interfaces*, *11*(47), 44133–44143. https://doi.org/10.1021/acsami.9b14082

Shokroo, E. J., Farsani, D. J., Meymandi, H. K., & Yadollahi, N. (2016). Comparative study of zeolite 5A and zeolite 13X in air separation by pressure swing adsorption. *Korean Journal of Chemical Engineering*, *33*(4), 1391–1401. https://doi.org/10.1007/s11814-015-0232-6

Shoppert, A. A., Loginova, I. V., Chaikin, L. I., & Rogozhnikov, D. A. (2017). Alkali Fusion-Leaching Method For Comprehensive Processing Of Fly Ash. *KnE Materials Science*, *2*(2), 89. https://doi.org/10.18502/kms.v2i2.952

Silva, D. P. S., Santos, A. T., Ribeiro, T. R. S., Solano, J. R. S., Cavalcanti, R. K. B. C., Silva, B. J. B., Quintela, P. H. L., & Silva, A. O. S. (2021). Monosodium glutamate-mediated hierarchical porous formation in LTA zeolite to enhance CO2 adsorption performance. *Journal of Sol-Gel Science and Technology*, *100*(2), 360–372. https://doi.org/10.1007/s10971-021-05644-5

Sircar, S. (2002). Pressure Swing Adsorption. *Industrial & Engineering Chemistry Research*, *41*(6), 1389–1392. https://doi.org/10.1021/ie0109758

SUGANO, Y., SAHARA, R., MURAKAMI, T., NARUSHIMA, T., IGUCHI, Y., & OUCHI, C. (2005). Hydrothermal Synthesis of Zeolite A Using Blast Furnace Slag. *ISIJ International*, *45*(6), 937–945. https://doi.org/10.2355/isijinternational.45.937

Taylor, J. H., Elmes, V. K., Hurt, A. P., & Coleman, N. J. (2020). Synthesis of feldspathoids and zeolite K–F from waste amber container glass. *Materials Chemistry and Physics*, *246*, 122805. https://doi.org/10.1016/j.matchemphys.2020.122805

Terzano, R., D'Alessandro, C., Spagnuolo, M., Romagnoli, M., & Medici, L. (2015). Facile Zeolite Synthesis from Municipal Glass and Aluminum Solid Wastes. *CLEAN – Soil, Air, Water*, *43*(1), 133–140. https://doi.org/10.1002/clen.201400091

W John Thomas, F. , & C. B. (1998). Adsorption technology and design. *Butterworth-Heinemann.*

Wang, J., Chen, Z., Shao, D., Li, Y., Xu, Z., Cheng, C., Asiri, A. M., Marwani, H. M., & Hu, S. (2017). Adsorption of U(VI) on bentonite in simulation environmental conditions. *Journal of Molecular Liquids*, *242*, 678–684. https://doi.org/10.1016/j.molliq.2017.07.048

Wang, P., Shen, B., Shen, D., Peng, T., & Gao, J. (2007). Synthesis of ZSM-5 zeolite from expanded perlite/kaolin and its catalytic performance for FCC naphtha aromatization. *Catalysis Communications*, *8*(10), 1452–1456. https://doi.org/10.1016/j.catcom.2006.12.018

Wang, S., & Peng, Y. (2010). Natural zeolites as effective adsorbents in water and wastewater treatment. *Chemical Engineering Journal*, *156*(1), 11–24. https://doi.org/10.1016/j.cej.2009.10.029

Worrall, W. E. (2013). Ceramic Raw Materials. *Institute of Ceramics Textbook Series. Elsevier.*

Wu, Y., Ren, X., & Wang, J. (2009). Facile synthesis and morphology control of zeolite MCM-22 via a two-step sol–gel route with tetraethyl orthosilicate as silica source. *Materials Chemistry and Physics*, *113*(2–3), 773–779. https://doi.org/10.1016/j.matchemphys.2008.08.008

Yao, G., Lei, J., Zhang, X., Sun, Z., & Zheng, S. (2018). One-Step Hydrothermal Synthesis of Zeolite X Powder from Natural Low-Grade Diatomite. *Materials*, *11*(6), 906. https://doi.org/10.3390/ma11060906

Zhu, X., Liu, Y., Yang, X., & Liu, W. (2017). Study of a novel rapid vacuum pressure swing adsorption process with intermediate gas pressurization for producing oxygen. *Adsorption*, *23*(1), 175–184. https://doi.org/10.1007/s10450-016-9843-4

Zimmermann, N. E. R., & Haranczyk, M. (2016). History and Utility of Zeolite Framework-Type Discovery from a Data-Science Perspective. *Crystal Growth & Design*, *16*(6), 3043–3048. https://doi.org/10.1021/acs.cgd.6b00272

APPENDIX

PUBLICATION

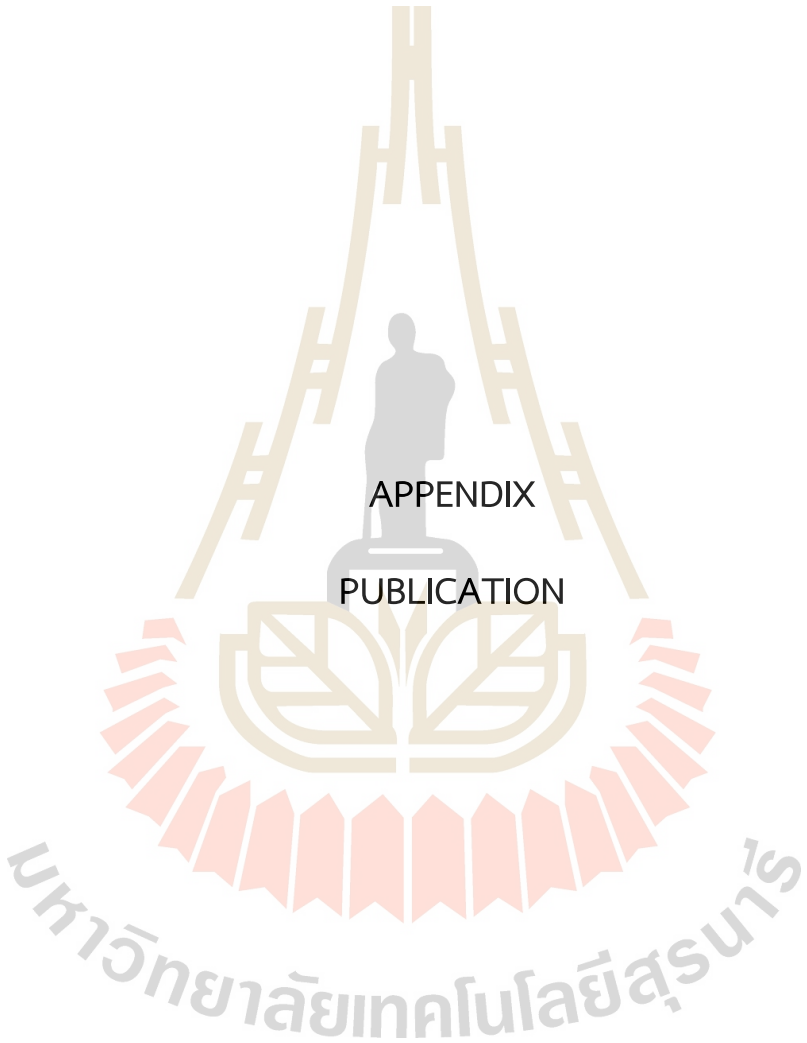

APPENDIX A

Available online at website: https://journal.bcrec.id/index.php/bcrec

Bulletin of Chemical Reaction Engineering & Catalysis, 20 (3) 2025, 553-559

Original Research Article

Preparation and Characterization of Zeolite A Synthesized from Narathiwat White Clay

Abhirak Sinchangreed[1], Sukasem Watcharamaisakul[1]*, Pattanaphong Janphuang[2]

[1]School of Materials Engineering, Suranaree University of Technology, Nakhon Ratchasima 30000, Thailand
[2]Synchrotron Light Research Institute, Nakhon Ratchasima 30000, Thailand.

Received: 16th July 2025; Revised: 18th August 2025; Accepted: 19th August 2025
Available online: 25th August 2025; Published regularly: October 2025

Abstract

Zeolite A is a widely used synthetic zeolite known for its high ion-exchange capacity and molecular sieving properties. This study explored the synthesis of zeolite A using Narathiwat white clay as a raw material. White clay, primarily composed of kaolinite ($Al_2Si_2O_5(OH)_4$), is considered a cost-effective source of aluminum and silicon for zeolite synthesis. The process involves the transformation of kaolinite into metakaolin via calcination, followed by hydrothermal crystallization under controlled conditions from natural white clay without conventional high-temperature calcination. Synthesized zeolite was characterized using X-ray diffraction (XRD), Differential Thermal Analysis (DTA), scanning electron microscopy (SEM), and X-ray fluorescence (XRF) spectroscopy to determine the elemental composition of the raw white clay and the synthesized zeolite A, while Fourier-transform infrared spectroscopy (FTIR) was used to confirm its structure and purity. Furthermore, the influence of the NaOH solution and the stability temperature of zeolite A are shown in this research. The optimum conditions for achieving zeolite A were calcined at 600 °C for 3 h in the first step, followed by using autoclaves at 200 °C for 24 h with a 3 M NaOH solution. The SEM results indicated that the Narathiwat white clay could be used to synthesize zeolite A, which exhibited a cubic morphology consisting primarily of silicon and aluminum. Notably, the crystallinity was influenced by the concentration of the NaOH solution employed. Moreover, the XRD and FTIR results demonstrate the feasibility of synthesizing high-quality zeolite A.

Keywords: Kaolinite; Hydrothermal synthesis; Autoclaves; Zeolite A

How to Cite: Sinchangreed, A., Watcharamaisakul, S., Janphuang, P. (2025). Preparation and Characterization of Zeolite A Synthesized from Narathiwat White Clay. *Bulletin of Chemical Reaction Engineering & Catalysis*, 20 (3), 553-559. (doi: 10.9767/bcrec.20445)

Permalink/DOI: https://doi.org/10.9767/bcrec.20445

1. Introduction

Zeolites are crystalline aluminosilicates with a three-dimensional porous structure possessing high value in various industrial applications [1]. Their unique framework includes silicon (Si), aluminum (Al), and oxygen (O) tetrahedra, forming channels and cavities that can selectively trap and release molecules [2,3]. Due to their molecular sieving, ion-exchange, and adsorption properties, zeolites are widely used in catalysis [4], water purification [5], gas separation [6], and detergent formulations [7]. Zeolite A has gained significant attention among different zeolite types due to its well-defined pore structure, high surface area, and excellent cation-exchange capacity. This makes it particularly useful in water softening, adsorption, and environmental remediation. While synthetic zeolites are commonly produced from pure chemical reagents such as sodium silicate and sodium aluminate [8,9], natural raw materials such as white clay are considered a cost-effective and eco-friendly alternative [10,11]. White clay, primarily composed of kaolinite ($Al_2Si_2O_5(OH)_4$), is a natural source of silicon and aluminum, which are essential for zeolite formation [12].

* Corresponding Author.
Email: sukasem@sut.ac.th (S. Watcharamaisakul)

Bulletin of Chemical Reaction Engineering & Catalysis, 20 (3), 2025, 554

Conventionally, synthetic zeolites are produced using pure chemical sources in silica and alumina, such as sodium silicate and sodium aluminate [13,14]. However, the production of these materials can be expensive and environmentally taxing. As a result, increasing attention has been directed toward using natural and low-cost raw materials such as clays, fly ash, and agricultural residues for zeolite synthesis [15,16]. In recent years, attention has shifted toward more sustainable synthesis approaches, driven by the need to reduce energy consumption, lower production costs, and minimize environmental impact. Clays are rich in silica and alumina, the essential components of zeolite frameworks, making them suitable and cost-effective precursors. Furthermore, clay-based synthesis often requires fewer chemical additives and can be conducted under hydrothermal conditions compared to conventional routes. Recent developments in green chemistry and materials science have enabled the optimization of clay activation processes, including thermal treatment and alkali fusion, to enhance their reactivity. These pathways to sustainable synthesis not only contribute to the circular economy by utilizing natural or industrial waste-derived clays but also align with environmental goals by reducing the carbon footprint associated with zeolite production. White clay consists of kaolinite and represents a promising alternative due to its abundance, low cost, and appropriate Si/Al ratio suitable for zeolite A formation [17]. The traditional method for producing zeolite A from natural kaolin begins with calcination, which decreases its resistance to chemical attack and converts it into an amorphous substance. This process yields metakaolin, which is then synthesized into zeolites through a hydrothermal reaction in an alkaline environment.

This research focuses on the synthesis of zeolite A from Narathiwat white clay, acquired from southern Thailand, through a hydrothermal process. The study aims to evaluate the feasibility of using white clay as a raw material by optimizing the synthesis conditions and characterizing the produced zeolite, thus developing a sustainable synthesis route. This study contributes to the advancement of environmentally friendly materials for industrial and environmental applications.

2. Materials and Methods

2.1 Preparation of Metakaolin and Zeolite A

The synthesis of zeolite A from white clay involves 2 steps as follows. The first step is metakaolinization, which involves the thermal treatment of raw white clay at a temperature of 600 °C for 3 h. The second step is the chemical treatment of the prepared metakaolin using sodium hydroxide (NaOH) solutions at concentrations of 1, 2, 3, and 4 M.

In the conventional hydrothermal synthesis technique, white clay is ground and screened through a sieve No.100 (aperture of 150 μm). Then, 200 grams of white clay powder in the particle range of 1-50 μm is calcined in a furnace at 600 °C for 3 h. This process converts kaolinite ($Al_2Si_2O_5(OH)_4$) into metakaolin ($Al_2Si_2O_7$). During this transformation, the structure of the kaolin changes, and volatile matter is released, leading to the formation of metakaolin, as illustrated in the following equation:

$$Al_2Si_2O_5(OH)_4\ (\text{kaolin}) \rightarrow Al_2Si_2O_7\ (\text{metakaolin}) + 2H_2O \quad (1)$$

A total of 20 g of metakaolin was treated with 100 mL of NaOH solutions at concentrations of 1, 2, 3, and 4 M. The mixture was placed in stainless steel autoclaves lined with Teflon and heated at 200 °C for 24 h to facilitate the exchange of sodium ions within the metakaolin structure. Following this treatment, the sample was washed with deionized water to eliminate unreacted NaOH until the pH reached about 7. After that, it was filtered and dried in an oven at 100 °C overnight. Different samples with different NaOH concentrations were prepared to determine the optimal concentration for synthesizing zeolite A.

2.2. Characterizations

The material characterization of synthesized zeolite A and Narathiwat white clay was analyzed on a powdered sample by Energy Dispersive Spectrometer X-ray Fluorescence (ED-XRF) (Horiba/XGT-5200) to determine the composition. Simultaneous Thermal Analysis (NETZSCH, STA449F3 / QMS403C) was used to analyze the thermal behavior of Narathiwat white clay. XRD analyzed the crystalline phases present in Narathiwat white clay, metakaolin, and synthesized zeolite A. An X-ray Diffractometer (Bruker D2 Phaser) with Cu kα radiation was operated at 40 kV and 30 mA. Data were collected in the 2θ range of 5-70°. The morphology of Narathiwat white clay and synthesized zeolite A was observed using a Scanning Electron Microscope (SEM-EDS - JEOL/JSM-6010LV). SEM micrographs were obtained at an operating voltage of U = 15 kV and a magnification of 1000X. FTIR spectra were recorded by a Fourier Transform Infrared Microscope Spectrophotometry (FT-IR Microscope/Bruker, TENSOR 27-Hyperion-2000) for the identification and characterization of the chemical composition of Narathiwat white clay and zeolite A.

3. Results and Discussion

3.1. XRF Analysis

X-ray fluorescence (XRF) spectroscopy was employed to determine the composition of the raw white clay and the synthesized zeolite A. This analysis aimed to evaluate the transformation of the clay material during the synthesis process and confirm the formation of a zeolitic structure based on compositional changes, particularly in the Si/Al ratio and sodium content.

Table 1 presents the comparative XRF results of various white clays and synthesized zeolite materials. The raw white clay was primarily composed of silica (SiO_2) and alumina (Al_2O_3), with minor quantities of iron oxide (Fe_2O_3), potassium oxide (K_2O), calcium oxide (CaO), and magnesium oxide (MgO). After synthesis, a marked increase in Na_2O content was observed in the zeolite A sample, indicating the successful incorporation of sodium into the crystal framework during hydrothermal treatment. The significant increase in Na_2O content observed during the synthesis process demonstrates a strong correlation with the formation mechanism and stabilization of the zeolite framework. Sodium ions (Na^+), derived from Na_2O, serve as essential structure-directing and charge-compensating agents, particularly in low-silica zeolites such as zeolite A (LTA-type). Their presence facilitates the development of a well-ordered aluminosilicate framework by balancing the negative charges resulting from isomorphic substitution of Si^{4+} by Al^{3+} within the tetrahedral network. Increased Na_2O concentration contributes to elevated alkalinity in the reaction medium, which plays a crucial role in promoting the dissolution of silica and alumina sources. This enhanced solubility accelerates the nucleation and subsequent crystallization of zeolite structures through a dissolution - reprecipitation mechanism. Moreover, the Na_2O content directly influences phase selectivity during hydrothermal synthesis. Lower sodium concentrations tend to yield amorphous or poorly crystalline phases, whereas elevated Na_2O levels favor the formation of sodium-rich crystalline zeolite phases such as zeolite A. This is attributed to the role of Na^+ in stabilizing the intermediate aluminosilicate species and promoting the assembly of the targeted microporous framework.

The Si/Al ratio of Narathiwat white clay was approximately 1.27, closely matching the theoretical ratio for zeolite A (NaA-type zeolite) synthesis as confirmed by the calculation below Table 1 [18], confirming successful structural transformation. The significant reduction in Fe_2O_3 and other impurities also suggests the improved purity and crystallinity of the final product. These results demonstrate the effectiveness of using white clay as a raw material for synthesizing zeolite A and achieving the elemental composition through the applied synthesis process.

3.2. Differential Thermal Analysis (DTA) of Narathiwat white clay

Figure 1 illustrates the DTA curve of Narathiwat white clay. DTA thermograms exhibit endothermic peaks with the maximum at 105 and 570 °C, which can be attributed to the removal of adsorbed water, dihydroxylation of clay minerals, and release of structural hydroxyl groups where kaolinite turns to metakaolin. Therefore, the calcined temperatures used in this experiment were around 600 °C according to the DTA results.

Table 1. The chemical XRF composition of white clays and zeolite A.

Element	Narathiwat white clay (wt%)	Lampang white clay (wt%)	Ranong white clay (wt%)	Zeolite (wt%)
SiO_2	54.222	64.478	73.519	43.841
Al_2O_3	36.285	24.763	13.223	35.654
Fe_2O_3	1.431	1.268	2.209	1.287
K_2O	2.145	3.973	3.285	2.023
TiO_2	0.078	0.046	0.089	0.033
CaO	0.184	0.212	0.104	0.121
MnO_2	0.045	0.246	0.071	0.018
Na_2O	4.223	4.196	5.232	16.456
MgO	1.387	0.818	2.268	0.567

(1). Si/Al calculation of Narathiwat white clay : SiO_2 = 54.222 × 258.18 / (100 × 60.08) = 2.33 mol; Al_2O_3 = 36.285 × 258.18 / (100 × 101.96) = 0.917 mol; Si/Al = 2.33 / (0.917 × 2) = 1.27
(2). Si/Al calculation of Zeolite A: SiO_2 = 43.841 × 1807.26 / (100 × 60.08) = 13.19 mol; Al_2O_3 = 35.654× 1807.26 / (100 × 101.96) = 6.32 mol; Si/Al = 13.19 / (6.32× 2) = 1.04

Bulletin of Chemical Reaction Engineering & Catalysis, 20 (3), 2025, 556

3.3. X-ray Diffraction (XRD)

Figure 2 illustrates the X-ray diffraction (XRD) pattern of Narathiwat white clay. The significant phases of Narathiwat white clay are kaolinite, illite, and quartz, which are impurities. Narathiwat white clay metakaolin, calcined at 600 °C, when compared with the XRD pattern of Narathiwat white clay, was found to have the kaolinite phase disappear after thermal treatment due to the dihydroxylation in molecules of white clay, resulting in the change of white clay structure from crystal to amorphous. According to the Differential Thermal Analysis (DTA) results, as shown in Figure 1, the Narathiwat white clay loses water by dihydroxylation at calcined temperature. Moreover, the X-ray diffraction (XRD) pattern of the synthesized zeolite A using NaOH concentrations of 3M displayed sharp and intense peaks at characteristic 2θ values. The synthesized products matched the characteristic peaks of zeolite A at 2θ values of 7.1, 10.1, 12.4, 16.2, 21.6, 24, 26, 27.2, 30, 30.9, 32.6, and 34.2 [19]. The presence of these well-defined peaks confirms the successful formation of pure zeolite A, with no detectable impurities or secondary phases such as sodalite or amorphous aluminosilicates. The intensity and sharpness of the peaks imply a high degree of crystallinity, which can ensure the microporous structure and uniform pore size distribution typical of zeolite A. These results align with previous studies, such as the research by Smaihi [19] and other contemporary works, which reported similar XRD patterns for high-purity synthetic zeolite A [20]. Besides, no significant broadening of peaks was observed, suggesting that the crystal domains are sufficiently large and well-ordered. This high crystallinity is critical for the ion-exchange capacity and molecular sieving performance of the material. Combined with the SEM and FTIR results, the XRD findings strongly support the successful synthesis of high-quality zeolite A. In addition, Figure 3 demonstrates the XRD patterns of zeolite A at different concentrations of NaOH solution. At 1 and 2M NaOH, the zeolite A pattern was not observed. The optimum conditions for synthesizing zeolite A were obtained when using NaOH concentrations of 3 and 4M, with the mixture heated to 200 °C for a 24 h reaction time.

3.4. SEM Micrographs

The micrographs in Figure 4 show that the crystallites of Narathiwat white clay are in a random orientation before treatment. In contrast, the SEM micrographs of the synthesized zeolite A in Figure 5 revealed uniform, well-defined cubic crystals, which are characteristic of the LTA-type framework. The particles appeared relatively homogeneous in terms of size and morphology, consistent with the values reported in the literature for conventionally synthesized zeolite A [21]. This regular cubic morphology indicates successful crystallization and effective control over the nucleation and growth phases during synthesis. The surfaces of the crystals appeared smooth and free of significant defects, with minimal signs of amorphous material or secondary phases, suggesting a high degree of purity. Slight agglomeration was observed in some regions, which is commonly reported in zeolite systems and may result from drying or interparticle interactions during sample preparation. However, the overall structural integrity of the crystals was not impacted. The well-defined crystal shape and absence of irregular structures support the high crystallinity observed in the XRD results, further confirming the successful formation of zeolite A.

3.5. Fourier Transform Infrared Analysis of Zeolite A from Narathiwat White Clay

The FTIR spectra for zeolite A and Narathiwat white clay are presented in Figure 6,

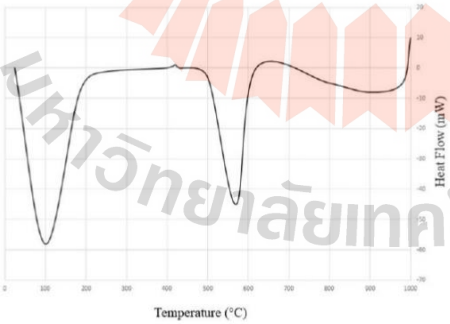

Figure 1. DTA curve of Narathiwat white clay.

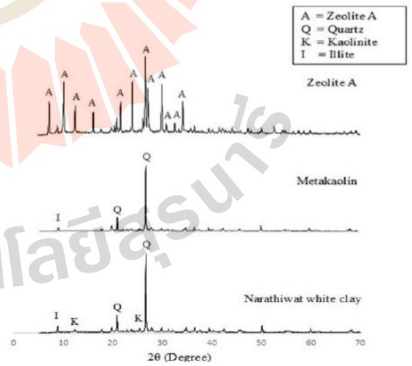

Figure 2. X-Ray diffraction pattern of Narathiwat white clay, metakaolin, and zeolite A.

along with the FTIR spectra of Narathiwat kaolin. The peaks observed at 3693 and 3622 cm^{-1} are linked to the stretching vibrations of hydroxyl groups within the structure of kaolin [22]. The peak at 3622 cm^{-1} specifically corresponds to the stretching vibration modes of the inner hydroxyl groups, mainly found in the octahedral and tetrahedral sheets. The peaks at 3693 cm^{-1} are associated with the stretching vibrations of the hydroxyl (OH) groups located on the inner surface, which are found on the surfaces of the octahedral sheets in the neighboring kaolin layer [23]. The peak at 1107 cm^{-1} is linked to the stretching vibrations of the Si-O bonds within the kaolin structure. In contrast, the peaks at 1029 cm^{-1} and 1002 cm^{-1} arise from the lattice vibrations of both Si-O-Si and Si-O-Al bonds. Moreover, the bending vibrations of the OH groups to the peaks at 910 cm^{-1} and 942 cm^{-1} correspond to the "surface OH bends" and the "inner OH bends", respectively. These vibrations of the OH groups are typically caused by the bonds in the Al-OH groups. The peaks at 790 cm^{-1} and 748 cm^{-1} were assigned to the Si-O-Si bonds, and finally, the 524 cm^{-1} peaks were assigned to the deformation of the vibration of the Si–O bonds [24]. The FTIR spectra of zeolite A illustrate broad bands around 466 cm^{-1}, which are related to the internal bending modes of the TO_4 (T = Si, Al). Additionally, bands at 550 cm^{-1} correspond to the vibrational modes of the double rings present in zeolite A. The prominent bands observed at 1002 cm^{-1} are linked to the T-O asymmetric stretching modes, while the band at 3446 cm^{-1}, along with the weaker band at 1650 cm^{-1}, is associated with water molecules and OH groups in zeolite A [25].

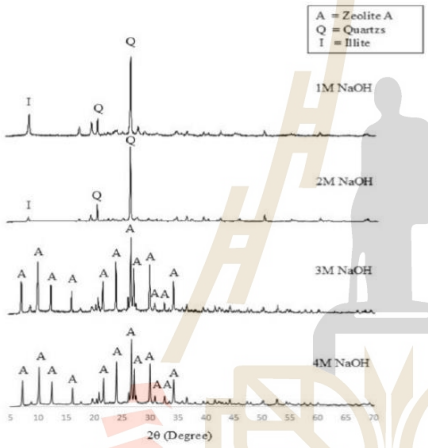

Figure 3. The XRD patterns of zeolite A prepared by heating at 200 °C in the NaOH solution at different concentrations (1, 2, 3, and 4 M).

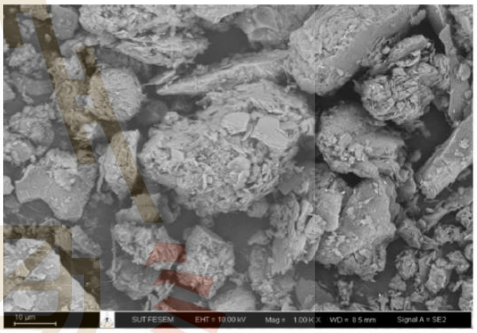

Figure 4. SEM micrograph of Narathiwat white clay.

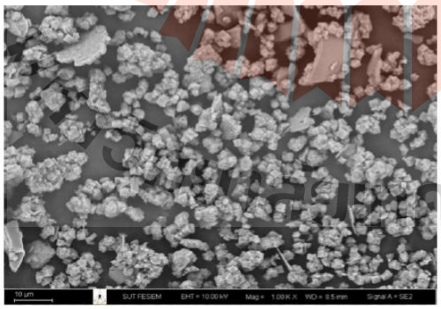

Figure 5. SEM micrograph of zeolite A.

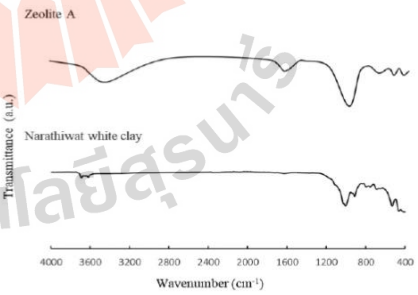

Figure 6. FTIR spectra of Narathiwat white clay and zeolite A.

4. Conclusions

This study successfully demonstrated the synthesis of zeolite A using locally sourced white clay (Narathiwat white clay) as a low-cost and environmentally friendly raw material. The first step starts with Narathiwat white clay calcined at 600 °C for 3 h. The synthesis parameters for zeolite A derived from Narathiwat white clay were optimized for the first time. The optimized parameters include a base of 3M NaOH, a crystallization time of 24 h, a temperature of 200°C, and a 24 h. The transformation of the clay into a crystalline zeolite structure was confirmed utilizing various characterization techniques. Differential thermogravimetric analysis further verified the thermal stability of the Narathiwat white clay, and its typical water loss behavior associated with the metakaolin structure for zeolite synthesis. XRF analysis confirmed the successful incorporation of sodium and an appropriate Si/Al ratio (~1.49), consistent with the zeolite A framework. The SEM results showed that the cubic crystal form was achieved. Overall, the results confirm that white clay is a viable and effective alternative raw material for synthesizing zeolite A. The synthesized product possesses properties suitable for applications in ion exchange, adsorption, and catalysis. This approach reduces production costs and promotes the utilization of abundant natural resources, contributing to sustainable material development.

Acknowledgments

The authors would like to acknowledge the Faculty of Materials Engineering, Suranaree University of Technology, and Synchrotron Light Research Institute for supporting the research fund.

CRedit Author Statement

Author Contributions: Sukasem Watcharamaisakul conceived the conceptualization, methodology, review, and editing of the manuscript. Abhirak Sinchangreed, author, performed methodology, formal analysis, investigation, validation, and writing-original draft. Pattanaphong Janphuang contributed to the experimental plan, measurement, data analysis, and revised the manuscript. All authors have read and agreed to the published version of the manuscript.

References

[1] Lin, Q.-F., Gao, Z.R., Lin, C., Zhang, S., Chen, J., Li, Z., Liu, X., Fan, W., Li, J., Chen, X., Camblor, M.A., Chen, F.-J. (2021). A stable aluminosilicate zeolite with intersecting three-dimensional extra-large pores. *Science*, 374 (6575), 1605–1608. DOI: 10.1126/science.abk3258

[2] Chen, K., Mousavi, S. H., Singh, R., Snurr, R. Q., Li, G., Webley, P. A. (2022). Gating effect for gas adsorption in microporous materials – mechanisms and applications. *Chemical Society Reviews*, 51 (3), 1139–1166. DOI: 10.1039/D1CS00822F

[3] Liu, X., Wang, C., Zhou, J., Liu, C., Liu, Z., Shi, J., Wang, Y., Teng, J., Xie, Z. (2022). Molecular transport in zeolite catalysts: depicting an integrated picture from macroscopic to microscopic scales. *Chemical Society Reviews*, 51(19), 8174–8200. DOI: 10.1039/D2CS00079B

[4] Kulprathipanja, S. (Ed.). (2010). *Zeolites in Industrial Separation and Catalysis*. Wiley. DOI: 10.1002/9783527629565.ch3

[5] Kallo, D. (2001). Applications of Natural Zeolites in Water and Wastewater Treatment. *Reviews in Mineralogy and Geochemistry*, 45(1), 519–550. DOI: 10.2138/rmg.2001.45.15

[6] Kosinov, N., Gascon, J., Kapteijn, F., Hensen, E.J.M. (2016). Recent developments in zeolite membranes for gas separation. *Journal of Membrane Science*, 499, 65–79. DOI: 10.1016/j.memsci.2015.10.049

[7] Cardoso, A.M., Horn, M.B., Ferret, L.S., Azevedo, C.M.N., Pires, M. (2015). Integrated synthesis of zeolites 4A and Na–P1 using coal fly ash for application in the formulation of detergents and swine wastewater treatment. *Journal of Hazardous Materials*, 287, 69–77. DOI: 10.1016/j.jhazmat.2015.01.042

[8] Al-nayili, A., Rzoqy, M. (2022). Local silica sand as a silica source in the synthesis of Y zeolite. *Asia-Pacific Journal of Chemical Engineering*, 17(5). DOI: 10.1002/apj.2824

[9] Foroughi, M., Salem, A., Salem, S. (2021). Characterization of phase transformation from low grade kaolin to zeolite LTA in fusion technique: Focus on quartz melting and crystallization in presence of NaAlO2. *Materials Chemistry and Physics*, 258, 123892. DOI: 10.1016/j.matchemphys.2020.123892

[10] Hassan, E.M., Abdul-Wahab, S.A., Abdo, J., Yetilmezsoy, K. (2019). Production of environmentally friendly cements using synthetic zeolite catalyst as the pozzolanic material. *Clean Technologies and Environmental Policy*, 21(9), 1829–1839. DOI: 10.1007/s10098-019-01752-7

[11] Lahnafi, A., Elgamouz, A., Jaber, L., Tijani, N., Kawde, A.-N. (2023). NaA zeolite-clay composite membrane formulation and its use as cost-effective water softener. *Microporous and Mesoporous Materials*, 348, 112339. DOI: 10.1016/j.micromeso.2022.112339

[12] Lecomte, I., Liégeois, M., Rulmont, A., Cloots, R., Maseri, F. (2003). Synthesis and characterization of new inorganic polymeric composites based on kaolin or white clay and on ground-granulated blast furnace slag. *Journal of Materials Research*, 18(11), 2571–2579. DOI: 10.1557/JMR.2003.0360

[13] Krachuamram, S., Chanapattharapol, K.C., Kamonsutthipaijit, N. (2021). Synthesis and characterization of NaX-type zeolites prepared by different silica and alumina sources and their CO2 adsorption properties. *Microporous and Mesoporous Materials*, 310. DOI: 10.1016/j.micromeso.2020.110632

[14] Yu, J. (2007). *Synthesis of Zeolites*. DOI: 10.1016/S0167-2991(07)80791-9

[15] El Bojaddayni, I., Emin Küçük, M., El Ouardi, Y., Jilal, I., El Barkany, S., Moradi, K., Repo, E., Laatikainen, K., Ouammou, A. (2023). A review on synthesis of zeolites from natural clay resources and waste ash: Recent approaches and progress. *Minerals Engineering*, 198, 108086. DOI: 10.1016/j.mineng.2023.108086

[16] -Murukutti, M., Jena, H. (2022). Synthesis of nano-crystalline zeolite-A and zeolite-X from Indian coal fly ash, its characterization and performance evaluation for the removal of Cs+ and Sr2+ from simulated nuclear waste. *Journal of Hazardous Materials*, 423, 127085. DOI: 10.1016/j.jhazmat.2021.127085

[17] Palomino, M., Corma, A., Rey, F., Valencia, S. (2010). New Insights on CO2 –Methane Separation Using LTA Zeolites with Different Si/Al Ratios and a First Comparison with MOFs. *Langmuir*, 26(3), 1910–1917. DOI: 10.1021/la9026656

[18] Ma, G., Bai, C., Wang, M., He, P. (2021). Effects of Si/Al Ratios on the Bulk-Type Zeolite Formation Using Synthetic Metakaolin-Based Geopolymer with Designated Composition. *Crystals*, 11(11), 1310. DOI: 10.3390/cryst11111310

[19] Smaihi, M., Barida, O., Valtchev, V. (2003). Investigation of the Crystallization Stages of LTA-Type Zeolite by Complementary Characterization Techniques. *European Journal of Inorganic Chemistry*, 2003(24), 4370–4377. DOI: 10.1002/ejic.200300154

[20] Wang, Q., Xu, W., Cai, J., Yu, Q., Min, J. (2024). Study on the Synthesis of LTA-Type Molecular Sieves from Coal Gangue and Aluminum Ash and Its Adsorption Properties towards Cu2+. *Crystals*, 14(4), 379. DOI: 10.3390/cryst14040379

[21] Youssef, H., Ibrahim, D., Komarneni, S. (2008). Microwave-assisted versus conventional synthesis of zeolite A from metakaolinite. *Microporous and Mesoporous Materials*, 115(3), 527–534. DOI: 10.1016/j.micromeso.2008.02.030

[22] Kloprogge, J. (2019). *The Kaolin Group: Hydroxyl Groups*. DOI: 10.1007/978-3-030-02373-7_3

[23] Jozanikohan, G., Abarghooei, M.N. (2022). The Fourier transform infrared spectroscopy (FTIR) analysis for the clay mineralogy studies in a clastic reservoir. *Journal of Petroleum Exploration and Production Technology*, 12(8), 2093–2106. DOI: 10.1007/s13202-021-01449-y

[24] Król, M., Minkiewicz, J., Mozgawa, W. (2016). IR spectroscopy studies of zeolites in geopolymeric materials derived from kaolinite. *Journal of Molecular Structure*, 1126, 200–206. DOI: 10.1016/j.molstruc.2016.02.027

[25] Montanari, T., Busca, G. (2008). On the mechanism of adsorption and separation of CO2 on LTA zeolites: An IR investigation. *Vibrational Spectroscopy*, 46(1), 45–51. DOI: 10.1016/j.vibspec.2007.09.001.

BIOGRAPHY

Mr. Abhirak Sinchangreed was born on June 20, 1994, in Nokok Subdistrict, Pak Thong Chai District, Nakhon Ratchasima Province, Thailand. He completed his primary education at Marie Thongchai School in Pak Thong Chai District and his secondary education at Marie Vithaya School in Mueang District, Nakhon Ratchasima Province. He received his Bachelor of Engineering in Chemical Engineering from Sirindhorn International Institute of Technology, Thammasat University, in 2017, and later pursued a Master of Engineering in Materials Engineering at Suranaree University of Technology, graduating in 2020.

He is currently working as a Community Development Specialist at the Department of Community Development, Ministry of Interior, Thailand.

During his graduate study, he received a Research and Development Fund (OROG), which was an external research funding source. His master's thesis is entitled "Synthesis of Zeolite Molecular Sieves for Medical Oxygen Concentrator." His research interests include zeolite synthesis, adsorption materials, and applications of porous materials in gas separation and oxygen concentrator systems.